INTEGRATION OF ELECTROFACIES AND GEOMECHANICAL CHARACTERISTICS OF SARAH FORMATION (POTENTIAL TIGHT GAS RESERVOIR), RUB' AL-KHALI BASIN, SAUDI ARABIA

BY

WALEED EJAZ

A Thesis Presented to the
DEANSHIP OF GRADUATE STUDIES

KING FAHD UNIVERSITY OF PETROLEUM & MINERALS

DHAHRAN, SAUDI ARABIA

In Partial Fulfillment of the
Requirements for the Degree of

MASTER OF SCIENCE

In

GEOPHYSICS

APRIL, 2016

KING FAHD UNIVERSITY OF PETROLEUM & MINERALS

DHAHRAN- 31261, SAUDI ARABIA

DEANSHIP OF GRADUATE STUDIES

This thesis, written by **Waleed Ejaz** under the direction of his thesis advisor and approved by his thesis committee, has been presented and accepted by the Dean of Graduate Studies, in partial fulfillment of the requirements for the degree of **MASTER OF SCIENCE IN GEOPHYSICS.**

Dr. Gabor Korvin
(Advisor)

Dr. Abdulaziz Al-Shaibani
Department Chairman

Dr. Ali Sahin
(Co-Advisor)

Dr. Salam A. Zummo
Dean of Graduate Studies

Dr. Abdulazeez Abdulraheem
(Member)

17/5/16
Date

Dr. Osman M. Abdullatif
(Member)

Dr. Michael A. Kaminski
(Member

Dedication

To my father Mr. Ejaz Akram Abid and my mother for their love, efforts and prayers.

To my uncle Mr. Naveed Ahmed Bhatti for his continuous encouragement and support.

ACKNOWLEDGMENTS

"In the name of Allah, The Most Gracious and The Most Merciful"

All praise belongs to Almighty Allah (SWT) for providing me this opportunity and giving me courage and perseverance to complete my masters successfully. I would like to thank the Higher Education Commission, Saudi Arabia and King Fahd University of Petroleum and Minerals for providing me academic platform and financial support during my studies.

My deepest gratitude and appreciation goes to my thesis advisors Prof. Gabor Korvin and Dr. Ali Sahin for their constant guidance, motivation and support during the course of my research. Their expertise, understanding, and patience, added considerably to my graduate experience. I also wish to express my deep gratitude and appreciation to Dr. Abdulazeez Abdulraheem, Dr. Osman M. Abdullatif and Prof. Michael A. Kaminski for their reviews, guidance, and efforts as my thesis committee members.

This study was conducted under the Project # 14-OIL468-04 supported by the KACST NSTIP Program. Samples were provided by the Ministry of Petroleum and Mineral Resources (Saudi Arabia). Supports of these organizations at every stage of study are fully acknowledged. My special thanks are due to Mr. Abdullah Al-Jof and Mr. Mohammad Saad Al-Ghamdi from the Ministry of Petroleum and Minerals (Dhahran) for their help and cooperation.

I would also like to thank several individuals for their support; Mr. Abdullah Alqubalee and Mr. Ayyaz Mustafa for their assistance throughout my thesis work, Mr. Mahmood M. Abdullah for his assistance with sample preparation, Mr. Mehboob Rasul, Mr. Syed Nizamuddin and Mr. Saheed Kolawole Adekunle for their cooperation in laboratory testing.

I would also like to express my deep gratitude to my uncle Mr. Naveed Ahmed Bhatti for his encouragement, support and motivation during my study at KFUPM. I am very thankful to my friends M. Hammad Malik, M. Asif Abbas, M. Haroon Tayyab, M. Saad Khan, and M. Abdur Rehman for their support and care through all these difficult years. Their good spirits always helped me to overcome setbacks and stay focused on my studies.

I would also like to acknowledge the support of Dr. Abdullatif A. Al-Shuhail and Dr. Abdulwahab A. Abokhodair with whom I took courses during my masters and learned a lot. I also owe thanks to all the faculty and students with whom I interacted during my stay at KFUPM.

TABLE OF CONTENTS

LIST OF TABLES

LIST OF FIGURES

ABSTRACT

Full Name : Waleed Ejaz

Thesis Title : Integration of Electrofacies and Geomechanical Characteristics of Sarah Formation (Potential Tight Gas Reservoir), Rub' Al-Khali Basin, Saudi Arabia

Major Field : Geophysics

Date of Degree : April, 2016

Tight gas resources provide a substantial amount of unconventional gas reserves, typically recognized by their low porosity and very low permeability that require effective stimulation (multistage hydraulic fracturing using horizontal wells) to produce economically. Reserves estimation and effective stimulation for economic production are challenging tasks in tight gas reservoirs. Successful accomplishment of these tasks require a better understanding of lithofacies associations, facies distribution, and their geomechanical properties. In other words, an effective integration of geology, geomechanics and petrophysics is needed to optimize development strategies and to reduce exploration risk.

This study involves the development of electrofacies from well logs using multivariate statistical methods and the development of 1-D Mechanical Earth Model (MEM) using well logs and core data to characterize a tight gas reservoir (Sarah Formation) and integration of results with electrofacies to understand the impact of geomechanical characteristics (brittleness/ fracability) on petrophysical properties.

The resulted electrofacies model is highly effective for identifying Sarah Formation major units and boundaries. The electrofacies model is also effective in identifying the overlying Silurian Qusaiba shales and the interbedded lithology of underlying Qasim Formation. This electrofacies model can be applied in other regions to recognize and assess the facies variation in Sarah Formation and in its equivalent formations (e.g. Zarqa Formation) in subsurface. The prepared 1-D MEM for Sarah Formation shows sharp changes in its mechanical properties and pore pressure which exhibit the presence of over-pressured and under-pressured zones within Sarah Formation. Changes in P-wave and S-wave velocities of Sarah Formation core samples show direct relation with porosity and density. The strength testing (Uniaxial Compression Test) of core samples shows high variability in strength properties and average values of Young's modulus and Poisson's ratio indicate high stiffness and brittle nature of Sarah Formation. The calculated in-situ stresses suggest that a reverse stress regime exists in the study area with a maximum stress gradient of 1.18 psi/ft. Further the integration of MEM with electrofacies helps to define mechanical properties through electrofacies as all major facies have characteristic response in terms of mechanical properties.

ملخص الرسالة

الاسم الكامل: وليد اعجاز

عنوان الرسالة: دمج الخصائص الجيوميكانيكية و الإلكترونيه لمتكون صارة (مكمن غازي واعد) في حوض الربع الخالي, المملكة العربية السعودية

التخصص: جيوفيزياء

تاريخ الدرجة العلمية: ابريل, 2016

توفر مصادر الغاز في الصخور المتراصة كميات كبيرة من احيتاطيات الغاز الغير تقليدية والتي تتميز بمسامية و نفاذية منخفضتين جداً عندها يتطلب التحفيز الفعال بواسطة التكسير الهيدروليكي متعدد المراحل في الآبار الأفقية حتى تنتج اقتصاديا. تقدير احتياط المكامن والتحفيز الفعال للإنتاج الاقتصادي يعتبر من المهام الصعبة في مكامن الغاز في الصخور المتراصة. إنجاح هذه المهام يتطلب فهم افضل لمجموعة الخواص الصخرية و توزيعها و خصائصها الجيوميكانيكية. بعبارة أخرى هناك حاجة ماسة لدمج الدراسات الجيولوجية مع الخواص الجيوميكانيكية و البتروفيزيائية لتحسين استراتيجيات التنمية والحد من مخاطر الاستكشاف. تتضمن هذه الدراسة تطوير الخصائص الإلكترونية للصخور من سجلات الآبار باستخدام أساليب احصائية ذات المتغيرات المتعددة وتطوير نموذج ميكانيكي ارضي أحادي الاتجاه من سجلات الآبار و المعلومات المتوفرة من الصخور لتوصيف الصخور المتراصة لمتكون صارة. و من ثم دمج النتائج مع الخصائص الإلكترونية للصخور لمحاولة فهم تأثير الخواص الجيوميكانيكية على الخواص البتروفيزيائية. يعتبر نموذج الخصائص الالكترونية للصخور أداة فعالة لتحديد حدود متكون صارة وكذلك لتحديد الوحدات الصخرية لهذا المتكون. يظهر في النموذج الميكانيكي الأرضي الذي تم أعداده تغيرات حادة في الخواص الميكانيكية للصخور و ضغط المسامات والتي تظهر وجود مناطق عالية الضغط وتحت الضغط في متكون صارة. بالإضافة إلى ذلك من خلال دمج النموذج الميكانيكي الارضي مع الخصائص الالكترونية للصخور يمكن تحديد الخصائص الميكانيكية للصخور من خلال الخصائص الالكترونية.

CHAPTER 1

INTRODUCTION

In an unconventional tight gas reservoir, it is important to precisely address geological characteristics including lithologies, diagenesis and depositional environments, besides fracture potential, reservoir development, resource density, and overall resource estimation (Naik, 2003). To address these requirements, a more detailed analysis of available data is needed. Most common data include core and well log data. To reduce the uncertainty in results, an effective integration of information from all types of datasets is needed.

Tight reservoirs commonly have no natural fractures, so they cannot produce economically without hydraulic fracturing. For hydraulic fracturing treatment, understanding of mechanical properties of all the layers above, within, and below the gas pay intervals is important. Basic mechanical rock properties such as Young's modulus, Poisson's ratio and in-situ stresses are required to design a hydraulic fracture treatment. These properties can be determined either through core testing or well logs and an integration of both gives more reliable results. Development of electrofacies will enable us to quantify these properties solely using well log data especially when the core data are limited.

The mechanical properties of rocks are in turn used to develop a Mechanical Earth Model (MEM) which provides the basis for classification of reservoir zones into brittle and ductile zones. Subsequently, an integration of this geomechanical earth model with electrofacies

developed using well log data can help in effective optimization of hydraulic fracturing design.

1.1 What is Tight Gas?

The term "tight gas" refers to the natural gas associated with very low permeability reservoirs. The German Society for Petroleum and Coal Science and Technology (DGMK) defined a tight gas reservoir as the one whose average effective gas permeability is less than 0.6 mD (Ghosh and Prelas, 2009).

Tight gas definition has evolved with time. Curtis (2002) defined tight gas reservoirs as having permeabilities less than 0.1 millidarcies. Holditch (2006) defined a tight gas reservoir as one that cannot produce economic volumes of gas unless the wells are stimulated by hydraulic fracturing treatment and by the use of horizontal wellbores.

Recently, Saudi Aramco used the following definition to refer tight gas reservoirs;

*"*Reservoirs that do not flow at commercial rates using Saudi Aramco's Standard drilling and completion procedures. The sands typically have <12% porosity and <1mD permeability, and require fracture stimulation (Hayton et. al., 2010)*".*

1.2 Tight Gas Exploration in Saudi Arabia

The main focus of tight gas exploration efforts in Saudi Arabia is the lower Paleozoic siliciclastic succession, which consists of mainly sandstones, with thicknesses of several thousand feet (Figure 1). Silurian Qusaiba Shale lies is in the middle of this succession. This succession, whose depth varies from outcrops to 20,000+ ft. deep zones in subsurface

across Saudi Arabia, has different reservoir qualities from conventional to distinctly tight (Hayton et. al., 2010).

Currently documented tight gas resources are located in Northwest Saudi Arabia and South Ghawar/ Rub' Al-Khali Basin (Figure 2). First attempt to explore these resources was made in 2006 by LUKOIL Saudi Arabia in Rub' Al-Khali. In this first attempt, nine wildcat wells were drilled and have come up with prospective tight gas discoveries at depths between 12,000 to 20,000 feet in High Temperature and High Pressure (HTHP) horizons with reservoir permeability of micro-Darcy levels (Bu-Khamseen et. al., 2010). Later the exploration activities were continued by Sino Saudi Gas (SSG) Limited and SRAC.

The prospective Northwestern field have a four-way closure that extends to a substantial area. In 1991, first well with gas from Sarah Formation was discovered in this area having low wellhead pressure and low flow rate. This well was reported an average porosity of 2% and extremely low permeability over a gross thickness of 100 ft. (Al-Zayer et. al., 20013). The first nearest production from Sarah Formation was reported from Risha gas field, Eartern Jordon in 1987 (Al-Zayer et. al., 20013).

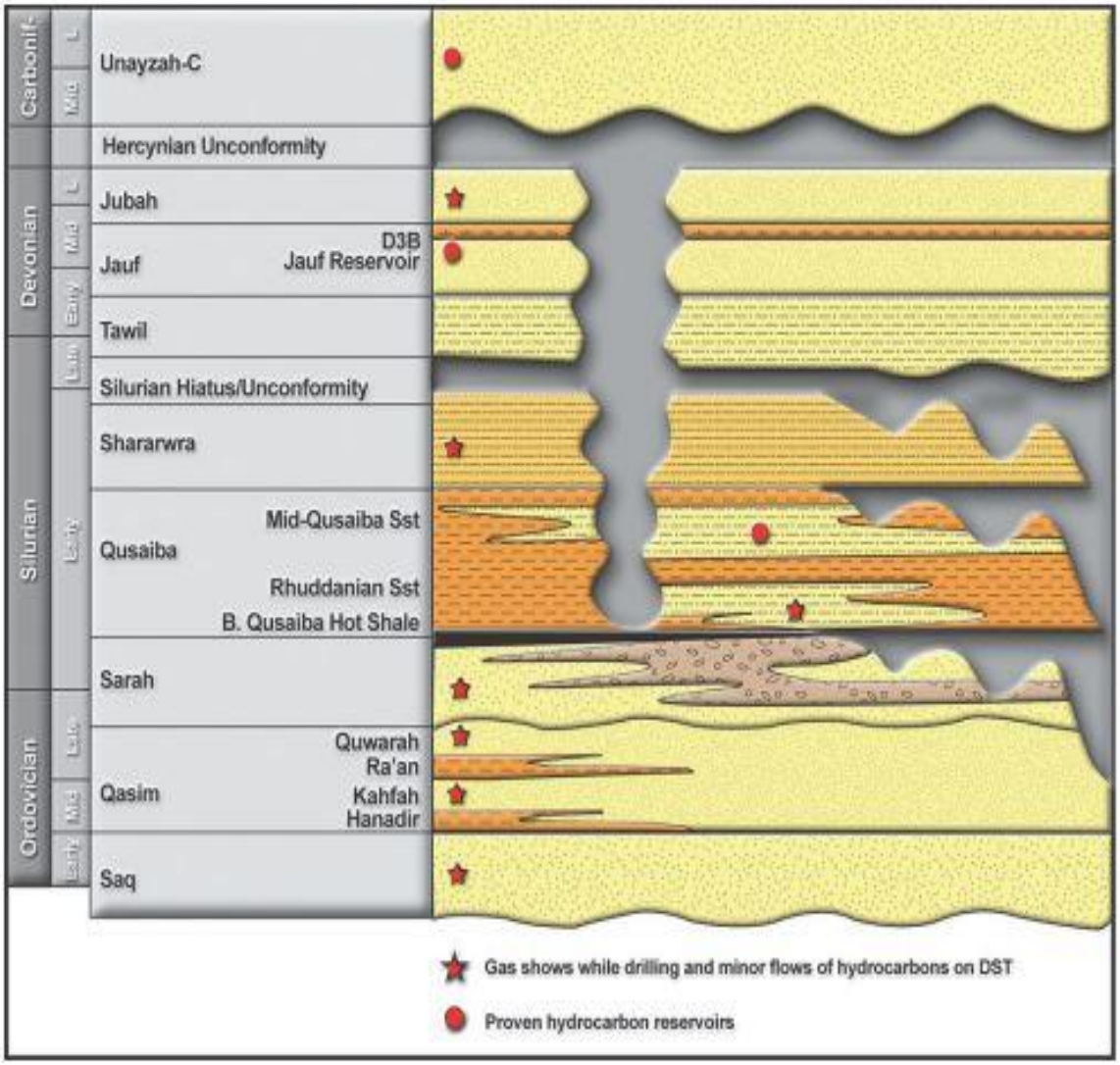

Figure 1.1 Idealized diagram of Lower Paleozoic succession of Saudi Arabia showing potential zones for gas (Hayton et. al., 2010)

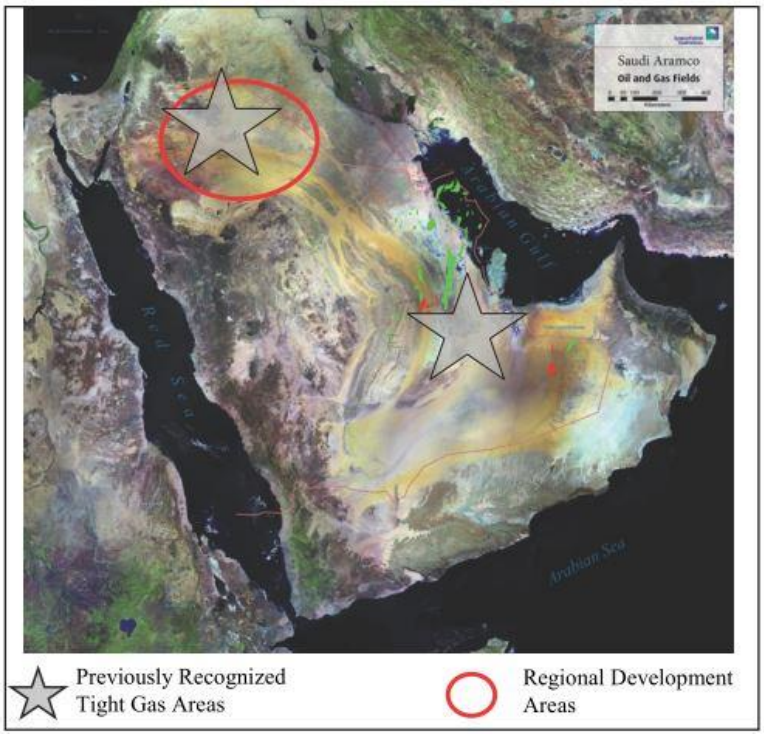

Figure 1.2 Tight gas resources of Saudi Arabia (Hayton et. al., 2010)

Exploration activity at South Ghawar and Rub' Al-Khali Basin confirmed the presence of significant tight gas resources in Late Ordovician Sarah and Middle Ordovician Qasim formations. According to Hayton et. al., (2010), the deep wells that penetrated Sarah and Qasim formations in Southern Saudi Arabia have the following key characteristics:

1. Excellent mud gas shows.
2. Gas columns are considerably greater than structural closures as indicated by mud gas shows and log data.
3. Minor gas flows in testing.
4. Conventional fracture stimulation is not effective in economic production of such reservoirs.

These results recognize Sarah and Qasim in Southern Saudi Arabia and Rub' Al-Khali as ~~a~~ problematic plays with poor reservoir quality, which when combined with the high temperature and high pressure of these deep reservoirs, makes exploration activity more challenging.

In northwestern Saudi Arabia, the tight gas play is relatively shallow as compared to southern Saudi Arabia which allows the use of conventional development technologies (Hayton et. al., 2010). Current conventional exploration wells in northwestern Saudi Arabia have provided additional data to help quantifying the tight gas potential of this region.

1.3 Study Area

The study area is located on the north eastern part of the Rub' Al-Khali Basin, Saudi Arabia as shown in the Figure 1.3.

Figure 1.3 Location of study area and distribution of wells

1.4 Geological setting of the study area

The Arabian Plate is surrounded by active tectonic activities. In the west and south west of the Arabian Plate, active sea floor spreading is present in Red Sea and Gulf of Aden which represents extensional regime. In the north and northwest, the Bitlis suture and the Zagros suture represent the compressional regime. Makran zone in the Gulf of Oman represents active subduction in the northeast of Arabian Plate and Dead Sea is the representative of transform movement (Figure 1.4) (Konert et al., 2001 and Johnson and Stern, 2010). Arabian Shield is occupying the western margin of Arabian Plate. The evolution of Arabian Shield has episodes of collision and extension which ended in the form of a stable craton with platform setting. The uplifting of Arabian Shield by Red Sea and Gulf of Aden rift systems influenced the sedimentation of Arabian Plate throughout its geological history (Powers et al., 1966).

Sarah Formation is deposited in confined paleo-valleys having variable thickness with maximum reported thickness of 350 m in outcrop. Sarah Formation is genetically related to Zarqa Formation and it cuts into Zarqa and Qasim Formation at places. Sarah Formation is a fining upward sandstone sequence having fluvial and glaciofluvial origin. The glacial deposits of Sarah or Zarqa Formations are separated by underlying Qasim or Saq Formations of pre-glacial origin by well define sub-Zarqa or sub-Sarah unconformities (Laboun, 2009).

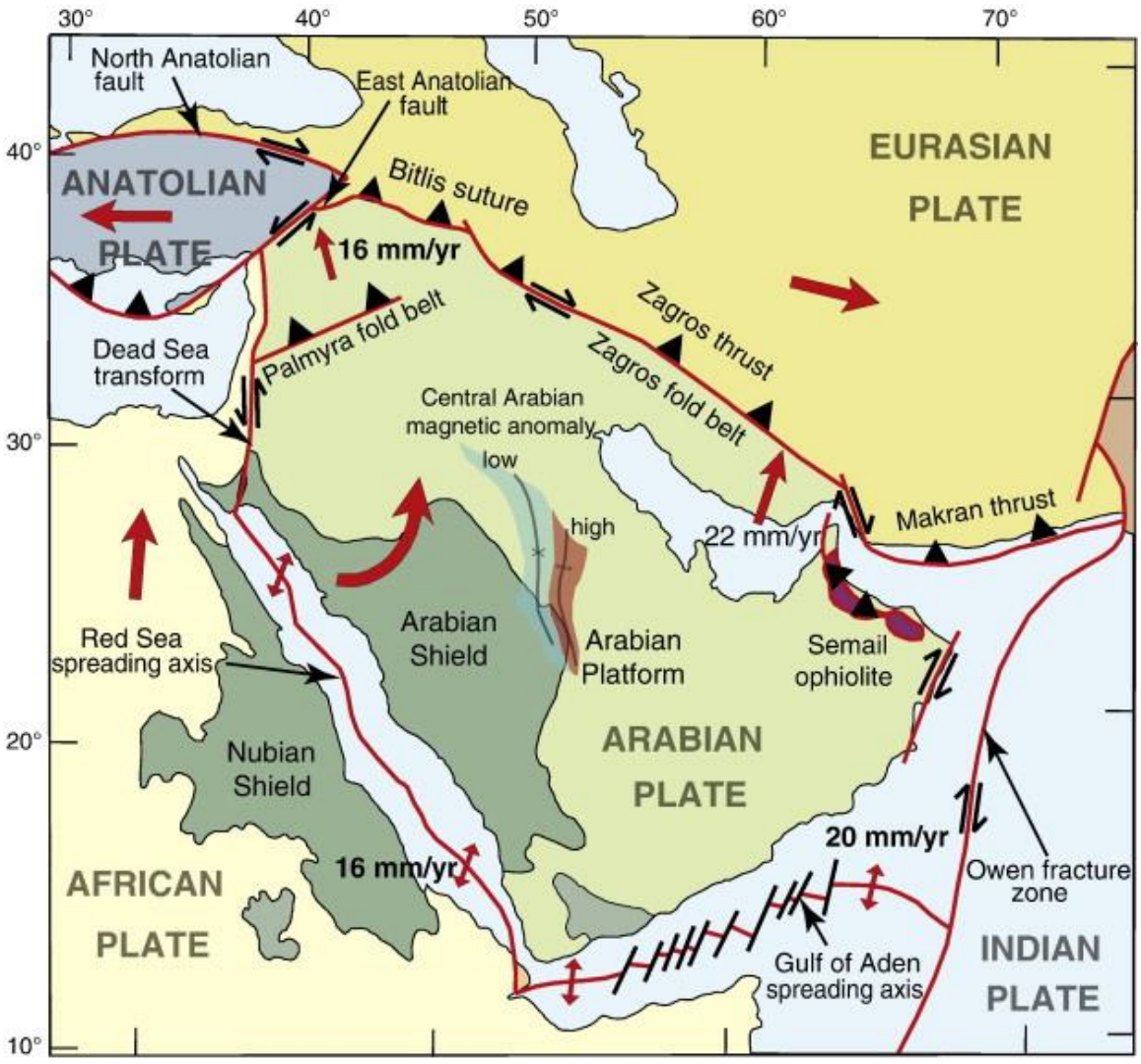

Figure 1.4 Tectonic elements of Arabian Plate boundaries (Johnson and Stern, 2010)

1.5 Database

This study is based on core and well log data from six wells. Cores represent Sarah Formation and have a total thickness of 148.4 ft. The basic information about wells are listed in Table 1.1. In Well-A, the cores are from the middle part of Sarah Formation which constitutes fine to coarse grain tight sandstone. The cores in Well-B, Well-C, Well-D and Well-E have been taken from the upper parts of the formation. On the other hand, the core from Well-F represents the transition zone between Sarah and Qusaiba.

Table 1.1 Core details of all wells

Well	Formation	Core Thickness (ft.)
A	Middle Sarah	29.2
B	Upper Sarah	29.1
C	Upper Sarah	37.9
D	Upper Sarah	13.8
E	Upper Sarah	29.8
F	Transition Zone	8.6
Total		**148.4**

1.6 Problem Statement

Tight gas sands (also known as low permeability gas sands) are the largest financial prospect in unconventional gas business. According to industry reports, it constitutes almost 70 percent of U.S unconventional gas production (Khlaifat et al., 2010).

Previously high costs and risk associated with tight sands projects were the major barriers to development. Now such barriers are somehow overcome by improved and cost effective

technologies in completion methods, but still reservoir modeling and production optimizing are challenging tasks to ensure economic production in such environments.

More time and effort should be spent to characterize reservoir properties in the early phase of a tight gas project to minimize the financial risk involved. Specially, to understand how rocks would respond to different fracking designs is important because an effective stimulation that makes gas flow to wellbore is key to economic tight gas production. Therefore, determination of petrophysical and geomechanical properties of a reservoir rock in any tight gas project is very critical.

There are six stages involved in the modeling and fracturing of a tight gas well.

1. Characterizing the reservoir rock
2. Petrophysics and rock-log calibration
3. 3D fracture design
4. Fracture production forecasting
5. Real-time monitoring
6. Post-frac evaluation

This study has focused on the first two phases of six stages listed above. The first one involves the determination of the formation's geomechanical properties that steer fracture stimulated reservoirs. It also involves rock typing through the use of well log data which provide electrofacies and integration of those electrofacies with geomechanical properties. The second phase involves the laboratory measurements of geomechanical properties that can be calibrated with logs to give actual geomechanical properties over the entire logged zone of interest.

1.7 Objectives

The aim of this study had been to investigate the geomechanical and petrophysical properties of the Sarah Formation as a tight gas reservoir. Specific objectives are stated as follows:

1. Determining electrofacies for Sarah Formation.
2. Building 1-D Mechanical Earth Model (MEM).
3. Integration of the MEM with electrofacies.

CHAPTER 2

LITERATURE REVIEW

The Literature review for this study is divided in three parts. First part focuses on regional studies of Sarah Formation and its tight gas potential. Second part includes different methods of developing electrofacies using multivariate statistical methods. Finally, the third part encompasses geomechanical characterization of tight gas reservoirs.

2.1 Sarah Formation

The Sarah Formation includes glacial and periglacial sediments filling paleovalleys. It was deposited during the Late Ordovician. Various structural features and paleotopography caused by glacial erosion during the era proves glaciation. Deposition of irregular and scattered pods of sediments throughout Saudi Arabia is due to the fluctuations in sea level (Al-Husseini et al. 1991). It has been recorded that the Arabian Plate was subjected to glaciation in two different time periods (Figure 2.1).

Sarah Formation consists of medium- to course-grained sandstones that are locally conglomeratic with rounded quartz pebbles. Glacial striations formed during Late Ordovician glacier advance were recognized in different areas. Sarah Formation is 26 meters thick at the type locality (Sarah Ridge, Jabal Habashi Quadrangle) and 85 meters thick at reference section on the eastern bank of Wadi U'aywij near Jal Az Zarqa. The thickness of Sarah Formation varies in different areas due to pre-existing paleotopography that had a considerable relief at places. The thickness also depends upon the relative

position within the paleovalley. At the axis, it is estimated to be 150 to 200 meters thick (Vaslet et. al., 1987a).

Clark-Lowes, (2005) reported the evidence for large scale palaeovalleys in Sarah Formation in northwestern Saudi Arabia and around Sarah Ridge in Al-Qasim area. He stated that Sarah Formation, which represents Ashgillian glacial deposits, is an important reservoir target in the North Africa and Arabia. Sarah Formation is a part of Late Ordovician deposits of a 600km long sedimentary system whose discontinuous outcrops extends from northwestern Saudi Arabia to northernmost North Africa (Michael 2015).

Clark-Lowes (2005) defined three facies associations in Sarah Formation as follows;

- Facies Association 1: Medium- and coarse-grained sandstones and diamictites
- Facies Association 2: Medium- and fine-grained sandstones
- Facies Association 3: Climbing-rippled fine-grained sandstones, siltstones and minor shales

The most abundant Facies Association 1 is overlain by Facies Association 2 in outcrop. Facies Association 3 is interbedded with Facies Association 1 at lateral positions in paleovalleys. Based on those facies associations, Clark-Lowes (2005) interpreted Sarah Formation as alluvial and fluvial glacial deposits.

Sarah formation is considered as an unconventional tight gas reservoir in the subsurface (Al-Mahmoud and Al-Ghamdi, 2010). Although the Hawban and Baqa members of Sarah Formation have good reservoir quality, their patchy geographical distribution may be considered as a major challenge.

The Sarah Formation has been considered as fluvial and marine sediments deposited in glacial paleovalleys by Al-Sharhan and Nairn (1997). The complex facies distribution, environment and paleogeography makes the prediction of reservoir quality difficult (Al-Mahmoud and Al-Ghamdi, 2010; Briner et al., 2010).

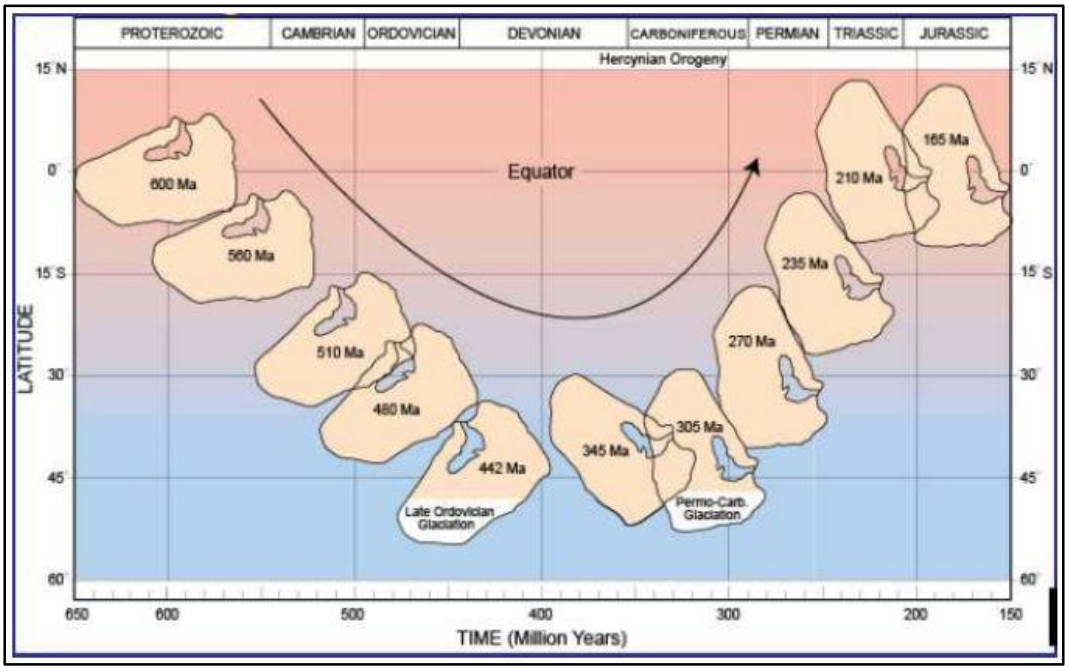

Figure 2.1 Change in Arabian Plate position during Paleozoic and early Mesozoic era (Konert et al., 2001)

Waseem (2013) studied the sedimentological and petrophysical heterogeneity of Sarah Formation in Al-Ilb paleochannel and interpreted the environment of Sarah Formation as glacial outwash braided river deposits with very good reservoir quality porosity and high permeability ranging between 53mD to 5D.

Islam (2014) studied several glacio-fluvial channels of the Sarah Formation within five paleovalleys in outcrops of central Arabia. He reported variation of porosity and permeability within investigated paleovalleys and concluded that porosity and permeability patterns in Sarah Formation are influenced by both depositional and diagenetic controls.

His lithofacies and reservoir heterogeneity analysis showed that those sediments are deposited in periods of ice advance and retreat and the Sarah Formation can be considered as heterogeneous to very heterogeneous reservoir.

Jarrah (2015) studied the relationship between lithofacies and geomechanical properties of Sarah Formation in outcrop in Al-Qaseem area, central Saudi Arabia. He found that his five defined lithological units have direct relation with five geomechanical units with strength ranging between low to extremely. He further found three types of fracture modes (opening mode, sliding mode and shear mode) which all reveals different stress regimes.

2.2 Electrofacies

For unconventional reservoirs, an integration of well log data with other data is important to reduce uncertainty in quantitative well log analysis (Euzen, 2014). The application of electrofacies characterization in reservoir evaluation and management has been widely recognized (Serra and Abbott, 1982 and Bucheb and Evans, 1994)

Electrofacies consists of distinct log responses that can offer valuable information about the mineralogy, fluid content, and hydraulic properties of a reservoir. These electrofacies can be often correlated with lithofacies from cores to give more accurate information about depositional and diagenetic characteristics of a reservoir through well log data (Lee et al. 2001).

Euzen et al. (2012) used well log cluster analysis and build electofacies to integrate conventional well log data with quantitative mineralogy data from cores and cuttings.

Gupta (2010) used high resolution electrofacies analysis through multivariate statistical technique to interpret heterolithic facies of thinly interbedded sandstones and mudstones from conventional well log data using core facies as a "training set". His electrofacies analysis is based on linear discriminant function analysis which involves two steps to classify facies: (1). Development of electrofacies database through core-defined facies. (2). Assigning electrofacies to unknown depth levels using electrofacies database and a linear discriminant function.

Ranger (2014) used discriminant analysis alone for developing electrofacies to get better interpretation of mixed and interbedded lithologies using well log data especially in areas of poor core control. Discriminant analysis is a multivariate statistical method utilizing a

control or training set of data from standardized wireline log readings and overlapping core recovery.

A linear discriminant function is calculated using this control set of data which is further used to identify from which facies (i.e. population) non-cored intervals are likely to originate (Gupta and Johnson, 2002). Applying this discriminant function to wireline parameters from cored wells and comparing the predicted facies with actual core can give an estimate of accuracy.

Euzen (2010) identified potential tight gas intervals by electrofacies classification using cluster analysis. Cluster analysis works by defining high density areas (clusters) of well log data in multivariate space that define electrofacies associated with a characteristic lithology and fluid content on the basis of similar log responses.

Lee et al. (2002) used a combination of principal components analysis (PCA), model-based cluster analysis (MCA), and discriminant analysis to identify electrofacies and then applied nonparametric regression techniques to predict permeability using well log data.

2.2.1 Electrofacies studies on Saudi Arabian reservoirs

Based on the work of pioneers of electrofacies (Serra and Abbott, 1982), AI-Sabti and AI-Bassam (1993) developed a 3D electrofacies model for Safaniya reservoir in Safaniya field (Saudi Arabia) using well logs from 573 wells. The Safaniya reservoir lies within Wasia Formation of Middle Cretaceous age. It comprises of thick, massive sands in the southern part of the field while the northern part has a complex geology with all types of sub-deltaic environments. The northern part contains mouth bars, distributary channels, crevasse splays, interdistributary bay shales, prodelta shales, and shallow marine shales and sands.

This model (AI-Sabti and AI-Bassam, 1993) which is based on a geological description of Safaniya reservoir in terms of 11-layers, was used by Saudi Aramco to understand the heterogeneity of Safaniya reservoir. It covered an area of 3900 sq. km., helped to understand the heterogeneity of such a large reservoir and to make reservoir management decisions. The maps and cross sections developed using this 3D electrofacies model provide 3D geological inputs for reservoir simulation modeling.

Clerke (2005) developed electrofacies for the Kuff-C gas reservoir using well log and mineralogical data and found a good agreement with geological facies developed by Tawil and Eid (Unpublished, Saudi Aramco Report) as well as grain type and grain size data.

Forsyth et al. (2011) developed electrofacies to improve the log derivation of permeability in tight gas intervals of Unayzah Formation. Five electrofacies were defined which helped to identify different tight gas intervals separately as well as improve the core data clustering. As shown in Figure 2.2, green and pink colored electrofacies have different permeability grouping representing different properties of rocks. The tight gas interval (pink colored electrofacies) is defined as a separate electrofacies category different from the tight gas interval (green colored electrofacies) which is above the main reservoir interval (Forsyth et al., 2011).

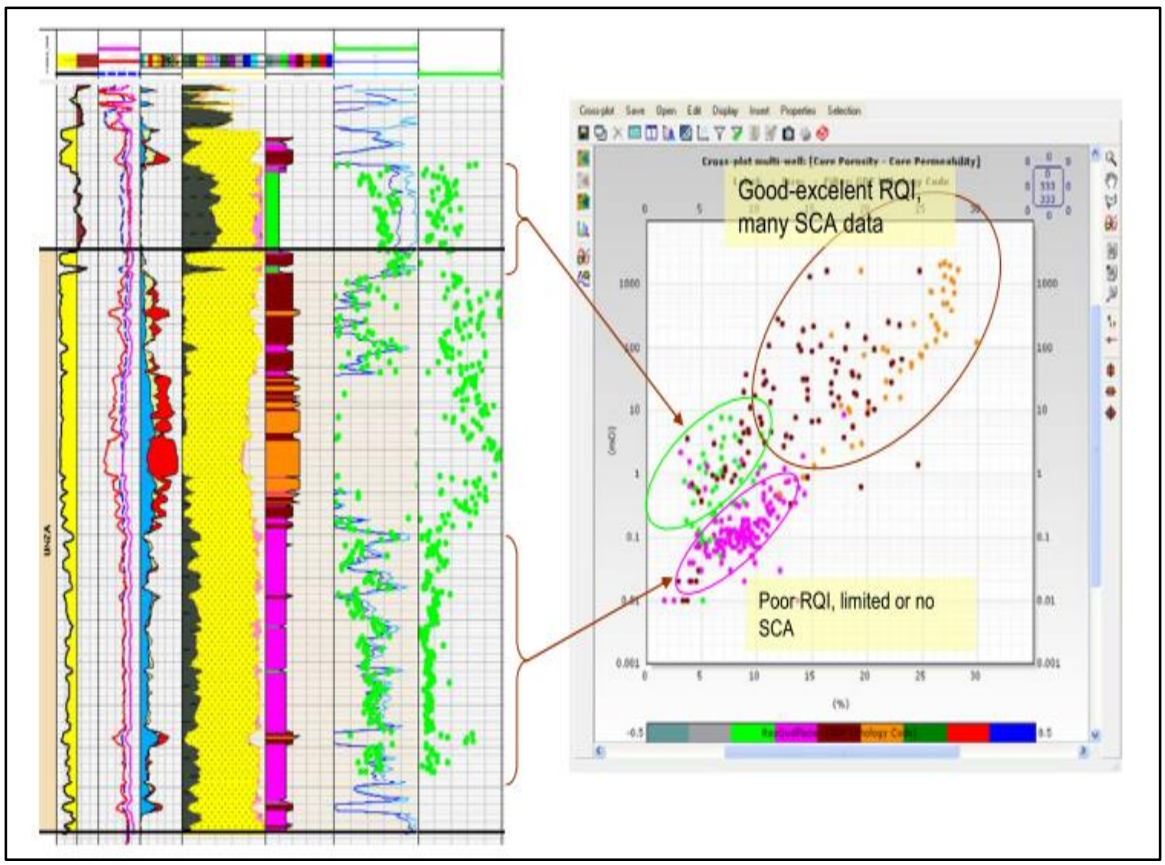

Figure 2.2 Comparing two (green and pink) electrofacies via core data clustering where the two electrofacies have different permeability (Forsyth et al., 2011)

2.3 Geomechanics

Geomechanics is used to predict and to manage rock deformation via understanding stress changes within the Earth. Unpredicted and unmanaged rock deformations can cause billions of dollar losses. In a reservoir with no information about the stress changes, problems like wellbore instability and tools lost in a borehole can occur. These problems result in loss of time and money along with delayed production (Ali et al., 2003).

Geomechanics plays a vital role in unlocking tight gas reserves by monitoring stress evaluation during different stages of reservoir development Addis and Yassir (2010) discussed the geomechanical engineering aspects of tight gas sands. They stated that in-situ stress magnitudes and orientations change as the reservoir pressure changes during drawdown and depletion. These stress changes have a direct impact on the placement of new wells and sweet spots enlargement.

Identification of sweet spots is an important task in the development of tight gas reservoirs. Depositional geology, diagenetic evolution, hydrodynamic properties as well as the structural geologic evolution of basins provide information about the sweet spots in tight gas reservoirs (Rushing et al., 2008).

Mechanical properties of rocks provide useful information for the evaluation of low permeability reservoirs. In this respect, Poisson's ratio and Young's modulus are the most important mechanical parameters (Solano et al. 2012).

The first step in a geomechanical study is to build a Mechanical Earth Model (MEM) which numerically represents Earth stresses as well as the mechanical properties of rocks in a specific stratigraphic section or a specific rock formation (Plumb et al. 2000). A MEM

relates dynamic elastic properties with laboratory measured static equivalents. This model contains profiles of elastic parameters, rock strength, pore pressure, Earth stresses and their directions. It addresses all drilling problems like wellbore instability, loss circulation and kick/flow which are related to the stress regime of the area and proposes solutions for further drilling (Afsari et al., 2009).

Adisornsuapwat (2012) built a 1-D MEM to improve hydraulic fracture design in a tight gas sandstone reservoir. Mechanical properties were derived using log data calibrated with laboratory test results from corresponding core. This model captures all information regarding the geomechanics of drilling and production (including rock mechanical parameters), rock failure mechanisms, in-situ stresses, geologic structure, stratigraphy and well geometry (Adisornsuapwat, 2012).

To calculate brittleness, several mechanical properties can be utilized such as Young's modulus, Poisson's ratio, cohesion, coefficient of friction, shear modulus, compressive and tensile strengths and their variation in different directions to account for anisotropy (Josh et al., 2012). Log based and laboratory approaches can be applied to determine the total organic matter, permeability, porosity, and mechanical parameters (Jacobi et al. 2008 and Parker et al. 2009). For optimizing the hydraulic fracture treatment, geomechanics, mineralogy, and petrophysics have to be integrated (Rickman et al., 2008).

CHAPTER 3

METHODOLOGY

3.1 Introduction

The methodology adopted in this study has been outlined in two parts. First part involves with the development of electrofacies using well log data and second part involves constructing the 1-D mechanical earth model and determining other geomechanical parameters. Later, the geomechanical parameters and mechanical earth model were integrated with electrofacies that enables the probable identification of these parameters through electrofacies. The integrated model, as a fundamental source of information, can resolve many problems related to drilling, fracturing and production from the tight gas reservoir.

In this thesis research, various techniques have been implemented in order to investigate and integrate the lithofacies, electrofacies and mechanical (elastic and failure) parameters of Sarah Formation. One hundred and forty-eight feet (148 ft.) of continuous subsurface cores from five wells representing Sarah Formation from Rub Al-Khali Basin, were used for the study. The available data also include well logs for the specific interval from five wells in the study area.

Electrofacies were developed using Interactive Petrophysics™ software based on the well log data. Different well log response combinations were used to develop electrofacies.

Subsequently, electrofacies that are most consistent with lithology and other petrophysical properties were selected for further analysis.

The geomechanical part includes laboratory measurements of mechanical properties of cores, estimation of geomechanical parameters using well log data and then core-log calibration to predict the mechanical behavior. First, the cores from all five wells were analyzed and described in terms of lithofacies based on grain size, texture and structures present. The plug locations for all cores are given in Appendix-A. Plugs were taken from all major lithofacies and used for laboratory analysis. Mechanical properties were determined using laboratory techniques for acoustic velocity measurements and uniaxial compression tests. Laboratory measured static results were then calibrated with log measured dynamic results to get continuous profiles of all geomechanical parameters along the well paths.

Geomechanical properties such as uniaxial compressive strength, Young's modulus, Poisson's ratio, cohesion, friction, ultrasonic velocities were measured. Ultrasonic velocity (primary and secondary waves) measurements were carried out to attain the stiffness in terms of dynamic Young's modulus and Poisson's ratio using Autolab 500 equipment. Ultrasonic velocity measurements were performed at different confining pressures in order to simulate reservoir conditions.

The compression test equipment was used to determine the uniaxial compressive strength (UCS). The static Young's modulus and Poisson's ratio were determined from the stress-strain results obtained from the UCS test. The tests were performed on all vertical and

horizontal samples in order to use their results to calibrate the dynamic Young's modulus and Poisson's ratio.

The methodology adopted is summarized in the following steps:

1. Taking plugs from cores considering all defined lithofacies
2. Laboratory measurement of geomechanical properties
3. Estimation of geomechanical properties using well log data
4. Calibration of static and dynamic geomechanical properties
5. Developing the 1-D mechanical earth model
6. Development of electrofacies using well log data
7. Integration of 1-D mechanical earth model and electrofacies

3.2 Acoustic Wave Velocity Measurements (ASTM D 2845)

The acoustic measurements on rock samples is performed in order to determine the compressional (primary or P-type) and shear (secondary or S-type) waves velocities which in turns yield dynamic elastic moduli i.e. Poisson's ratio and Young's modulus. In this study, acoustic measurements were conducted on 17 sandstone samples using acoustic measurement equipment AUTOLAB 500 (Figure 3.1). The tests were performed under different confining pressures to have compressional and shear wave velocities at simulated reservoir conditions.

The ultrasonic velocity measurement system yields velocities of compressional and shear wave (P and S waves) and their variation with changes in confining pressures. The main elements of the equipment are: (1) the ultrasonic transducer assembly, (2) the pressure

vessel and pressure intensifiers mounted in a safety enclosure, and (3) a data acquisition system.

A typical ultrasonic transducer assembly is shown in Figure 3.2. This unit is a matched set of transmitting and receiving transducers capable of propagating a compressional wave (P) and two polarized shear waves (S1 and S2) through a rock specimen. The vibration directions for two shear waves are oriented at 90^0 to each other. The transducers operate at confining pressure up to 100 MPa.

The confining pressure is developed with a manually operated pressure intensifier rated to 100 MPa. The intensifier is controlled with a manually operated hydraulic pump. To fully simulate the reservoir conditions, the pressure vessel may be externally heated to temperatures up to 115 ^{0}C. At each set of simulated reservoir conditions, time series are collected and stored for one compressional and two orthogonally polarized shear waves. At the conclusion of an experiment, the first arrivals of the compressional and shear waves are picked. The velocities are computed from these picked travel time values. The experimental data is then plotted. Data plots include wave forms collected at each pressure for each wave type, as well as a tabular output of all the information on the rock specimen including sample size, porosity, density, as well as P and S wave velocities under different environmental conditions.

Figure 3.1 Ultrasonic wave velocity measurement system

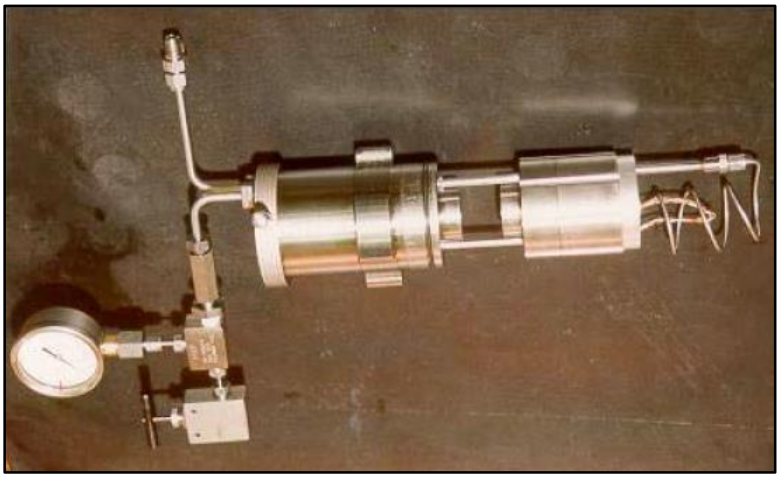

Figure 3.2 Ultrasonic transducer assembly

3.2.1 Sample Preparation

The following basic steps have been taken during the sample preparation:

1. Measure the dimensions (length and diameter) of plug sample. Record at least 5 readings of length and diameter at five different locations and take the average of them. Also note down the weight of sample (in grams).
2. Make sure the plug length is between 2 to 2.5 inches and diameter is 1.5 inches in order to accommodate in the sample holder.
3. Apply couplant at the end faces of the plugs in order to fill surface irregularities.
4. Place the plug in the rubber sleeve and put it between the two steel platens of the sample holder.
5. Tighten the two ends of plug on to the sample holder with clamps. Make sure the clamps are tightened on the steel platens and not on the plugs.

3.2.2 Experiment Procedure

The experimental procedure is summarized in the following steps:

1. Remove approximately 150 ml of oil from the test chamber and fill it back into the reservoir through the funnel.
2. Make sure all the valves on the front panel are off.
3. Make Confining Intensifier (CI) knobs to down position and open Fill/Drain valve. Keep pumping till it gets harder (approximately for 10 minutes). Immediately make CI knobs to off position and close Fill/Drain valve.
4. Open Relief valve and slowly press the plug inside. Lock the plug by rotating clockwise.
5. Connect the transmitter and receiver cables on the sample holder.

6. Close the Relief valve. Make CI knobs up. Open Vessel On/Off valve. Start pumping in order to reach the required confining pressure (CP).
7. Use the AutoLab software to record the acoustic measurements.
8. After collecting the measurements, remove the cables attached to sample holder.
9. Close the vessel using On/Off valve and slightly open the Relief valve and Fill/Drain valve with purpose to release pressure. Make the two CI knobs at down position. Keep opening the Relief and Fill/Drain valves further slowly.
10. Make the CI knobs to Off position. Turn the sample holder anticlockwise such that it should get relieved from the groove (Unlock).
11. Close back Relief and Fill/Drain valves. Open Vessel On/Off valve. Bring CI knobs to Up position. Slightly open Fill/Drain valve.
12. Keep pumping (approx. 5 min.) so that confining pressure is applied and sample holder should come out slowly.
13. After the sample holder comes out, gently pull it off and wait for 20 minutes for the oil to be dripped completely.

3.2.3 Data Acquisition

1. Open the AutoLab software. Click the "Acquire Data" tab. This will open a new window wherein the sample information (density, length and diameter) has to be entered. Other information related to the plug such as plug number, formation name should be entered in order to identify the plug being tested. After entering sample information click "Done". This will automatically open a window that displays the confining pressure being applied and the temperature electronically.

2. As mentioned earlier, after reaching a CP of 7 MPa, click “Capture” in order to transmit the acoustic waves. Then click “Accept” to record the data. Repeat this for 14, 21, 28, and 35 MPa, respectively.

3. Once readings are recorded, click “Stop Data Acquisition” tab. Then click the “Process Data” tab in order to select the arrival times of P and S waves at different CP applied.

3.3 Unconfined Compressive Test (ASTM D 2938)

The uniaxial or unconfined compressive strength (UCS) test is the most common laboratory test undertaken in rock mechanics studies. The UCS test is the basic test in numerous design methods. Applications of this test comprise the following: (i) estimation of the onset of compression or shear failure, (ii) estimating rock modulus for calculation of displacements and settlements, (iii) estimating the Poisson’s ratio.

The UCS test procedure is conducted as follows:

1. The plug is mounted in a cell between the top and bottom steel platens. It is then fitted with one axial and one circumferential strain gauge.
2. The cell is connected to the displacement signal conditioning box via a cable breakout box. At this point, the strain gauges are preset within their working range.
3. The cell is then positioned on the hydraulic frame ram piston.
4. The computer program is used to run the hydraulic ram, raise the piston, and establish sample-load cell contact.

5. Axial load is then applied automatically at a predetermined fixed strain rate using the system's triaxial program. Axial load, axial stress, average axial strain, and radial strain are automatically recorded and saved in a file.

CHAPTER 4

GEOMECHANICAL CHARACTERIZATION

In this study, geomechanical analysis was conducted for Sarah Formation to evaluate its potential as a tight gas reservoir. Geomechanical analysis included the determination of rock mechanical parameters experimentally as well as using well-log data and building a 1-D Mechanical Earth Model (MEM) based on those parameters as discussed in the following sections.

4.1 Importance of geomechanics in tight gas reservoir

The critical factors involved in establishing a successful tight gas play are proper reservoir evaluation and development planning. Geomechanical analysis is important both for the evaluation of reservoir quality and development as it helps to increase the understanding of reservoir facies in terms of weak zones (sweet spots), stress magnitudes and stress anisotropy (Stotts et al., 2007).

The important mechanical parameters which define the deformational behavior of rocks are Poisson's ratio and Young's modulus. Young's modulus is a measure of stiffness that determines rock's ability of fracture containment while Poisson's ratio, (the ratio of transverse to axial strain) explains the behavior of rock under stress. Rocks with high Young's modulus and low Poisson's ratio tend to be more brittle and are favorable for hydraulic fracturing. On the contrary, low Young's modulus and high Poisson's ratio are

representative of ductile behavior which acts as a barrier for fracture propagation (Rickman et al., 2008).

A Mechanical Earth Model (MEM) is built to account for the stresses and their behavior during drilling, completion and hydraulic fracturing. The MEM helps to reduce drilling costs and to improve long term production performance in a tight gas reservoir. Quantifying and understanding the stresses present in the subsurface are important to mitigate the hazards associated with them. Other aspects of reservoir evaluation and development are also affected by Earth's stresses. Fracture propagation and initiation are influenced by stress magnitudes and orientation. Strong compressional stresses may cause borehole breakout in weak formations (Ali et al., 2003).

The integration of geomechanics with mineralogy and reservoir facies helps to optimize the hydraulic fracturing treatment. It has been reported that the cost of hydraulic fracturing can be significantly reduced by identifying and characterizing reservoir facies in terms of their mineralogy, organic matter content and geomechanical properties (Jacobi et al., 2008).

4.2 Dynamic and Static Elastic Moduli

The determination of rock mechanical properties such as dynamic and static moduli, shear strength is essential in many reservoir monitoring and production tasks such as hydraulic fracturing, estimation of reserves and wellbore stability. The elastic moduli can be dynamic or static based on the method used to measure them. Dynamic moduli are obtained through ultrasonic compressional and shear wave velocity measurements at in-situ or in laboratory

conditions under different confining pressures. On the other hand, the static moduli are obtained through stress-strain measurements in laboratory.

The dynamic moduli often differ from the static ones as they come from a different source of information. At low confining pressure, dynamic moduli are generally higher than static moduli (Simmons and Brace, 1965; King, 1969; and Chen and Johnston, 1981). Walsh and Brace (1966) concluded that this difference is due to the presence of high complaint cracks that affect dynamic deformation differently than static deformation. The values of static moduli approach dynamic values in rocks with low concentration of cracks.

In this study, both dynamic and static moduli are measured for Sarah Formation. Dynamic moduli are obtained through continuous log-measured compressional and shear wave velocities. Moreover, dynamic moduli are also measured in laboratory using core samples under different confining pressures. Static moduli were derived from stress-strain measurements obtained from uniaxial compression strength test on core samples.

4.2.1 Sampling for geomechanical testing

46 plugs were taken for acoustic and unconfined compressive strength (UCS) testing from cores of five wells constrained by the required specifications described as follows;

For acoustic measurements, the plug's diameter should be 1.5 inch and its length should be equal to or larger than 2 inches. So the selection of plugs was restricted by the plug dimensions' requirement as it is not possible to recover a plug of this dimension from all available cores and all facies. Further, as the cores are broken and fractured at many levels, it has been impossible to recover an intact plug for all facies of interest. Summary of all plugs taken for acoustic measurements is given in Table 4.1.

For UCS testing, the main requirements are that the plugs should be taken vertically from cores and the ratio of diameter to length should be 1 by 2. Therefore, the plugs are taken vertically from all major facies with dimensions of 1″×2″. Plugs selection was again restricted by the fractured condition of cores and locations from where a vertical plug of 2 inch can be taken. Summary of all plugs taken for UCS testing is given in Table 4.4. All plug locations are presented in Appendix A.

4.2.2 Dynamic Moduli Measurements

Dynamic moduli measurement methods are based on wave propagation. Continuous velocity measurements are more commonly available at in-situ conditions from well log data so calculating dynamic moduli is rather easy as compared to the static one, which is expensive and involves destructive testing on core samples. Calculation of elastic moduli from well-log data will be discussed later in Section 4.3.

A method involving the use of laboratory velocity measurements is also adopted to calculate dynamic moduli. During the measurements, reservoir conditions are simulated by changing confining pressure. The details of this method are outlined in the following section.

4.2.2.1 Acoustic Measurements

Acoustic measurements were performed on 16 sandstone samples using Autolab 500 equipment. The core sample is fitted in a transducer (Figure 4.1) and then this transducer is placed in the main assembly unit (Figure 4.2). Compressional and shear waves are passed through the sample vertically on different stages of confining pressure and their first arrival

times are measured. After measuring, first arrival picking is performed manually. Based on those picked arrival times and pre-determined information on sample dimensions and density, Young's modulus and Poisson's ratio are calculated at five stages of confining pressure.

A typical ultrasonic transducer assembly is shown in Figure 4.1. The unit is a matched set of transmitting and receiving transducers capable of propagating and receiving a compressional wave (P) and two polarized shear waves (S1 and S2) through a rock specimen. The vibration directions for two shear waves are oriented at 90^0 to each other. The transducers operate at confining pressures up to 100 MPa.

Figure 4.1 Autolab 500 for acoustic measurements

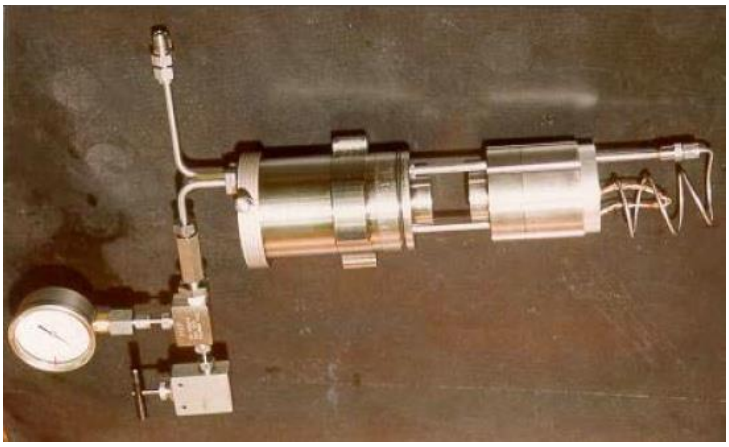

Figure 4.2 Ultrasonic transducer assembly

Before conducting test, some pre-test measurements (Table 4.1) were made to compute bulk density from measured core sample dimensions and weights. These pre-test measurements and calculated bulk density are necessary to calculate elastic parameters from acoustic results.

Table 4.1 Pre-test values for acoustic measurements

Well No.	Sample No.	Length (cm)	Diameter (cm)	Average Length	Average Diameter	Volume (cc)	Weight (gms)	Density (gms/cc)	Depth (ft)
E	2H	5.18	3.77	5.186	3.786	58.38262	147.11	2.52	14807
		5.18	3.78						
		5.2	3.8						
		5.19	3.79						
		5.18	3.79						
	8H	5.2	3.78	5.2	3.782	58.4166	142.93	2.45	14813
		5.2	3.78						
		5.2	3.78						
		5.2	3.78						
		5.2	3.79						
	12V	5.36	3.78	5.363	3.784	60.31147	150.06	2.49	14817.1
		5.365	3.79						
		5.36	3.78						
		5.36	3.78						
		5.37	3.79						
	16H	5.575	3.78	5.57	3.782	62.57317	153.38	2.45	14820.9
		5.57	3.78						
		5.565	3.79						
		5.575	3.78						
		5.565	3.78						
	24H	5.5	3.79	5.493	3.798	62.23138	154.25	2.48	14829
		5.49	3.8						
		5.49	3.8						
		5.485	3.8						
		5.5	3.8						
	30H	5.185	3.795	5.185	3.792	58.55653	146.78	2.51	14835.2
		5.18	3.79						
		5.18	3.79						
		5.19	3.79						
		5.19	3.795						
A	68H	5.34	3.72	5.345	3.726	58.2805	141.05	2.42	16693.5
		5.345	3.73						
		5.35	3.72						
		5.35	3.725						
		5.34	3.73						
	73H	5.47	3.72	5.472	3.712	59.21775	140.74	2.38	16700.1
		5.46	3.715						
		5.465	3.7						
		5.47	3.7						
		5.47	3.71						

(table continued)

Well No.	Sample No.	Length (cm)	Diameter (cm)	Average Length	Average Diameter	Volume (cc)	Weight (gms)	Density (gms/cc)	Depth (ft)
A	81H	4.76	3.72	4.77	3.725	51.98294	124.66	2.40	16708
		4.77	3.72						
		4.76	3.725						
		4.77	3.73						
		4.77	3.73						
	88H	4.9	3.72	4.908	3.733	53.71683	127.1	2.37	16714.8
		4.91	3.72						
		4.905	3.735						
		4.91	3.73						
		4.91	3.73						
	89V	5.58	3.72	5.587	3.727	60.95191	153.32	2.52	16715
		5.59	3.73						
		5.59	3.73						
		5.585	3.725						
		5.58	3.72						
	95V	5.25	3.74	5.253	3.743	57.80121	136.05	2.35	16720.9
		5.26	3.73						
		5.26	3.73						
		5.255	3.735						
		5.26	3.74						
F	116	5.025	3.83	5.023	3.833	57.96031	146.059981	2.52	18662.3
		5.02	3.82						
		5.03	3.82						
		5.025	3.83						
		5.02	3.83						
	118	5.07	3.83	5.075	3.832	58.52978	153.933335	2.63	18664
		5.08	3.82						
		5.08	3.835						
		5.075	3.835						
		5.07	3.83						
D	33H	4.47	3.83	4.474	3.822	51.32952	144.94	2.82	17208.2
		4.48	3.82						
		4.485	3.82						
		4.47	3.835						
		4.48	3.82						
	40H	4.77	3.815	4.782	3.817	54.71971	145.49	2.66	17221.5
		4.78	3.82						
		4.785	3.82						
		4.88	3.81						
		4.88	3.81						

The measured compressional and shear wave velocities were used to calculate dynamic elastic parameters. As pointed out earlier, acoustic measurements were performed on 16 core plugs from 4 wells. Velocity measurements were taken on all plugs under five stages of confining pressure ranging from 7 Mpa to 35 Mpa. The acoustic measurement results for one of the samples from Well-E are shown in Table 4.2 and Figure 4.3a, b, c. These results indicate considerable increase in compressional and shear velocity with an increase in confining pressure. The same trend is followed by Young's modulus and Poisson's ratio (Table 4.2). On the contrary, some results show very little increase in compressional wave velocity with increasing confining pressure and so the difference in Young's modulus and Poisson's ratio is small. An example of such behavior from Well-D is given in Table 3 and Figure 4.4a, b, c. All other results from 16 plug samples are presented in Appendix-B.

Table 4.2 P and S wave velocities with confining pressure for Sample 8H (Well-E)

Event	Confining Pressure	Vp	Vs (1)	Vs (2)	Young's modulus	Poisson's ratio
	MPa	m/s	m/s	m/s	Gpa	
0	7	3364	2169	2056	25.68	0.174
1	14	3731	2428	2276	31.72	0.17
2	21.1	4021	2546	2438	36.16	0.188
3	28	4234	2684	2561	40.06	0.189
4	35.1	4395	2758	2659	42.91	0.194
5	28.2	4298	2714	2606	41.24	0.19
6	21.4	4149	2656	2505	38.65	0.185
7	14.2	3924	2505	2377	34.58	0.184
8	7.2	3493	2281	2183	28.19	0.155

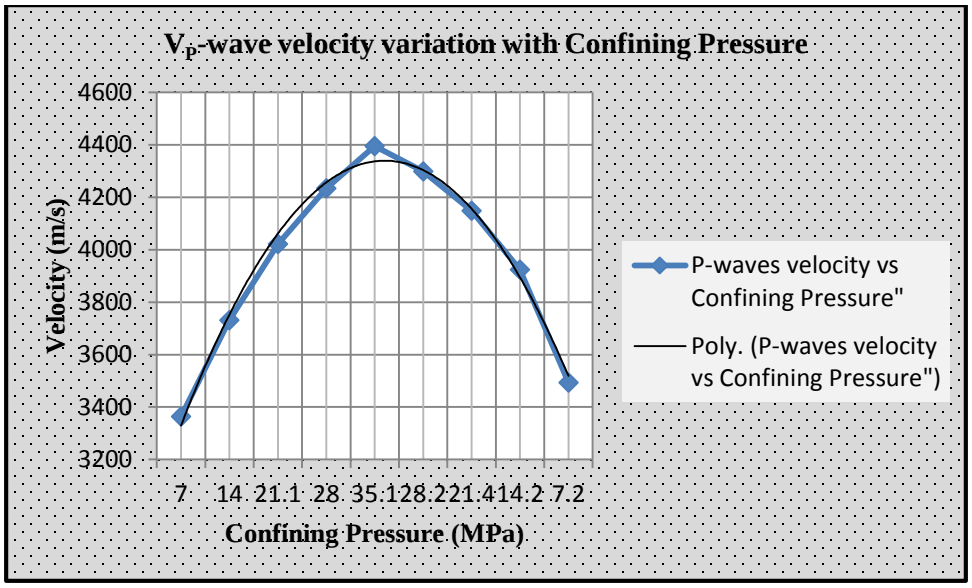

Figure 4.3a V_P-wave velocity variation with confining pressure for Sample 8H (Well-E)

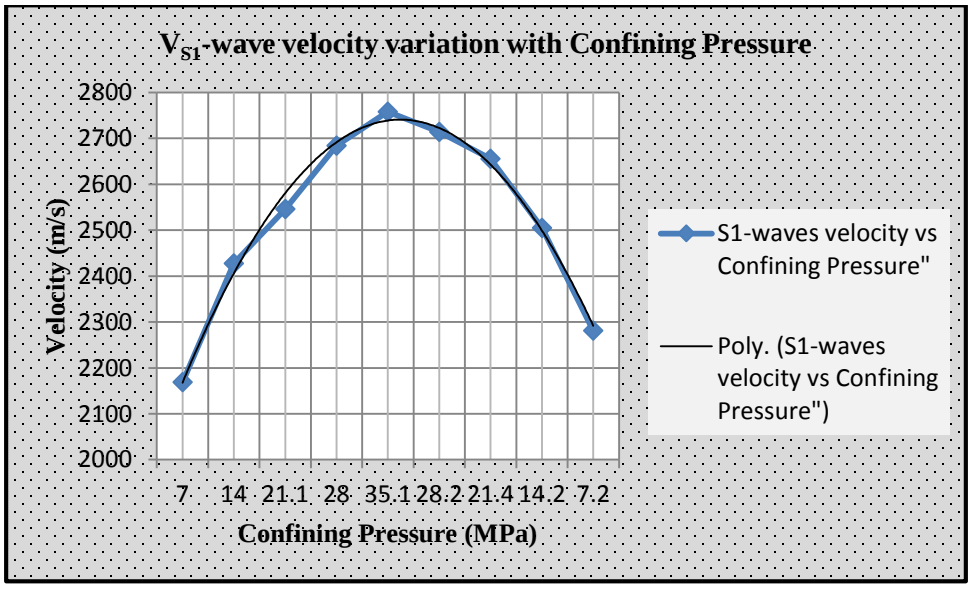

Figure 4.3b V_{S1}-wave velocity variation with confining pressure for Sample 8H (Well-E)

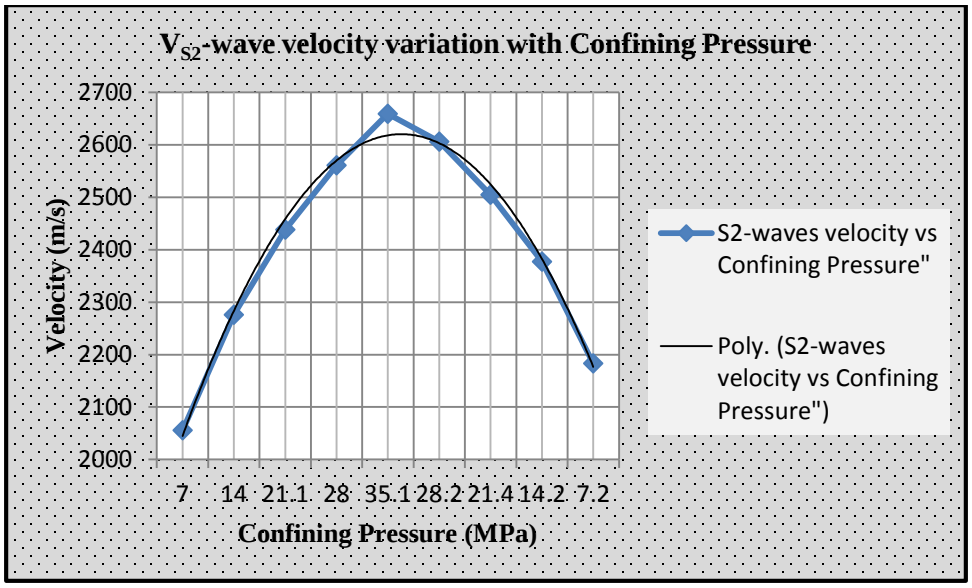

Figure 4.3c V_{S2}-wave velocity variation with confining pressure for Sample 8H (Well-E)

Table 4.3 P and S wave velocities with confining pressure for Sample 40H (Well-D)

Event	Confining Pressure	Vp	Vs (1)	Vs (2)	Young's modulus	Poisson's ratio
	MPa	m/s	m/s	m/s	Gpa	
0	7.1	5502	3226	3372	70.6	0.219
1	14.1	5550	3246	3394	71.62	0.221
2	21	5582	3257	3411	72.3	0.223
3	28	5615	3257	3420	72.73	0.227
4	35	5632	3268	3422	73.07	0.228
5	28.1	5615	3257	3418	72.7	0.227
6	21.1	5582	3257	3414	72.35	0.222
7	14.1	5550	3246	3394	71.62	0.221
8	7.3	5502	3226	3372	70.6	0.219

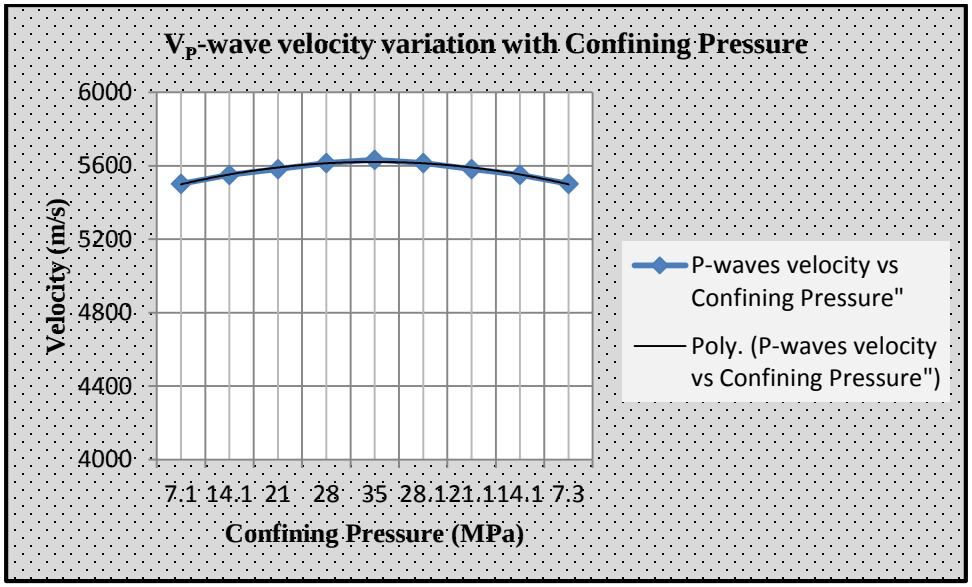

Figure 4.4a V_P-wave velocity variation with confining pressure for Sample 40H (Well-D)

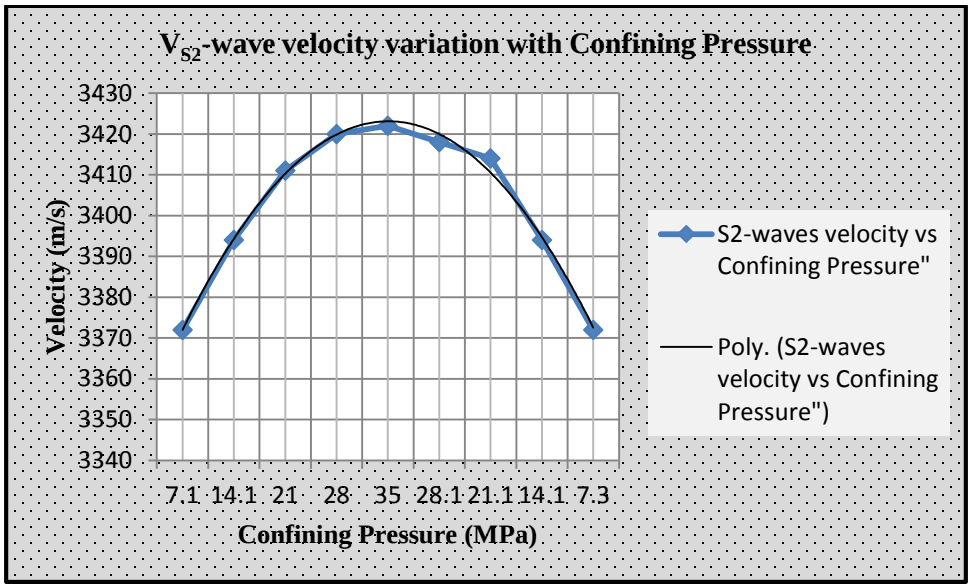

Figure 4.4b V_{S1}-wave velocity variation with confining pressure for Sample 40H (Well-D)

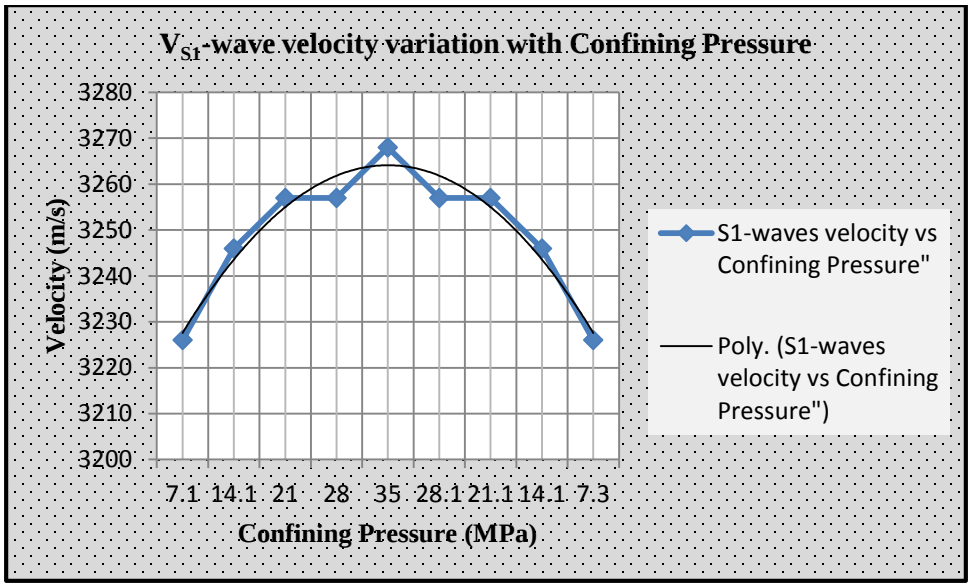

Figure 4.4c V_{S2}-wave velocity variation with confining pressure for Sample 40H (Well-D)

4.2.3 Static Moduli Measurements

Static elastic moduli are usually obtained in laboratory either by uniaxial compression test or triaxial compression test. In this study, uniaxial compression test was performed on 19 plug samples from six wells.

4.2.3.1 Uniaxial Compression Test

Uniaxial compression test (also called unconfined compression test) is the most important test to measure rock strength (unconfined compressive strength) and to estimate mechanical parameters of rocks. Several important concepts related to a typical result from the uniaxial compression test are shown in Figure 4.5 (Fjaer et al. 1992):

- In the elastic region the specimen will return to its original state after the stress is released.

- Hardening region is where the sample undergoes plastic deformation with increasing ability to sustain load.
- Softening region is where the specimen's ability to withstand stress decreases as deformation increases.

Brittle rocks show little strain in linearly elastic manner before failure while ductile rocks deform in a non-elastic, non-recoverable way before breaking showing more plastic or inelastic behavior defining a ductile failure.

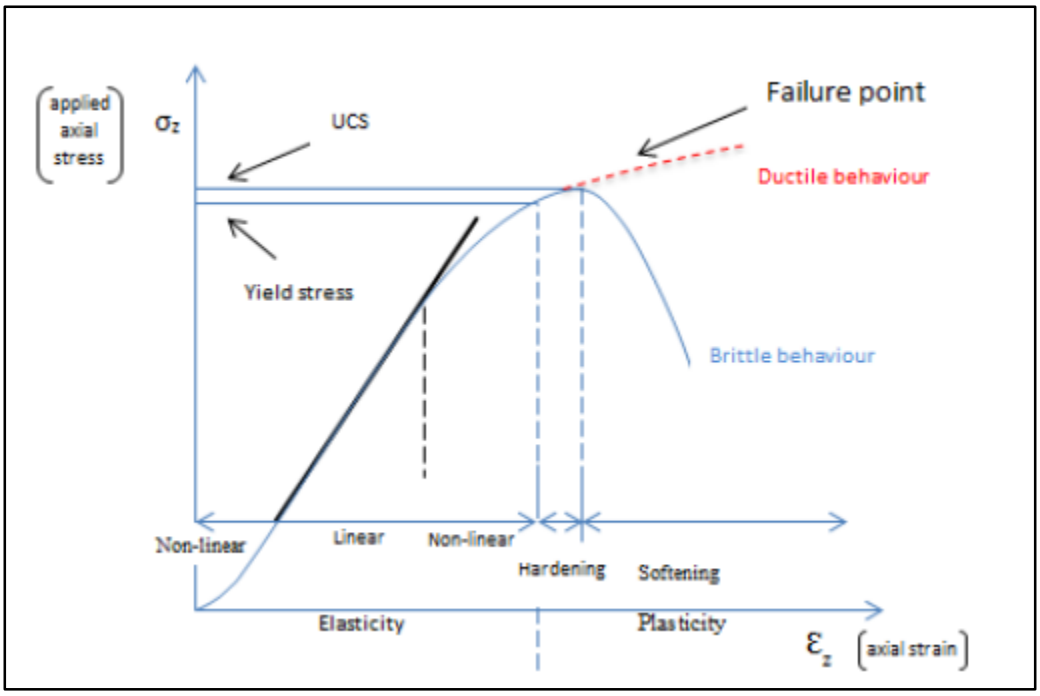

Figure 4.5: Failure modes in a uniaxial compression test (Modified from Fjaer et al., 1992)

19 new vertical plugs (1"x 2") were prepared from the cores of all five wells. Plugs were taken considering all major facies present. End face grinding was performed on each plug to make their faces parallel to each other to get accurate testing results.

In this test, core samples are attached with strain gauges (Figure 4.6), which measure the axial and lateral strain along with the applied stress till failure. A data logger is attached to the testing apparatus to record the results (Figure 4.7). Static moduli were derived from stress-strain measurements obtained from uniaxial compression strength test on 19 core samples. Two representative stress-strain measurement results from Well-E are illustrated in Figure 4.8 and Figure 4.9.

Figure 4.6 Samples attached with strain gauges

Figure 4.7 Uniaxial compression testing assembly

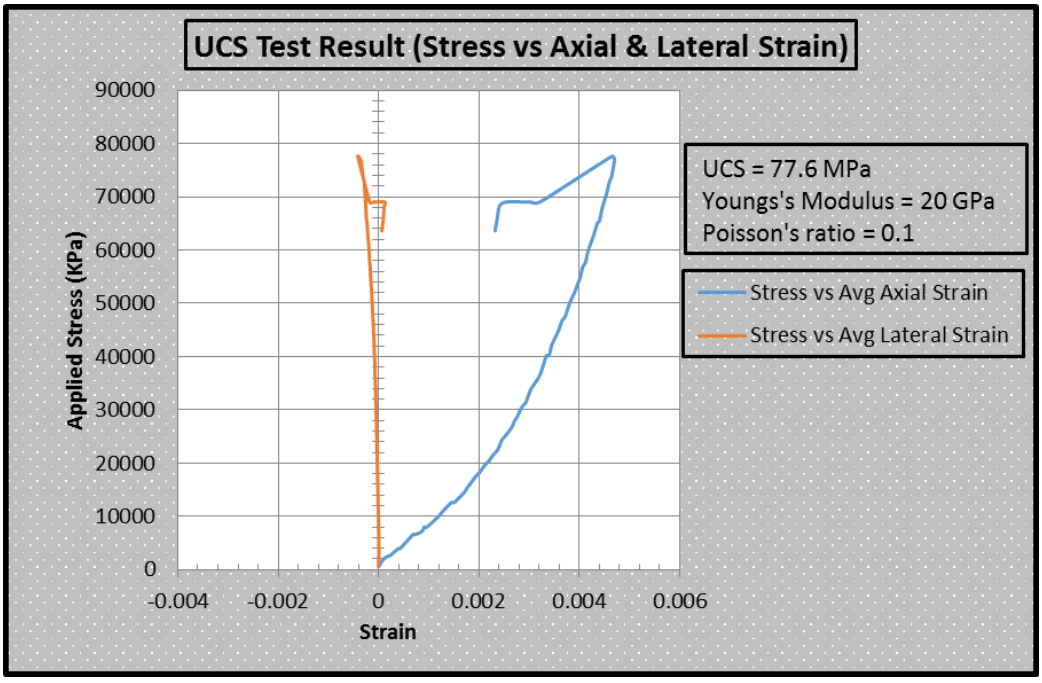

Figure 4.8 UCS test result for sample W5, Well-E

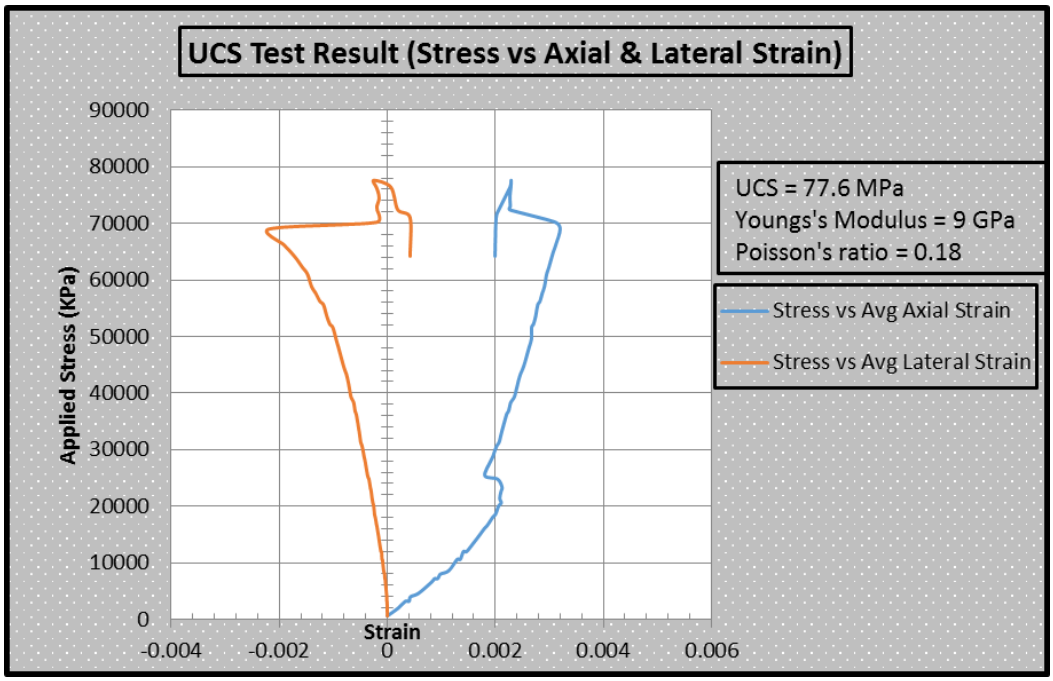

Figure 4.9 UCS test result for sample W6, Well-E

It is obvious from the graphs (Figure 4.8 and 4.9) that the both samples got fractured at about 77.7 Mpa which is their unconfined compressive strength (UCS). The failure of sample W5 (Figure 4.8) is more plastic (non-elastic) as it shows more strain (about 0.05) before getting fractured while the failure of sample W6 (Figure 4.9) tends to be brittle as it shows small strain (about 0.03) before failure. Young's Modulus is calculated from the slope of axial strain vs stress and Poisson's Ratio is obtained using the slope of lateral strain vs stress. The summary of all UCS results is given in Table 4.4. Samples with no results indicate broken samples while plugging due to natural fractures present in the core. Stress-strain plots for are all 19 plugs are presented in Appendix C.

Table 4.4 Summary of all UCS results

Sr #	Well #	Sample #	Lithology	Young's Modulus (GPa)	Poisson's Ratio	UCS (MPa)	UCS (psi)
1	A	A1	Sandstone	-	-	-	-
2		A2	Sandstone	60	0.3	71	10298
3		A3	Sandstone	70	0.2	75.6	10965
4		A4	Sandstone	-	-	-	-
5		A5	Sandstone	40	0.16	60.2	8731
		Average		**56.67**	**0.22**	**68.93**	**9997.95**
6	B	B1	Sandstone	50	0.25	85	12328
7		B2	Sandstone	20	0.1	74.4	10791
8		B3	Sandstone	10	0.2	65.6	9514
9		B4	Sandstone	20	0.1	85	12328
10		B5	Sandstone	-	-	-	-
		Average		**25**	**0.16**	**77.5**	**11240.45**
11	C	C1	Sandstone	40	0.16	154.8	22452
12		C2	Sandstone	50	0.25	63	9137
13		C3	Sandstone	60	0.2	160.8	23322
14		C4	Sandstone	70	0.175	95	13779
15		C5	Sandstone	40	0.2	92.4	13402
16		C6	Sandstone	100	0.18	116.6	16911
		Average		**60.00**	**0.19**	**113.77**	**16500.49**
17	D	D1	Sandstone	-	-	-	-
18		D2	Sandstone	80	0.4	82.4	11951
19		D3	Sandstone	80	0.4	158.2	22945
		Average		**80**	**0.4**	**120.3**	**17448.07**
20	E	E1	Sandstone	40	0.3	117.2	16998
21		E2	Sandstone	40	0.3	63.6	9224
22		E3	Sandstone	20	0.2	42.8	6208
23		E4	Sandstone	40	0.2	128.6	18652
24		E5	Sandstone	30	0.1	77.6	11255
25		E6	Sandstone	30	0.18	77.6	11255
26		E7	Sandstone	-	-	-	-
		Average		**33.33**	**0.21**	**84.57**	**12265.38**

4.3 1-D Mechanical Earth Model (MEM)

Mechanical Earth Model (MEM) is a quantitative way to show Earth's in situ stresses and the mechanical properties of rocks in a field or basin. Understanding the geomechanics of the well drilled helps to minimize the risk related to geomechanical properties. Understanding the stressed state of Earth is important for effective and safe drilling operations. MEM helps to reduce issues created by Earth's stresses like wellbore instability, predicting overpressure zones and fracture orientation for hydraulic fracturing etc (Husain et al., 2003).

The MEM captures all information regarding the geomechanics of drilling and production (including rock mechanical parameters), rock failure mechanisms, in-situ stresses, geologic structure, stratigraphy and well geometry (Adisornsuapwat, 2012). To calculate brittleness, several mechanical properties are required such as Young's Modulus, Poisson's Ratio, cohesion, coefficient of friction, shear modulus, compressive and tensile strengths and their variation in different directions to account for anisotropy (Josh et al., 2012). Log based and laboratory approaches can be applied to determine the total organic matter, permeability, porosity, and mechanical parameters (Jacobi et al. 2008; and Parker et al. 2009). For optimizing the hydraulic fracture treatment, geomechanics, mineralogy, and petrophysics are integrated (Rickman et al. 2008). The MEM contains the following components as illustrated in Figure 4.10;

1. Framework Model
2. Mechanical Stratigraphy
3. Rock Mechanical Properties
4. Earth Stresses

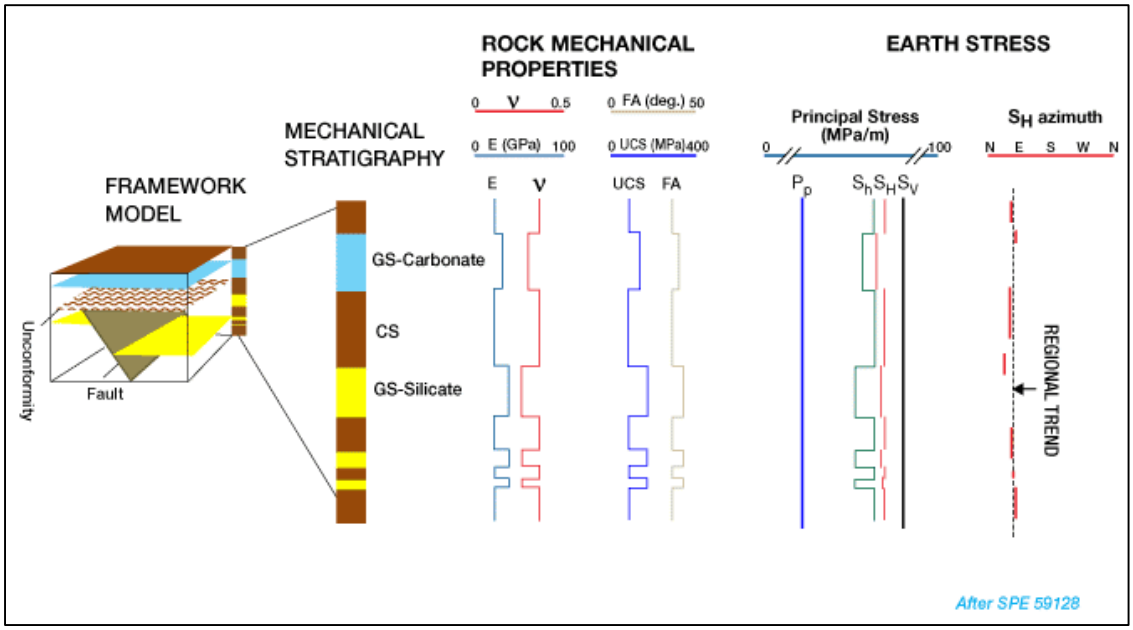

Figure 4.10 Schematic representation of a 1-D MEM

4.3.1 Applications of MEM

The MEM is important for effective exploitation of hydrocarbons especially in unconventional reservoirs such as shale gas or tight gas reservoirs. It integrates information from the fields of geology, rock mechanics, geophysics and petrophysics to characterize subsurface rock formations in a way that can help to reduce risk involved in oil field operations (Husain et al., 2003).

1. MEM provides a means for;
    - Predicting wellbore stability and reservoir deformation.
    - Optimizing field development plans.
    - Diagnosing problems related to subsurface rock deformation.
2. MEM drilling applications include pre-drilling planning and during the drilling wellbore stability management.

3. MEM completion applications include sanding risk analysis, completion design, hydraulic fracturing simulation planning and design.

4.3.2 MEM Workflow

The MEM workflow is represented as a series of ten interdependent steps. The sequence of these steps reflects a logical progression of data processing; each step builds on one or more previous steps. Figure 4.11 shows the recommended sequence of building a MEM. Data from all available sources can be utilized in building and upgrading a MEM in the life cycle of the reservoir. Table 4.5 shows the sources of information used to build a MEM.

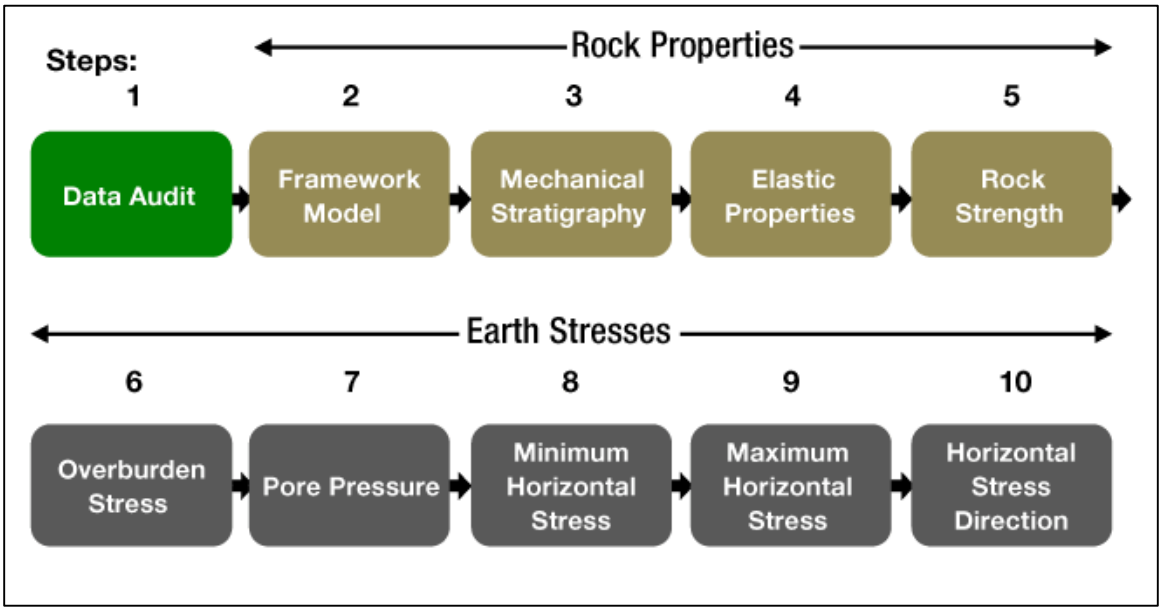

Figure 4.11 MEM Workflow

Table 4.5 Sources of information used to build a MEM (After Plumb et al., 2000)

Property profiled	Source logs	Other sources
Mechanical stratigraphy	Gamma ray, density, resistivity, sonic compressional velocity (V_p)	Cuttings, cavings, sequence stratigraphy
Pore pressure (P_p)	V_p, check-shot survey, resistivity	Interval velocity from seismic data, formation-integrity test, daily drilling reports
Overburden stress (σ_v)	Bulk density	Cuttings
Stress direction	Oriented multiarm calipers, borehole images, oriented velocity anisotropy	Structural maps, 3D seismic data
Minimum horizontal stress (σ_h)	V_p and sonic shear velocity (V_s), wireline stress tool	P_p, leakoff tests, extended leakoff tests, microfrac, step-rate injection tests, local or regional database, daily drilling reports, modeling
Maximum horizontal stress (σ_H)	Borehole images	P_p, σ_h, rock strength, database, wellbore stress model
Elastic parameters [Young's modulus (E), shear modulus (G), Poisson's ratio (v)]	V_p and V_s, bulk density	Database, laboratory core tests, cavings
Rock-strength parameters [unconfined compressive strength (UCS), friction angle (Φ)]	V_p and V_s, bulk density, mechanical stratigraphy	Database, laboratory core tests, cavings
Failure mechanisms	Borehole image, oriented multiarm caliper	Daily drilling reports, cavings

4.3.3 Mechanical Stratigraphy

The MEM for Well-C presented here have a total depth of 1000 ft. The stratigraphic units encountered in those 1000 ft. are as follows;

- Qusaiba Member, Qalibah Formation 415 ft.
- Baq'a Sandstone Member, Sarah Formation 55 ft.
- Baq'a Shale Member, Sarah Formation 20 ft.
- Sarah Formation 240 ft.
- Quwarah Member, Qasim Formation 270 ft.

4.3.4 Calculating Elastic Parameters

Elastic property profiles, Young's modulus, and Poisson's ratio are calculated using sonic and density log data. Figure 4.12 illustrates the process of calculating these profiles. Calibration of dynamic elastic parameters is carried out using static elastic parameters which are obtained from UCS testing of core samples. Continuous profiles of dynamic and calibrated Young's Modulus and Poisson's ratio were attained (Figure 4.13 a, b).

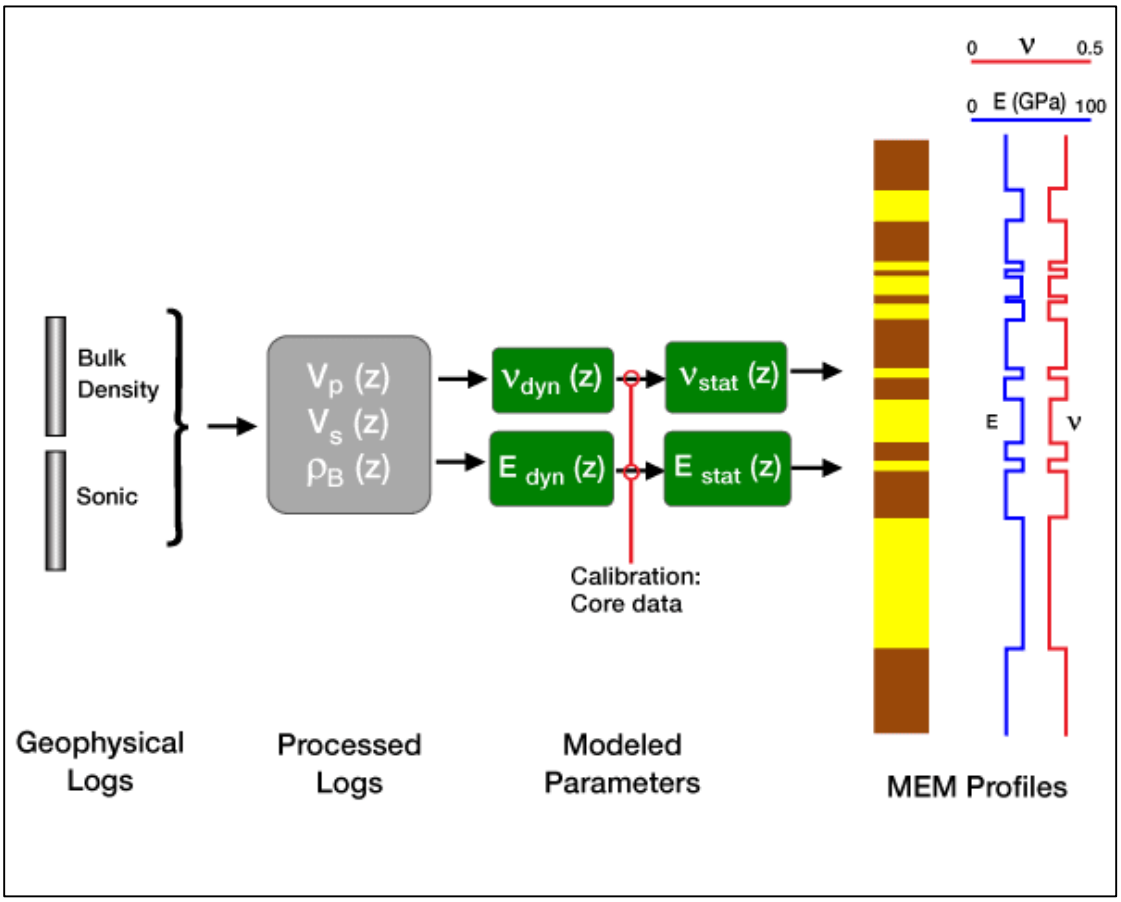

Figure 4.12 Process of constructing elastic property profiles

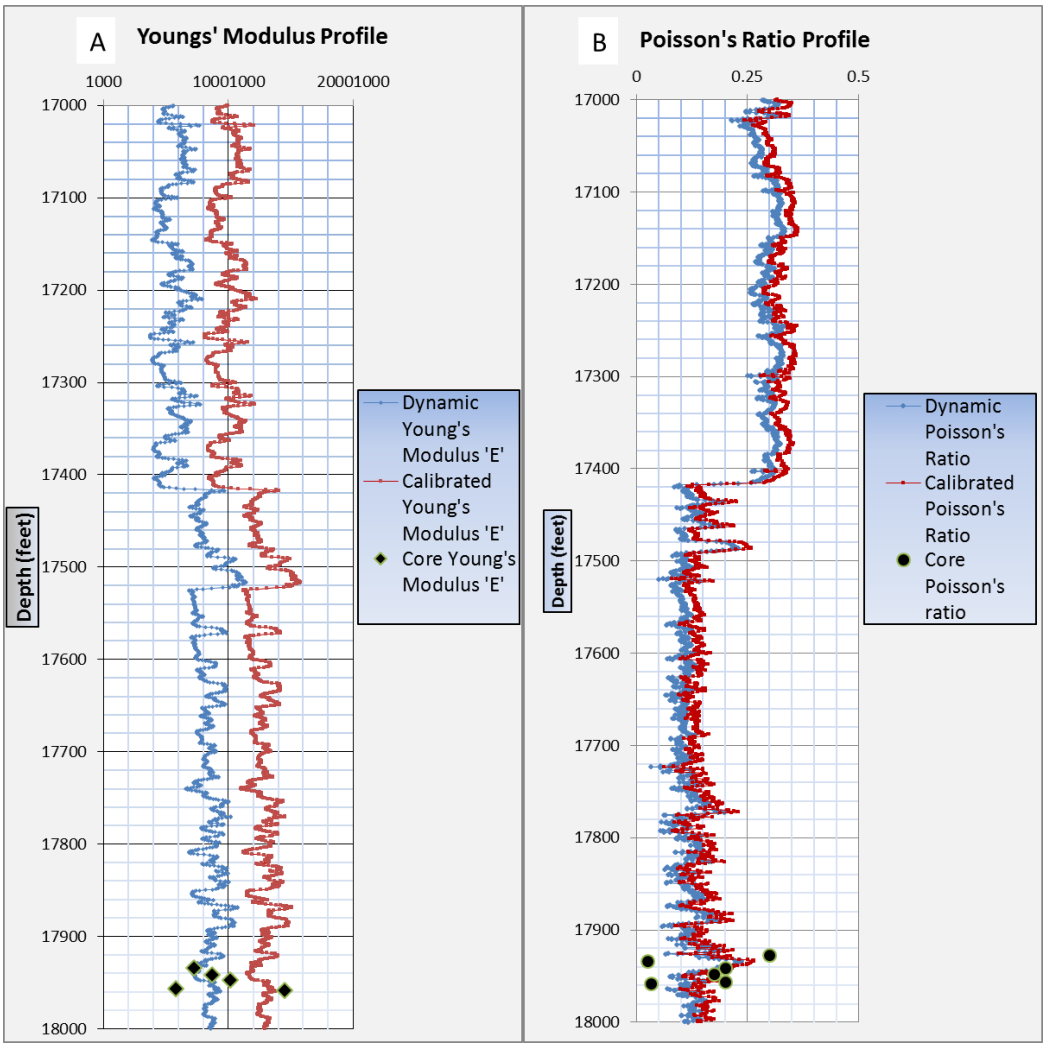

Figure 4.13 Elastic parameters for Well-C: (a) Young's Modulus profile, (b) Poisson's ratio profile

4.3.5 Calculating Strength Parameters

Profiles of rock strength parameters, Unconfined Compressive Strength (UCS), Angle of friction, and Cohesion are derived from elastic property profiles (Figure 4.14). Calibration of these profiles is recommended with laboratory uniaxial or triaxial strength measurements on cores whenever possible. In this work, calibration is done by uniaxial compression test (UCS) on 19 core samples. The profiles showing variations of failure

parameters (cohesion, friction, UCS, and tensile strength) with depth are given in Figures 4.15 a, b, c.

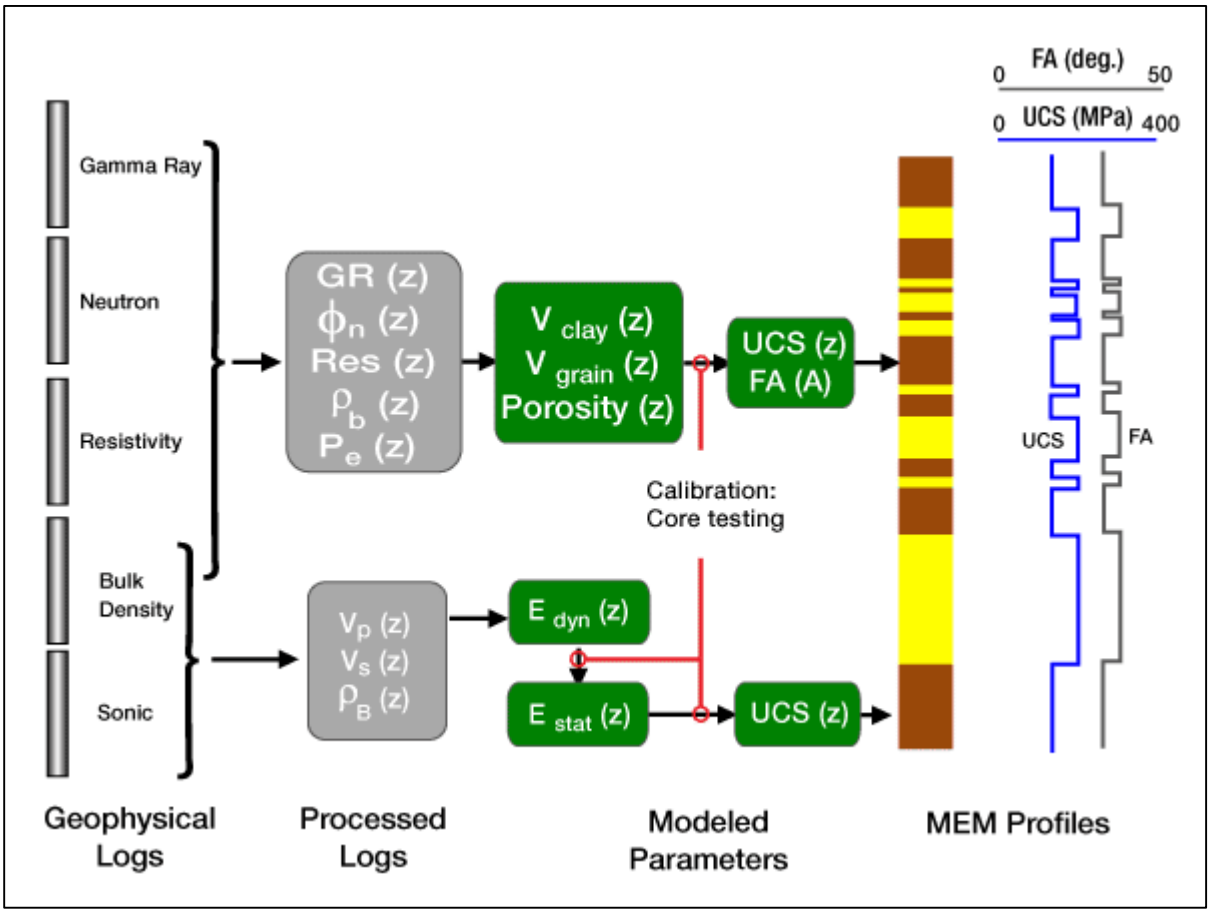

Figure 4.14 Methods of constructing profiles of rock strength parameters

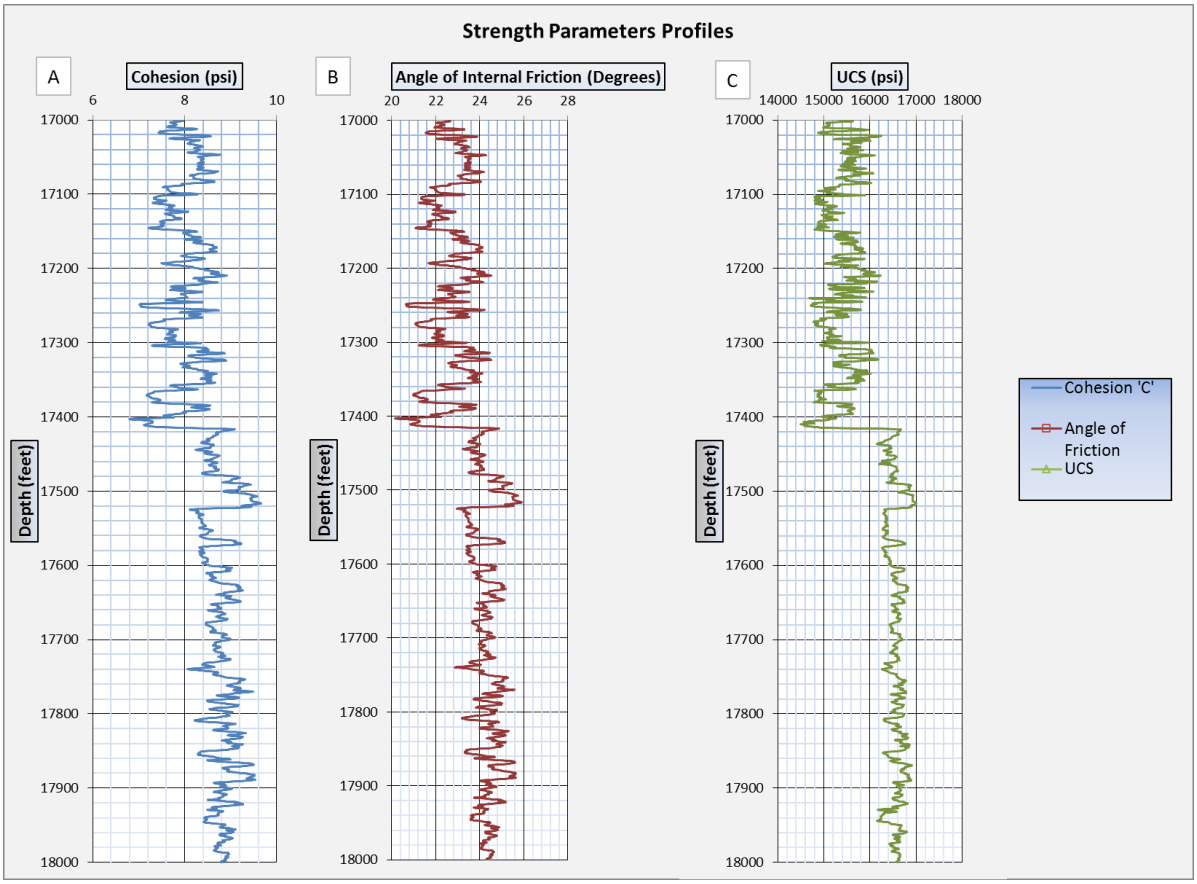

Figure 4.15 Strength parameters for Well-C: (a) Cohesion Profile, (b) Angle of Friction profile, (c) Uniaxial Compressive Strength profile

4.3.6 Calculating Earth Stresses

Overburden stress is calculated by integrating bulk density over depth. The pore pressure (P_p) profile is modeled using Eaton's method (Eaton, 1975). This method can take compressional wave velocity (V_p) or deep resistivity and overburden stress as input data (Figure 4.16). It is important to calibrate pore pressure profile because of its impact on drilling safety and Earth stress calculation. Un-calibrated pore pressure profiles often show the general trend of pressure vs. depth, but the magnitude of pressure can be seriously in error. In this study, the pore pressure profile was estimated using compressional wave velocity and overburden stress as shown in Figure 4.17.

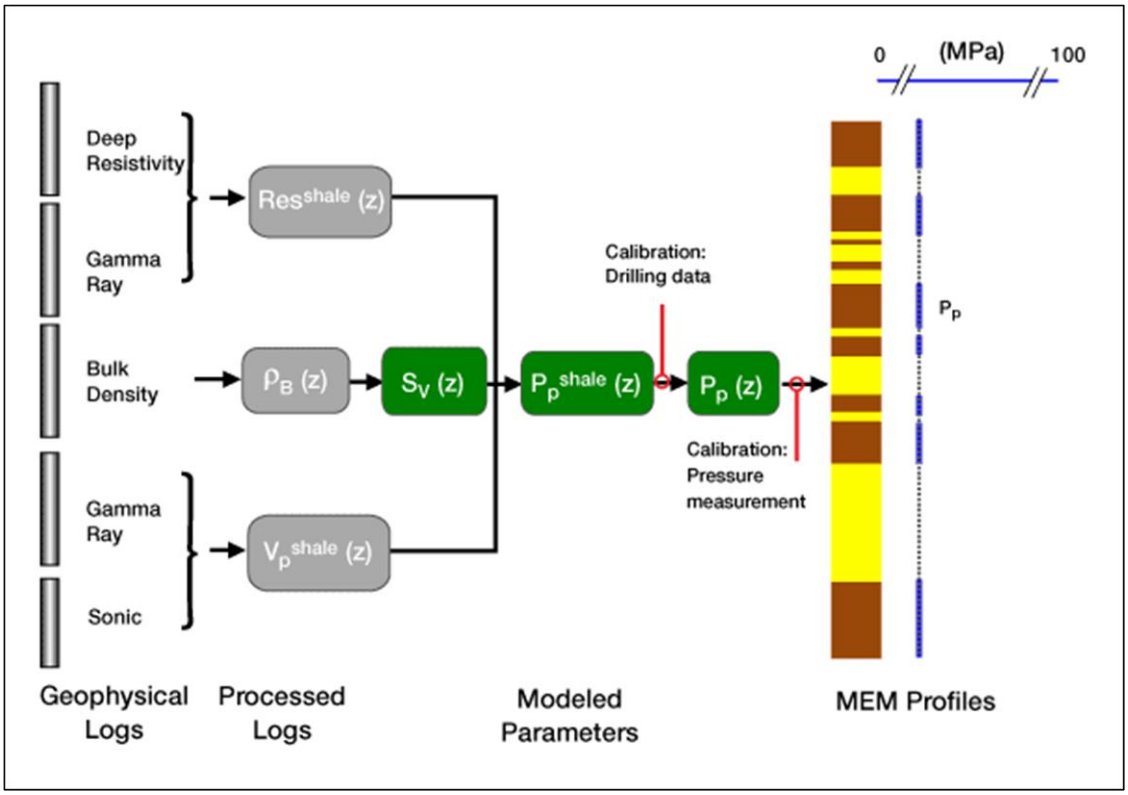

Figure 4.16 Process of calculating pore pressure

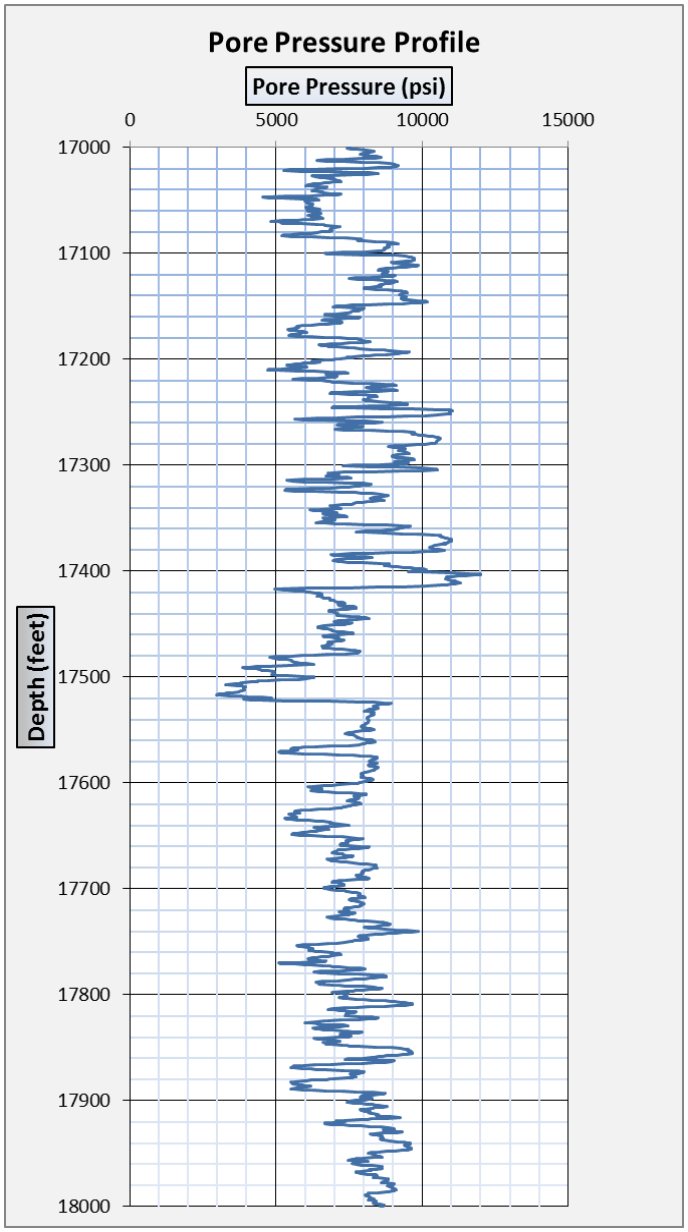

Figure 4.17 Pore pressure profile showing variation abrupt changes in pore pressure for Well-C

Minimum and maximum horizontal stresses were determined using strain corrected method (Blanton and Olson, 1999). Extended leak-off test or hydraulic fracturing data were used to estimate the minimum horizontal stress, and strain factor which are further used to estimate the maximum horizontal stress. Minimum horizontal stresses were determined using extended leak-off test data.

The pressure was measured at the surface so we need to add hydraulic gradient to the measured pressure. Using the minimum horizontal stress, strain factor was determined and maximum horizontal stress was obtained at the same depth. For the determination of minimum horizontal stress 'σ_h' (Equation 1) and maximum horizontal stress 'σ_H' (Equation 2), the strain corrected model (Blanton and Olson, 1999) was used.

$$\sigma h = [(\nu/(1-\nu)\,(\sigma v - \alpha Pp) + \alpha Pp + \left[\frac{E\nu\varepsilon}{1-\nu^2}\right] \qquad \text{Equation (1)}$$

$$\sigma h = [(\nu/(1-\nu)\,(\sigma v - \alpha Pp) + \alpha Pp + \left[\frac{E\varepsilon}{1-\nu^2}\right] \qquad \text{Equation (2)}$$

The magnitude and directions of in-situ stresses are essential in order to assess the hydraulic fractures orientation. Stress profiles are shown below in Figure 4.17a, b, and c.

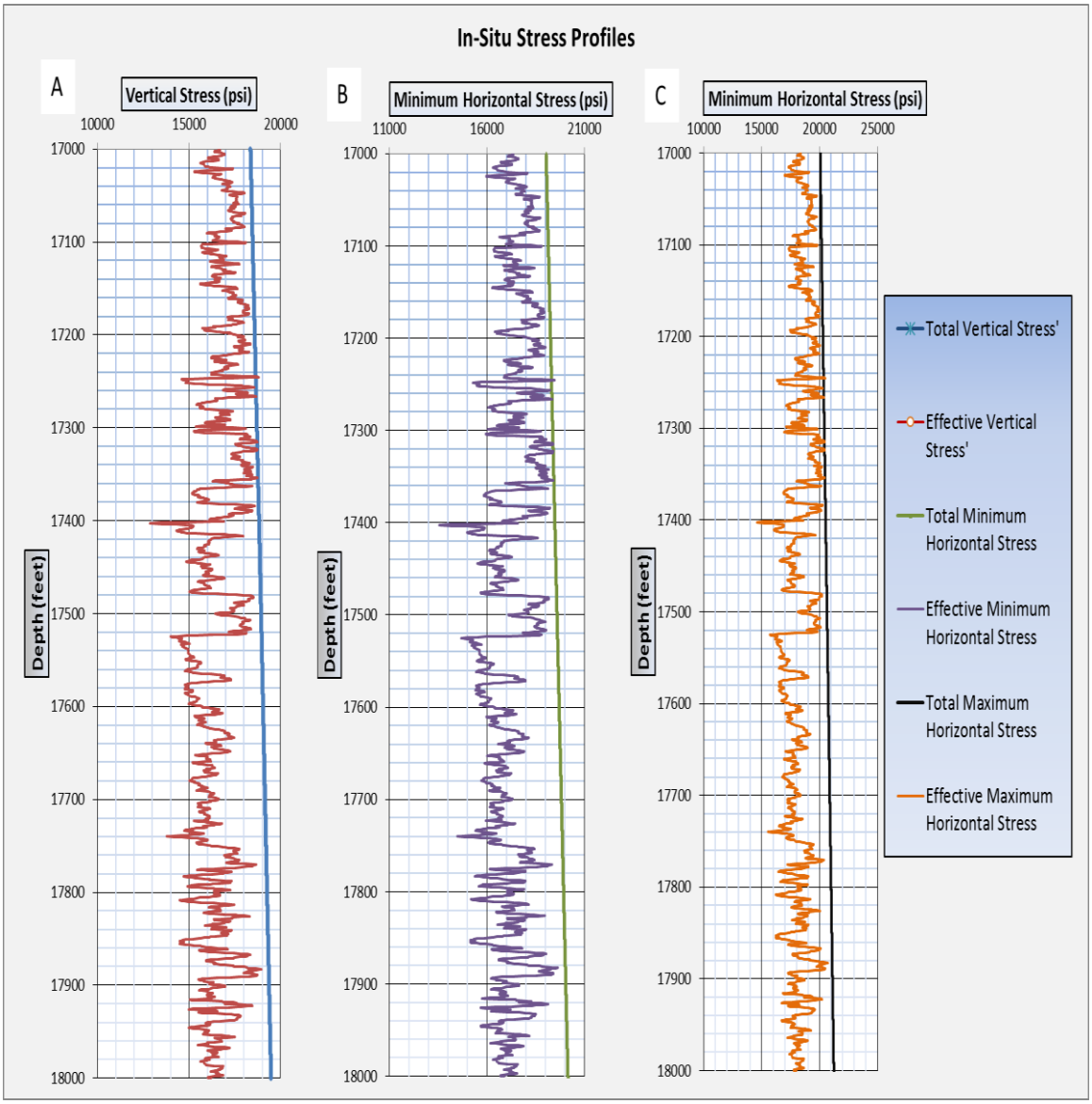

Figure 4.18 In-Situ stress parameters for Well-C: (a) Vertical stress profile, (b) Maximum Horizontal Stress, (c) Minimum Horizontal Stress

4.3.7 Construction of Safe Mud Weight Window

An important application of the MEM is to define the safe mud weight to avoid any serious problem during drilling. Figure 4.18 shows a schematic wellbore stability forecast using a safe mud weight window.

Keeping in mind the four limits (two upper and two lower) for safe drilling operation, safe mud weight window was determined (Figure 4.19). The four limits for mud weight (Fjaer et al., 2008) are defined as:

1) 1st Upper limit to avoid borehole collapse. Mud weight should be less than this limit to avoid shear failure or collapse that cause stuck pipe, tight hole etc. problems.

$$P_w \leq \frac{1}{tan^2\beta+1}\left[(3\sigma_h - \sigma_H)tan^2\beta - \alpha P_f(tan^2\beta - 1) + C_o\right] \quad (3)$$

2) 2nd Upper limit to avoid induced fractures. Mud weight should be less than this limit to avoid fractures that cause loss circulation.

$$P_w \leq 3\sigma_h - \sigma_H - T_o + P_p \quad (4)$$

3) 1st Lower limit to avoid borehole collapse. Mud weight should be higher than this limit to avoid shear failure or collapse that cause stuck pipe, tight hole etc. problems.

$$P_w \geq \frac{1}{tan^2\beta+1}\left[(3\sigma_H - \sigma_h) + \alpha P_f(tan^2\beta - 1) - C_o\right] \quad (5)$$

4) 2nd Lower limit is formation pressure. Mud weight should be higher than formation pressure in order to avoid kick or blowout problems.

The recommended safe mud weight calculated for Sarah Formation is in between 11000 psi to 29000 psi.

It should be noted that in addition to the above-mentioned limits, mud weight should also be less than the fracture gradient to avoid the reopening of already existing natural fractures. Normally, the fracture gradient is taken as equal to the minimum horizontal stress.

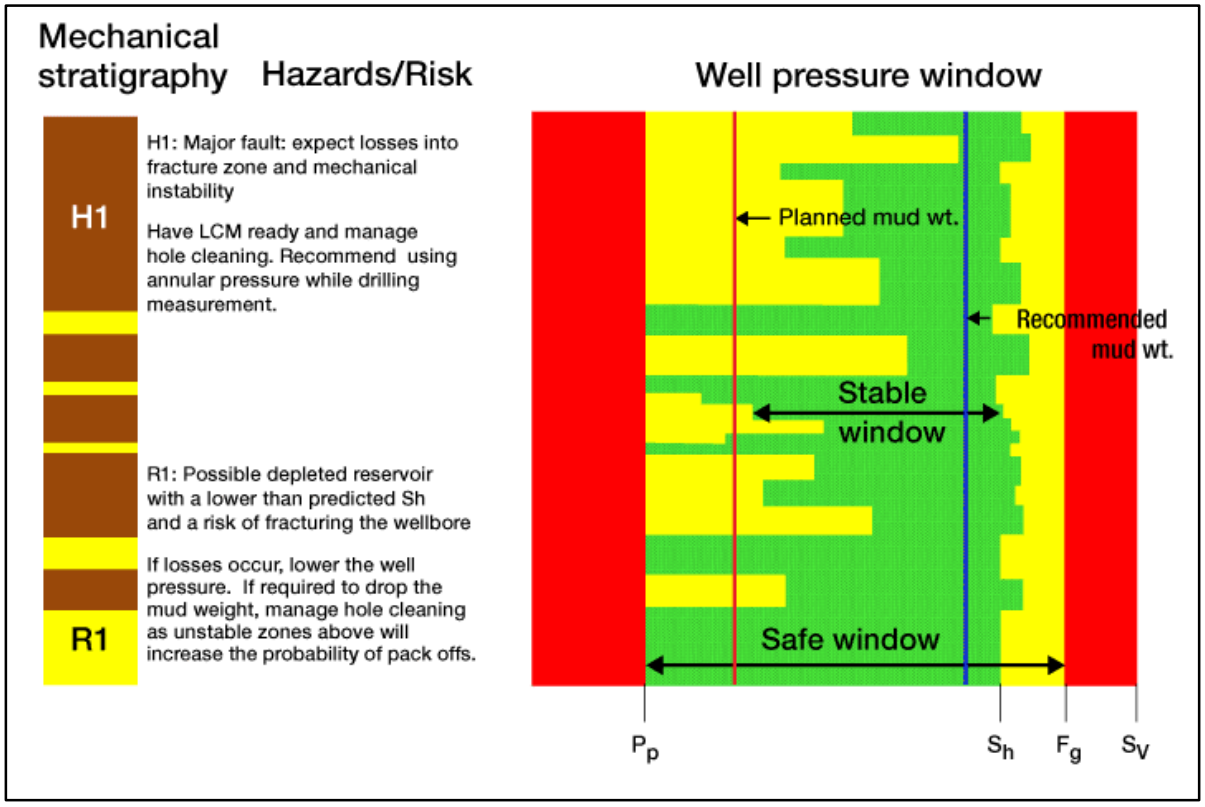

Figure 4.19 Wellbore stability forecast using safe mud weight window (After Afsari et al., 2009)

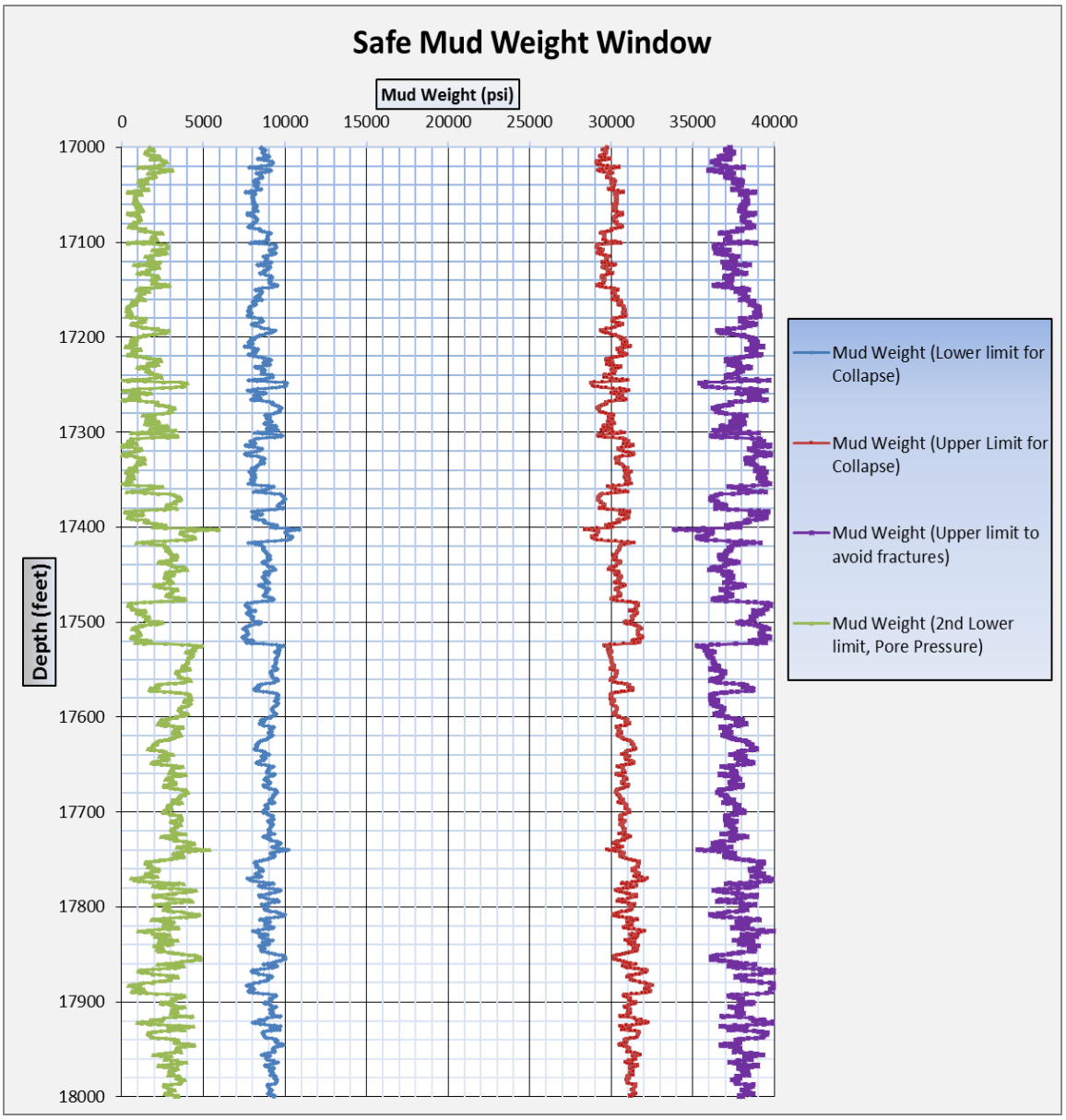

Figure 4.20 Safe Mud weight window for safe drilling operations for Well-C

CHAPTER 5
PETROPHYSICAL ROCK TYPING

5.1 Introduction

Delineation of the lateral and vertical extent of facies in an unconventional tight gas reservoir is important for designing completion strategies for their successful exploitation. Placement of fracturing perforations and isolation packers are the challenging tasks in hydraulic fracturing strategy which normally requires detailed lithological data. Due to the scarcity of core data, well log data is the only source of information to define facies in the subsurface. Core recovery and testing for different petrophysical parameters are costly and time consuming. Moreover, core testing gives discrete results while well logs provide a continuous record of reservoir petrophysical properties.

Identification and mapping of rock facies are the first steps in building a reservoir model. Statistical methods are commonly adopted to identify and to classify lithofacies from well-log data. These methods can be supervised or unsupervised. The most common supervised technique is the use of artificial neural network which requires training based on available data and prior knowledge. The training of the network involves much more effort and time and it is often case specific. On the other hand, unsupervised techniques involve the use of multi-variant statistical methods like principal component analysis and cluster analysis which are based on automatic reorganization of data patterns (John et al., 2005). In this study, an unsupervised approach was adopted using the principal component method and cluster analysis to classify facies in Sarah Formation.

This chapter includes the description of methods used and steps to develop electrofacies for Sarah Formation and their integration with geomechanical properties.

5.2 Cluster Analysis

Cluster Analysis uses standard statistical routines to allow to cluster the data into groups and to produce an electrical facies log. Cluster analysis is a multivariate analysis which identifies groups of objects that are similar to each other, but different from objects in other groups. For example, by clustering the mineral contents of a rock sample, you can study its origin and distribution in the study area.

Clustering involves the grouping of data points into classes based on similarities and dissimilarities. In the multidimensional space of well log data, similarities and dissimilarities are measured in terms of the distances between data points (Euzen et al., 2010). Some important aspects of cluster analysis are listed as follows:

1. Choosing the variables for clustering is crucial as the clustering method cannot differentiate between relevant and irrelevant variables. So the variable selection should be based on some conceptual considerations as the clusters formed are very much dependent on the variables selected (Cornish, 2007). In case of well log data, each log which corresponds to a physical property measured in a specific well is considered as a variable. In this study, the selection of logs to be used in clustering is based on their impact in identification of tight gas sandstone facies and their geomechanical properties.

2. Choosing a clustering method is also important. One has to select a clustering method which is effective in capturing geological features and is easily applicable and

interpretable. In this study, K-means clustering is used (a type of non-hierarchical clustering) which is capable of dealing with large set of data.

5.2.1 K-means clustering

K-means clustering (MacQueen, 1967) is a relocation clustering method which works using an iterative approach. The number of clusters should be defined before running the clustering and this number should remain the same during the iteration process. This method assigns each data point to the nearest cluster and iteratively keeps on moving points from one cluster to another until it minimizes the within-cluster sums of squares difference between cluster mean and data points. After each iteration, it calculates the mean of each cluster and then works with this new mean value to move the data points. The iterations run until the mean value of clusters stops changing (Fraley and Raftery 1998).

The number of clusters to be formed should be chosen wisely based on the spread and size of the data set. An effective way to find the number of clusters to be used is to run k-means clustering with different number of clusters and analyzing their sum of squares. Every cluster should have enough data points which are comparable to the total number of data points (Milligan and Cooper, 1985).

5.3 Principal Component Analysis

Principal Component analysis (PCA) is a handy statistical method which is used to analyze high dimensional data sets. Visualization of large data set is made easy by applying PCA which reveals strong patterns of a data set and highlight the variations present in it. PCA is a tool to recognize patterns in multidimensional data sets in a way that highlights their similarities and dissimilarities. PCA's main advantage is the reduction of dimensions by recognizing patterns in the data sets. This technique has been successful in Petrophysics and Geology as a preliminary method of combining multiple logs into a single one or into two logs without losing information. The principal component curves can be used for various tasks like Multi-Well tops correlation (Smith, 2002). In this study, Principal Component method is used in initiating cluster analysis by reducing the dimensions of data set and identifying major clusters in the data to start with.

5.4 Electrofacies

Electrofacies were first introduced by Serra and Abbott (1982) as facies that are uniquely based on well log responses as log measurements are a function of rock properties. Different logs represent different properties of rock formation, for example a resistivity log gives information about formation fluid and degree of cementation while a gamma ray log is an indicative of radioactive content of a rock. Any well log response can be used to develop an electrofacies depending upon the lithology and scope of the work.

In this study, electrofacies were developed in three wells for the same depth zone represented by the Mechanical Earth Model (MEM) described in the previous chapter. A software known as the Interactive Petrophysics has been used to develop these

electrofacies. Cluster analysis module was used to make clusters of well log data and to group them using different cluster consolidation options available as discussed below.

5.4.1 Selection of Variables

The variables used are the ones represented in well log curves. Every well log curve represents a physical property of rocks along the well path. So the selection of well log curves should be based on the rocks characteristics to be identified. In this work, the objective of making electrofacies is to characterize Sarah Formation and its geomechanical characteristics. Since Sarah Formation is a tight sand, well log curves should be sensitive to evaluate tight sandstone and their geomechanical properties. Therefore, the following well logs were used:

1. Compressional wave travel time (DTCO)
2. Shear wave travel time (DTSM)
3. Gamma ray (GR_EDTC)
4. Deep resistivity (LLD)
5. Long spaced photoelectric effect (PEFL)
6. Thermal neutron porosity (TNPH)
7. Formation potassium concentration (HFK)
8. Dry weight fraction (Quartz, Feldspar and Mica) (WQFM_WALK2)

The depth zone and well log curves used for Well-C are given in Figure 4.1. This module gives options to select different depths to build and to run the model developed. Different wells can also be selected to build and run the cluster analysis model.

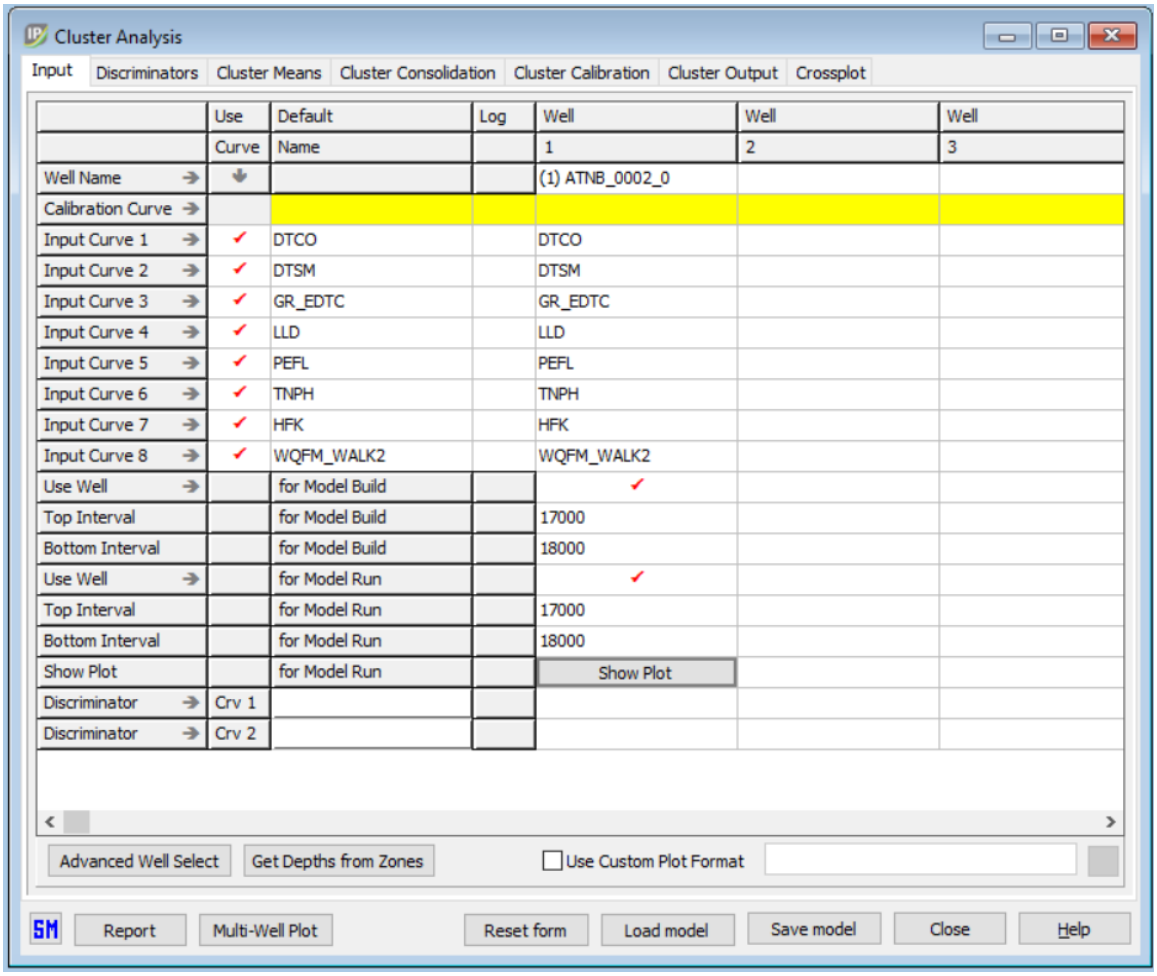

Figure 5.1 Custer analysis module user interface showing well logs selected for Well-C

5.4.2 Clustering of variables

K-means clustering was applied to cluster well log data as mentioned before. The number of clusters to be formed was selected as 10 before running the analysis. The same data set is used for model run as for building this model. K-means clustering first calculates the mean value for each curve. To calculate the mean value, every cluster should be initialized with some value. This initialization was performed using the "Seed Clusters" options available in the software. This option carries out principal component analysis on the data

set. The data is then divided into the decided number of clusters and then the mean value of each cluster is calculated iteratively as explained in Section 5.2.1.

After seeding and clustering, the software gives the number of points in each cluster and the spread of each cluster. The mean and standard deviation of each well log curve corresponding to a cluster were also calculated to analyze their contribution to that specific cluster. The number of points in ten clusters formed for Well-C and their corresponding mean and standard deviation of each well log curve are shown in Figure 4.2.

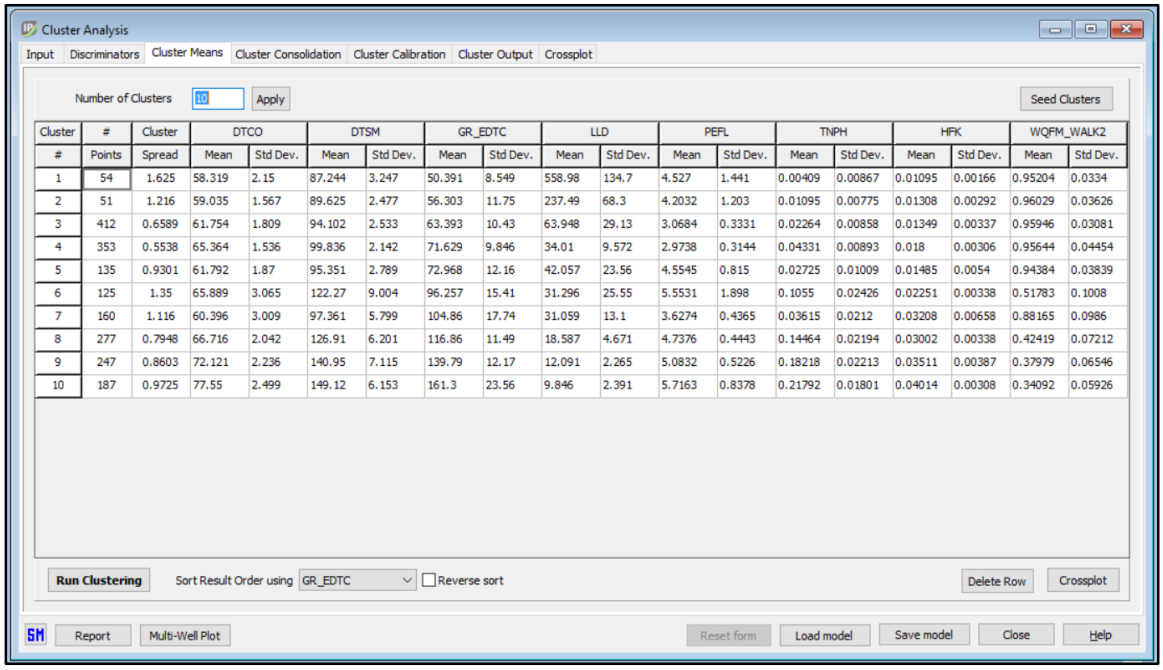

Cluster #	# Points	Cluster Spread	DTCO Mean	DTCO Std Dev.	DTSM Mean	DTSM Std Dev.	GR_EDTC Mean	GR_EDTC Std Dev.	LLD Mean	LLD Std Dev.	PEFL Mean	PEFL Std Dev.	TNPH Mean	TNPH Std Dev.	HFK Mean	HFK Std Dev.	WQFM_WALK2 Mean	WQFM_WALK2 Std Dev.
1	54	1.625	58.319	2.15	87.244	3.247	50.391	8.549	558.98	134.7	4.527	1.441	0.00409	0.00867	0.01095	0.00166	0.95204	0.0334
2	51	1.216	59.035	1.567	89.625	2.477	56.303	11.75	237.49	68.3	4.2032	1.203	0.01095	0.00775	0.01308	0.00292	0.96029	0.03626
3	412	0.6589	61.754	1.809	94.102	2.533	63.393	10.43	63.948	29.13	3.0684	0.3331	0.02264	0.00858	0.01349	0.00337	0.95946	0.03081
4	353	0.5538	65.364	1.536	99.836	2.142	71.629	9.846	34.01	9.572	2.9738	0.3144	0.04331	0.00893	0.018	0.00306	0.95644	0.04454
5	135	0.9301	61.792	1.87	95.351	2.789	72.968	12.16	42.057	23.56	4.5545	0.815	0.02725	0.01009	0.01485	0.0054	0.94384	0.03839
6	125	1.35	65.889	3.065	122.27	9.004	96.257	15.41	31.296	25.55	5.5531	1.898	0.1055	0.02426	0.02251	0.00338	0.51783	0.1008
7	160	1.116	60.396	3.009	97.361	5.799	104.86	17.74	31.059	13.1	3.6274	0.4365	0.03615	0.0212	0.03208	0.00658	0.88165	0.0986
8	277	0.7948	66.716	2.042	126.91	6.201	116.86	11.49	18.587	4.671	4.7376	0.4443	0.14464	0.02194	0.03002	0.00338	0.42419	0.07212
9	247	0.8603	72.121	2.236	140.95	7.115	139.79	12.17	12.091	2.265	5.0832	0.5226	0.18218	0.02213	0.03511	0.00387	0.37979	0.06546
10	187	0.9725	77.55	2.499	149.12	6.153	161.3	23.56	9.846	2.391	5.7163	0.8378	0.21792	0.01801	0.04014	0.00308	0.34092	0.05926

Figure 5.2 Clusters' spread and their corresponding mean and standard deviation of each well log curve for Well-C

The effectiveness of the model and the contribution of each well log curve to the clusters generated can be determined using the multi curve cross-plot module. This module plots all curves with each other separately so that the contribution of each curve (variable) used

can be analyzed. Some of the crossplots showing poor and good contribution from Well-C are illustrated in Figures 5.3 and 5.4. In Figure 5.3, the crossplot between LLD and PEFL is clearly separating red cluster from other clusters while in Figure 5.4 the red cluster is overlapped by other clusters in a crossplot between HFK and WQFM_WALK2.

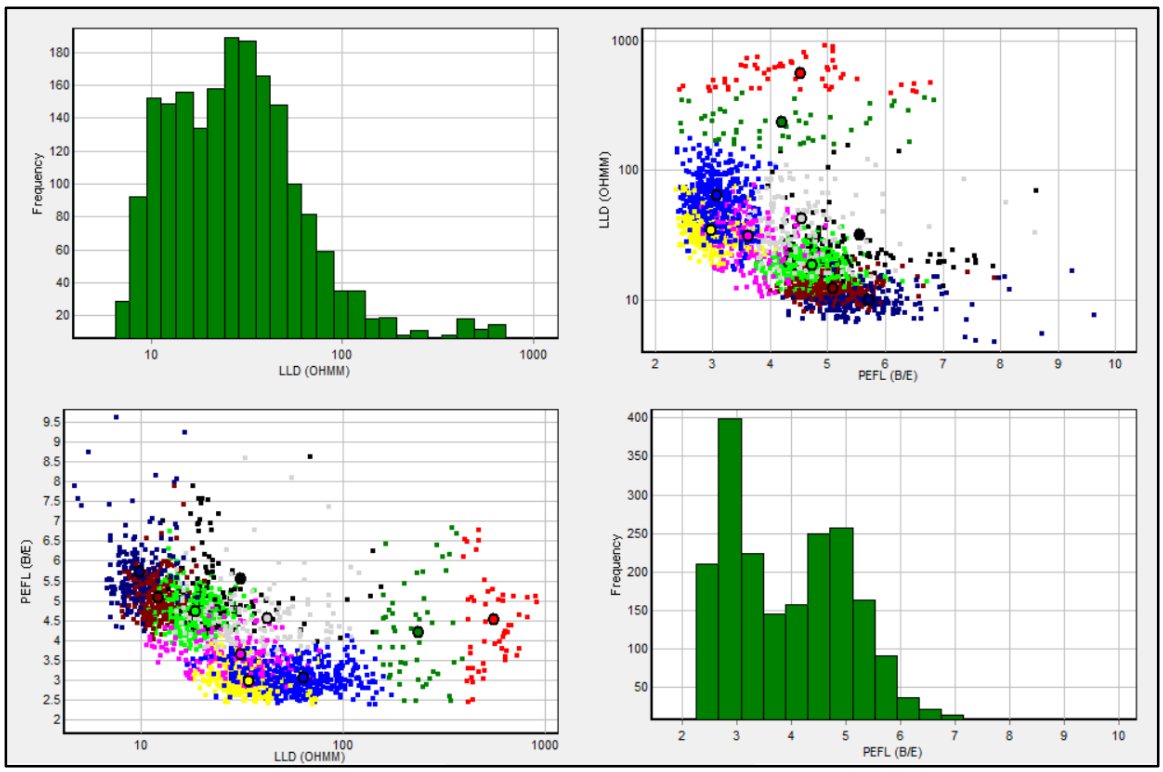

Figure 5.3 Multi curve crossplots showing good clustering between Deep Resistivity (LLD) and Photoelectric Effect (PEFL) log for Well-C

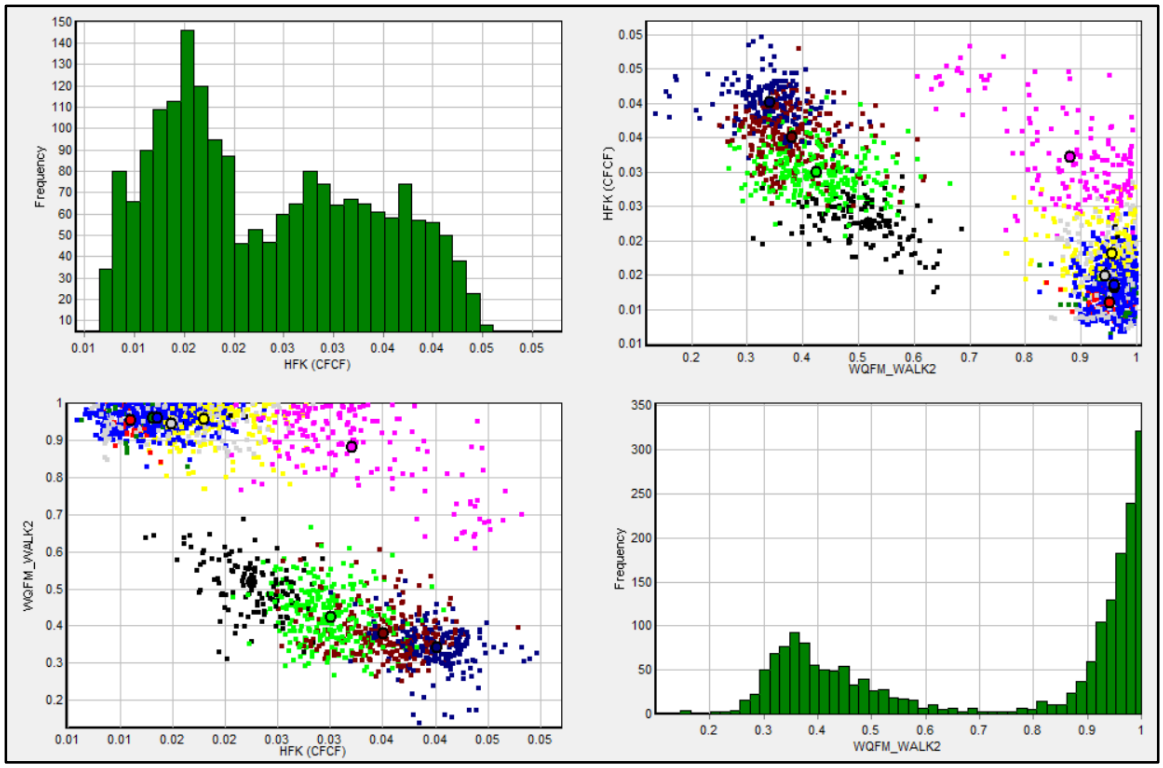

Figure 5.4 Multi curve crossplots showing bad clustering between Formation Potassium Concentration (HFK) and Dry Weight Fraction Quartz+Feldspar+Mica (WQFM_WALK2) log for Well-C

5.4.3 Cluster consolidation

Cluster consolidation was done to give geological meaning to electrofacies by combining alike clusters. It can be done manually or using hierarchical clustering. In this work, hierarchical clustering was used which groups the closest clusters based on the distance between them. All clusters are merged in this way to a single cluster and the result is shown as a dendrogram. Different methods can be used to form the dendrogram. We have adopted the method which minimizes the within-cluster sum of squares distance and gives good results by separating different rock lithologies into different clusters. The number of groups to be formed should be defined before conducting consolidation. Dendrogram for the

cluster consolidation of Well-C was constructed and illustrated in Figure 5.5. It shows the merged clusters and their order of merging as given on the top of each branch. In this model, ten clusters were merged in six groups and each group is considered as a separate facies with its unique characteristic response in all well log curves used.

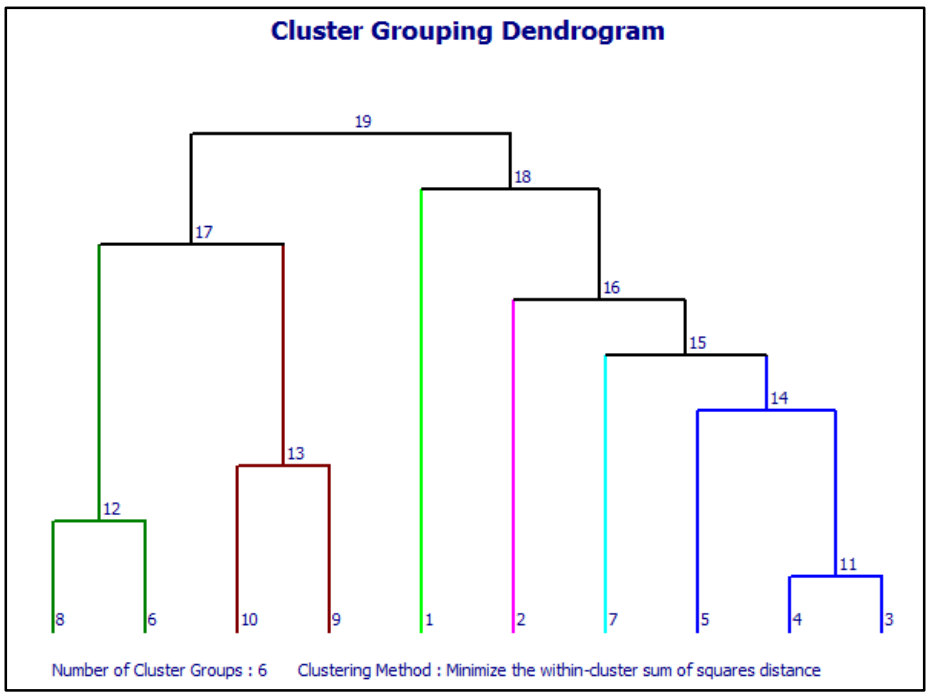

Figure 5.5 Dendrogram of cluster consolidation for Well-C

The grouping of clusters can be analyzed by the cluster randomness plot which gives information about how random or organized is a group of clusters by calculating their apparent randomness. This plot shows how random is the grouping as compared to a completely random grouping.

The randomness plot for cluster consolidation of Well-C is given in Figure 5.6. Higher values show more arranged grouping of clusters while a lower value refers to more randomness. A value of 1 means that the cluster is totally random.

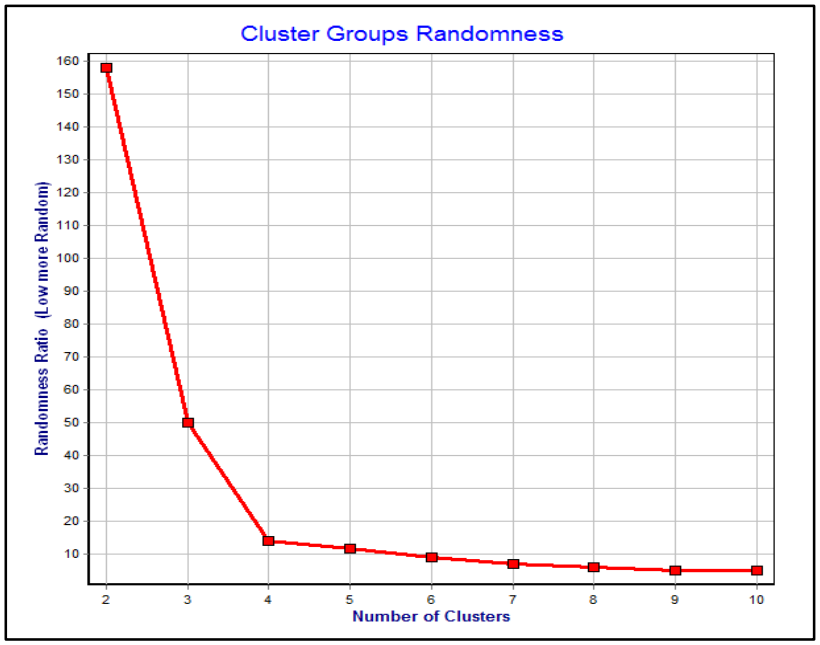

Figure 5.6 Cluster randomness plot for Well-C

5.4.4 Facies Model

The result of clustering can be shown in the form of a facies model. Six facies were defined (Figure 5.7) and assigned with different colors to be distinguished from each other. The clusters included in every facies are also given.

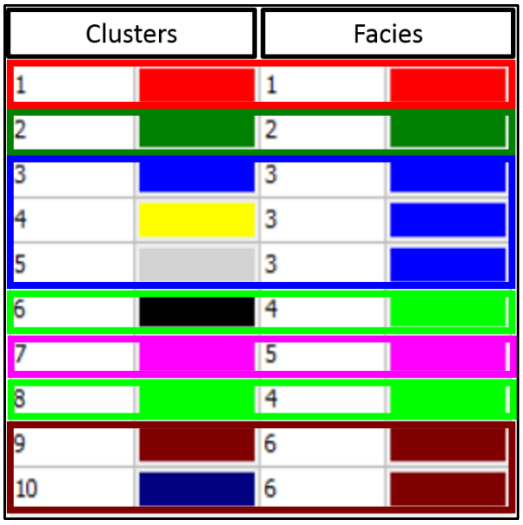

Figure 5.7 Faices and their corresponding clusters for Well-C

The electrofacies developed for Well-C along with the well logs used are shown in Figure 5.8. The second last track in Figure 5.8 is showing all ten clusters formed and the width of each cluster is based on the distance between clusters as shown in the track before. The last track is showing six facies after cluster consolidation. The defined clusters and electrofacies association with interpreted lithologies based on the information available from mud log data and literature on the geological formations present in the area is given in Table 5.1.

Table 5.1 Electrofacies accosiation with lithologies

Clusters	Facies	Associated Lithologies
1	1	Shale
2	2	Shale
3	3	Sandstone
4	3	Sandstone
5	3	Sandstone
6	4	Shale
7	5	Mudstone
8	4	Shale
9	6	Shale
10	6	Shale

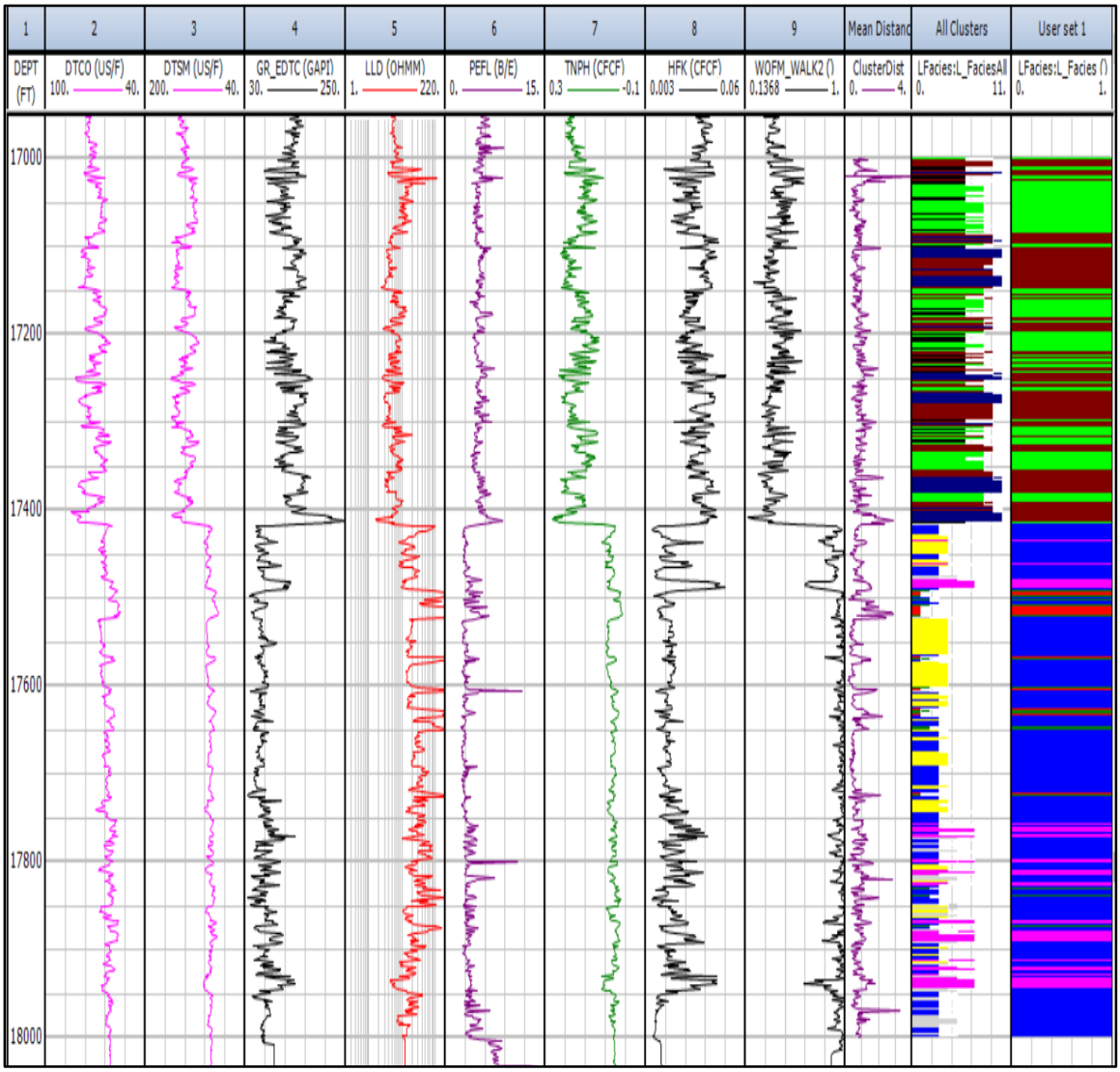

Figure 5.8 Electrofacies model and well logs used for Well-C

In Figure 5.9, the depth interval from 17000 ft. to 17415 ft. comprised of Facies-4 and Facies-6, which is actually the lower part of Qusaiba Formation. The interval from 17415 ft.to 17490 ft. is Baq'a Formation which consists of sandstone and is dominated by Facies-3. Baq'a Formation is underlain by Sarah Formations (17490 ft.-17730 ft.) which comprises of Facies-3 dominantly with thin portions of Facies-1, Facies-2 and Facies-5. The lowest portion of the facies model from 17730 ft. to 18000 ft. is the upper part of Qasim Formation which contains alternations of Facies-3 and Facies-5.

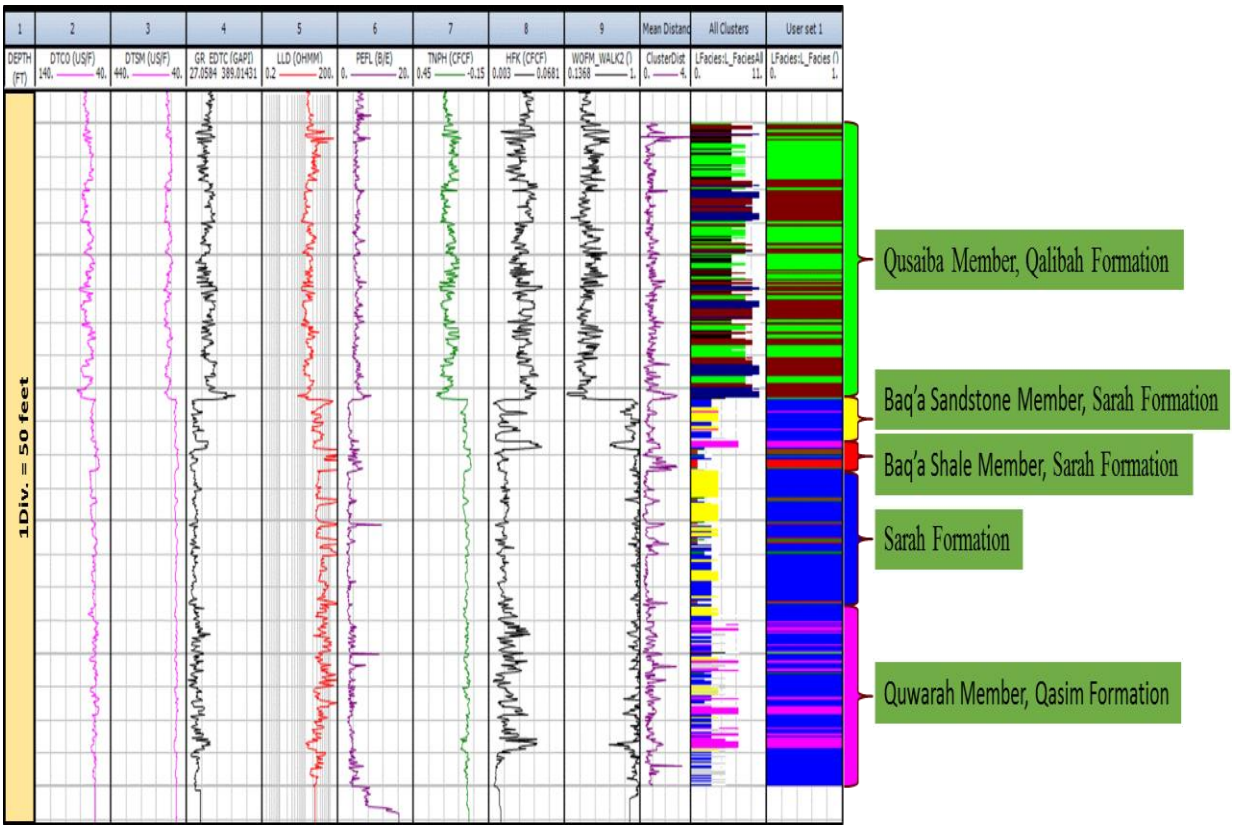

Figure 5.9 Electrofacies model correlation with geological formations for Well-C

5.5 Integration of electrofacies with geomechanical characteristics

One of the objectives in this study is the interpretation of electrofacies with respect to their geomechanical characteristics. As every facies in the model developed is unique so it should have its own unique geomechanical characteristics. For this purpose, all the profiles developed for the MEM in Section 4.5 were compared with the corresponding electrofacies (Figure 5.10). The results show that all major and minor facies in the model have good matches with elastic and strength parameters profiles. It is obvious from the Figure 5.10 that every facies defined has a unique trend in all geomechanical profiles which is the characteristic of that facies. The model also has a good correlation with pore pressure profile and safe mud weight window which is based on the stresses calculated as shown in Figure 5.11.

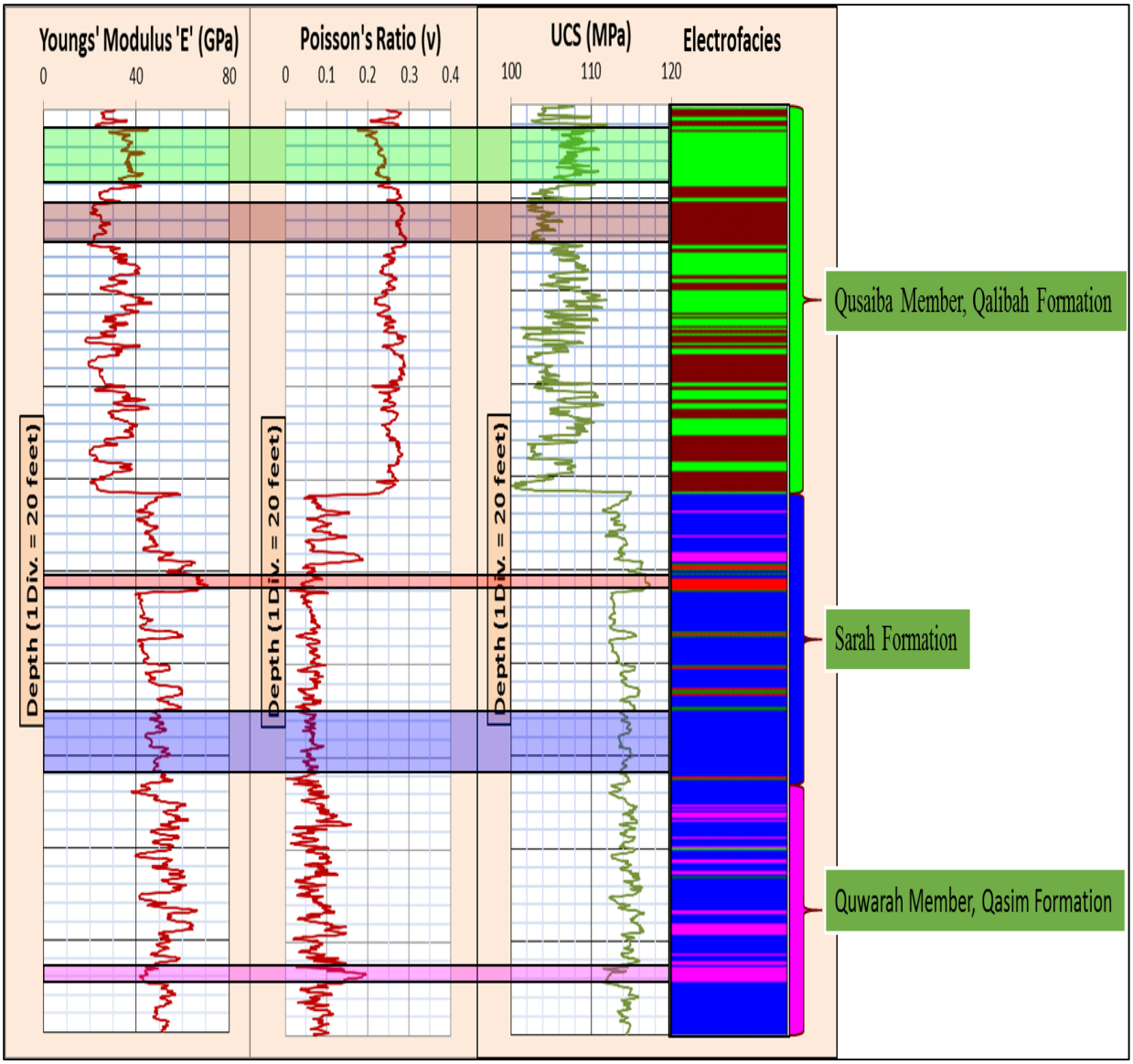

Figure 5.10 Electrofacies model correlation geomechanical parameters showing unique responses in terms of (a) Young's modulus (b Poisson's ratio (c) Unconfined compressive strength (UCS) for Well-C

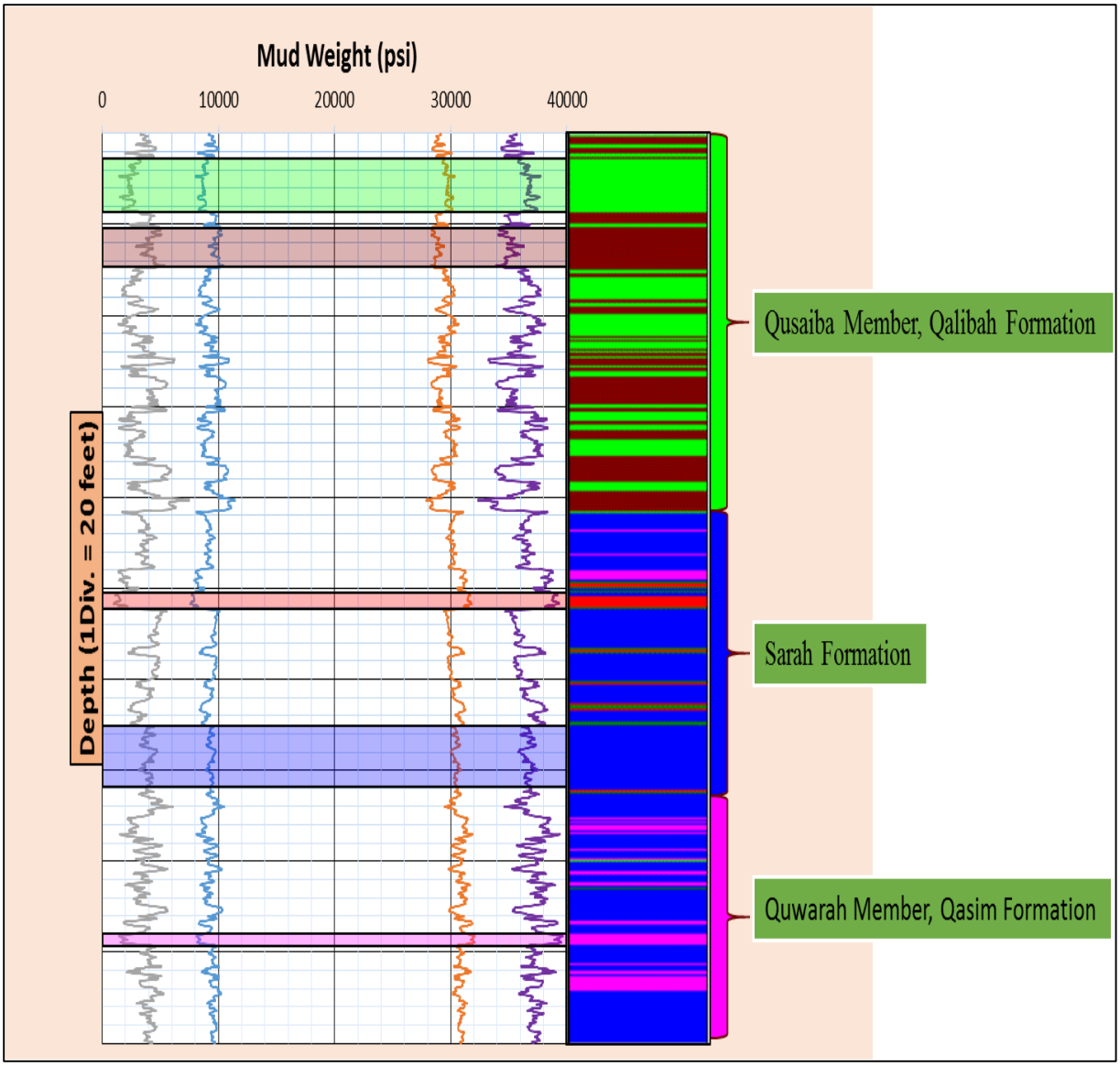

Figure 5.11 Electrofacies model correlation showing unique responses in terms of (a) Safe mud weight window (b) Pore Pressure for Well-C

CHAPTER 6

CONCLUSIONS AND RECOMMENDATIONS

6.1 Conclusions

6.1.1 Electrofacies Characterization

The constructed electrofacies model for Sarah Formation in subsurface has led to the following conclusions:

- The results revealed that the electrofacies model is highly effective for identifying Sarah Formation boundaries.
- The electrofacies model for Sarah Formation has led to the identification of three units:
    - Baq'a Sandstone Member
    - Baq'a Shale Member
    - Sarah Formation
- The well log suite that best characterize the Paleozoic secession including lower Qusaiba Formation, Sarah Formation and Upper Qasim Formation using electrofacies model include the following:
    - Compressional wave travel time (DTCO)
    - Shear wave travel time (DTSM)

- Gamma ray (GR_EDTC)
- Deep resistivity (LLD)
- Long spaced photoelectric effect (PEFL)
- Thermal neutron porosity (TNPH)
- Formation potassium concentration (HFK)
- Dry weight fraction (Quartz, Feldspar and Mica) (WQFM_WALK2)

6.1.2 Geomechanical Characterization

- Changes in P-wave and S-wave velocities of Sarah Formation core samples show direct relation with porosity and density.
- The Strength testing (Uniaxial Compression Test) of core samples shows high variability in strength properties.
- Sharp changes in mechanical properties and pore pressure exhibited the presence of over-pressured and under-pressured zones within the formation.
- Average values of Young's modulus and Poisson's ratio indicate high stiffness and brittle nature of the formation.
- The reverse stress regime exists at the study area with a maximum stress gradient of 1.18 psi/ft.
- The required mud weight for safe drilling operation is ranging from 11,000 psi to 29,000 psi for Sarah Formation interval.

- Integration of MEM with electrofacies helps to define mechanical properties through electrofacies.

6.2 Recommendations

Some recommendations to be considered in similar type of future studies are as follows;

- To assess the accuracy of electrofacies model, it should be used in other regions to recognize Sarah Formation or its equivalent formations (e.g. Zarqa Formation) in subsurface.

- The efficiency of electrofacies model can be improved using variables from additional wells.

- Triaxial compressive testing should be performed to get more accurate values for failure parameters (c and Φ) and to better understand the geomechanical behavior under reservoir pressure conditions.

- To enhance the reliability of the MEM, field test data such as the extended leak-off tests should be used.

- Reservoir Simulation should be run using calculated dynamic and static elastic moduli to define fracture stimulation treatment. This will help in assessing fracture compatibility, containment, and complexity within Sarah Formation.

- A 3D MEM should be built incorporating elastic and failure parameters extracted for seismic data and more scattered wells for better delineation of the variations in mechanical properties and Earth stresses.

- Complete reservoir characterization needs integration of geochemical data and geomechanical properties.

References

Addis, M. A., and Yassir, N. (2010). An Overview of Geomechanical Engineering Aspects of Tight Gas Sand Developments. SPE/DGS Saudi Arabia Section Technical Symposium and Exhibition, 4-7 April, Al-Khobar, Saudi Arabia. doi:10.2118/136919-MS

Adisornsuapwat, K., Phuat-tan, C., Anis, L., Vantala, A., Juman, R., and Boyce, B. (2011). Enhanced Geomechanical Modeling with Advanced Sonic Processing to Delineate and Evaluate Tight Gas Reservoirs. SPE Middle East Unconventional Gas Conference and Exhibition, 31 January-2 February, Muscat, Oman. doi:10.2118/142813-MS

Afsari, M., Ghafoori, M., Roostaeian, M., Haghshenas, A., Ataei, A., and Masoudi, R. (2009). Mechanical Earth Model (MEM): An Effective Tool for Borehole Stability Analysis and Managed Pressure Drilling (Case Study). SPE Middle East Oil and Gas Show and Conference, 15-18 March, Manama, Bahrain. doi:10.2118/118780-MS

Ali, A. H. A., Brown, T., Delgado, R. et al. (2003). Watching Rocks Change—Mechanical Earth Modeling. Oilfield Rev. 15 (1): 22–39

El-Deek, I. (2014). Sedimentological Heterogeneity of the Late Ordovician Glacio-Fluvial Sarah Formation, Al-Qaseem Area, Saudi Arabia: Impact on Petrophysical Properties and Reservoir Quality. MSc Thesis, King Fahd University of Petroleum and Minerals, Saudi Arabia

Al-Mahmoud, M. J., and Al-Ghamdi, I. (2010). An Overview of Tight Gas Reservoirs in Saudi Arabia. Second Middle East Tight Gas Reservoirs Workshop - Exploration and Development Strategies 12-15 December 2010, Manama, Bahrain. doi:10.3997/2214-4609.20145641

Al-Zayer, A., Mesdour, R., Al-Faleh, K., Basri, M., and Utaibi, A. (2013, May 19). Practical Well Testing Analysis Considerations in Heterogeneous Sandstone. SPE Saudi Arabia Section Technical Symposium and Exhibition, 19-22 May, Al-Khobar, Saudi Arabia. doi:10.2118/168092-MS

Babker, J. M. A. (2015). The relationship between litho-stratigraphy and geomechanical properties of Sarah Formation outcrop analogue, Central Saudi Arabia. MSc Thesis, King Fahd University of Petroleum and Minerals, Saudi Arabia

Briner, A. P., Hulver, M., Azzouni, A., and Harvey, C. (2010). Regional Reservoir Quality of a Tight Gas Play: the Ordovician Sarah Formation in the Rub' Al Khali Basin of Southern Saudi Arabia. Second Middle East Tight Gas Reservoirs Workshop - Exploration and Development Strategies 12-15 December 2010, Manama, Bahrain.

Bucheb, J. A., and Evans, H. B. (1994). Some Applications Of Methods Used In Electrofacies Identification. The Log Analyst. 35 (01).

Bu-Khamseen, R. H., Sierra, L., Young, D. A., and Machala, M. S. (2010). First Successful Tight Gas Reservoir Completion and Fracture Stimulation in Sarah Formation, Rub Al-Khali Empty Quarter of Saudi Arabia. SPE Deep Gas Conference and Exhibition, 24-26 January, Manama, Bahrain. doi:10.2118/130722-MS

Clark-Lowes, D. D. (2005). Arabian glacial deposits: recognition of paleovalleys within the Upper Ordovician Sarah Formation, Al Qasim district, Saudi Arabia, Proceedings of Geologists Association. 116: 331-347.

Cornish, R. (2007). Statistics: 3.1 cluster analysis. Retrieved March 7, 2016, from: http://mlsc.Iboro.ac.uk/resources/statistics/clusteranalysis.pdf.

Eaton, B. A. (1975). The Equation for Geopressure Prediction from Well Logs. Fall Meeting of the Society of Petroleum Engineers of AIME, 28 September-1 October, Dallas, Texas. doi:10.2118/5544-MS

Euzen, T. (2012). Well log cluster analysis and electrofacies classification: a probabilistic approach for integrating log with mineralogical data. CSPG CSEG CWLS Joint Annual Convention, Calgary. Open Geosciences. 6 (3): 393–402

Euzen, T., Delamaide, E., Feuchtwanger, T., and Kingsmith, K. D. (2010). Well Log Cluster Analysis: An Innovative Tool for Unconventional Exploration. Canadian Unconventional Resources and International Petroleum Conference, 19-21 October, Calgary, Alberta, Canada. doi:10.2118/137822-MS

Euzen, T., Power, M., Crombez, V., Rohais, S., Petrovic, M., and Carpentier, B. (2014). Lithofacies, Organic Carbon and Petrophysical Evaluation of the Montney and Doig Formations (Western Canada): Contribution of Quantitative Cuttings Analysis and Electrofacies Classification. CSPG CSEG CWLS Joint Annual Convention, 12-16 May 2014, Calgary.

Forsyth, D., Al Musharfi, N. M., and Al Marzooq, A. M. (2011). Tight Gas Petrophysical Challenges in Saudi Aramco. SPE/DGS Saudi Arabia Section Technical Symposium and Exhibition, 15-18 May, Al-Khobar, Saudi Arabia. doi:10.2118/149048-MS

Fraley, C., and Raftery, A. E. (1998). How Many Clusters? Which Clustering Method? Answers via Model-Based Cluster Analysis. The Computer Journal, 41(8), 578–588. doi:10.1093/comjnl/41.8.578

Gupta, R., and Johnson, H. D. (2001). Characterization of heterolithic deposits using electrofacies analysis in the tide-dominated Lower Jurassic Cook Formation (Gullfaks Field, offshore Norway). Petroleum Geoscience, 7 (3): 321–330. doi:10.1144/petgeo.7.3.321

Gupta, R., and Johnson, H. D. (2002). High-resolution facies architecture of heterolithic tidal deposits: an integrated outcrop and electrofacies analysis of a complex reservoir. In Geological Applications of Well Logs, 13: 161–184.

Hayton, S., Heine, C., and Gratto, B. E. (2010). Tight Gas Exploration in Saudi Arabia. SPE Deep Gas Conference and Exhibition, 24-26 January, Manama, Bahrain. doi:10.2118/131065-MS

Holditch, S. A. (2006). Tight Gas Sands. Journal of Petroleum Technology. 58 (06): 86 - 93 doi:10.2118/103356-JPT

Husseini, M. I. (1989). Tectonic and depositional model of Late Precambrian - Cambrian Arabian and adjoining plates. American Association of Petroleum Geologists Bulletin, 73(September): 1117–1131.

Jacobi, D. J., Breig, J. J., LeCompte, B., Kopal, M., Hursan, G., Mendez, F. E., Longo, J. (2009). Effective Geochemical and Geomechanical Characterization of Shale Gas Reservoirs From the Wellbore Environment: Caney and the Woodford Shale. SPE Annual Technical Conference and Exhibition, 4-7 October, New Orleans, Louisiana. doi:10.2118/124231-MS

John, A. K., Lake, L. W., Torres-Verdin, C., and Srinivasan, S. (2005). Seismic-Based Facies Identification and Classification Using Simple Statistics. SPE Annual Technical Conference and Exhibition, 9-12 October, Dallas, Texas. doi:10.2118/96577-MS

Konert G, Afifi AM, Al-Hajri S, de Groot K, Al Naim, A.A., Droste H. J. (2001). Paleozoic stratigraphy and hydrocarbon habitat of the arabian plate. AAPG Memoir 74: 483-515

Konert, G., Afifi, A.M., Hajri, S.A, and Droste, H. J. (2001). Paleozoic stratigraphy and hydrocarbon habitat of the Arabian Plate. GeoArabia, 6: 407-442.

Konert, G., Afifi, A. M., Al-Hajri, S. A., de Groot, K., Al Naim, A., and Droste, H. J. (2001). Paleozoic stratigraphy and hydrocarbon habitat of the Arabian Plate. Petroleum Provinces of the Twenty-First Century, 74(January 2001): 483–516.

Laboun, A. A. (2010). Paleozoic tectono-stratigraphic framework of the Arabian Peninsula. Journal of King Saud University - Science, *22*(1): 41–50.

Law, B. E., and Curtis, J. B. (2002). Introduction to unconventional petroleum systems. AAPG Bulletin, 86(11): 1851–1852. doi: 10.1306/61EEDDA0-173E-11D7-8645000102C1865D

Lee, S. H., Kharghoria, A., and Datta-Gupta, A. (2002). Electrofacies Characterization and Permeability Predictions in Complex Reservoirs. SPE Reservoir Evaluation and Engineering 5 (03): 237 - 248. doi:10.2118/78662-PA

M., Esteban, L., Delle Piane, C., Sarout, J., Dewhurst, D. N., and Clennell, M. B. (2012). Laboratory characterisation of shale properties. Journal of Petroleum Science and Engineering, 88-89: 107–124. doi:10.1016/j.petrol.2012.01.023

MacQueen, J. B. (1967). Some Methods for classification and Analysis of Multivariate Observations. 5th Berkeley Symposium on Mathematical Statistics and Probability 1967, 1(233): 281–297.

Milligan, G. W., and Cooper, M. C. (1985). An examination of procedures for determining the number of clusters in a data set. Psychometrika, 50(2): 159–179.

Parker, M. A., Buller, D., Petre, J. E., and Dreher, D. T. (2009). Haynesville Shale-Petrophysical Evaluation. SPE Rocky Mountain Petroleum Technology Conference, 14-16 April, Denver, Colorado. doi:10.2118/122937-MS

Plumb, R., Edwards, S., Pidcock, G., Lee, D., and Stacey, B. (2000). The Mechanical Earth Model Concept and Its Application to High-Risk Well Construction Projects. IADC/SPE Drilling Conference, 23-25 February, New Orleans, Louisiana. doi:10.2118/59128-MS

Powers, R.W., Ramirez, L.F., Redmond, C.D. and Elberg, E.L. (1966). Geology of the Arabian Peninsula, Sedimentary geology of Saudi Arabia. Geological Survey Professional Paper 560-D, United States Government Printing Office, Washington, 147pp.

Ranger, M. J. (2014). Determining Facies from Wireline Logs using Discriminant Analysis, Geoconvention May 12-16, 2014, Alberta, Canada.

Razzaq, W. (2013). Sedimentological and Petrophysical Characterization of Sarah Formation with the Aid of Gis, Central Saudi Arabia. MSc Thesis, King Fahd University of Petroleum and Minerals, Saudi Arabia

Rushing, J. A., Newsham, K. E., and Blasingame, T. A. (2008). Rock Typing: Keys to Understanding Productivity in Tight Gas Sands. SPE Unconventional Reservoirs Conference, 10-12 February, Keystone, Colorado, USA. doi:10.2118/114164-MS

Sahin, A., Hassan, H. M. (1998). Enhancement of Permeability Variograms using Outcrop Data. The Arabian Journal for Science and Engineering. 23(1C): 137-144

Serra, O., and Abbott, H. T. (1982). The Contribution of Logging Data to Sedimentology and Stratigraphy. Society of Petroleum Engineers Journal 22 (01): 117 - 131.

Solano, N. A., Clarkson, C. R., and Krause, F. (2012). Quantification of cm-Scale Heterogeneities in Tight-Oil Intervals of the Cardium Formation at Pembina, WCSB, Alberta, Canada. SPE Canadian Unconventional Resources Conference, 30 October-1 November, Calgary, Alberta, Canada. doi:10.2118/162837-MS

Stern, R. J., and Johnson, P. (2010). Continental lithosphere of the Arabian Plate: A geologic, petrologic, and geophysical synthesis. Earth-Science Reviews, 101 (2010) 29–67. doi:10.1016/j.earscirev.2010.01.002

Vaslet D. (1987a). Early Paleozoic glacial deposits in Saudi Arabia, a lithostratigraphic revision. Saudi Arabian Deputy Ministry for Mineral Resources Technical Record BRGM-TR-07-1, p. 24.

Weibel, R., Kristensen, L., Olivarius, M., Leth Hjuler, M., Mathiesen, A., and Nielsen, L. H. (2012). Investigating Deviations from Overall Porosity−Permeability Trends. Thirty-Sixth Workshops on Geothermal Reservoir Engineering, Stanford University, California. SGP-TR-194

Appendix - A

Locations of Core Plugs

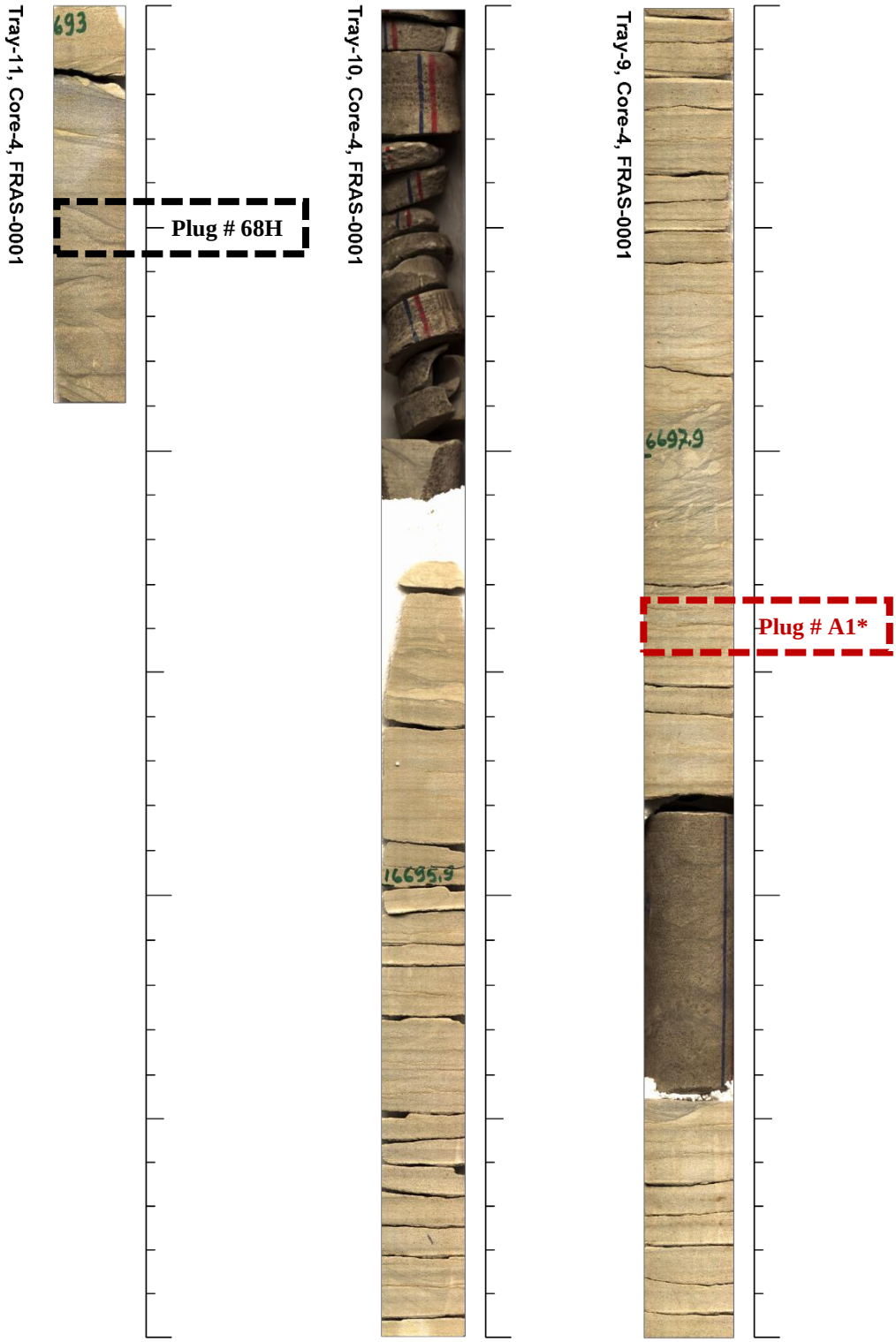

Well-A, Tray 11, 10 and 9

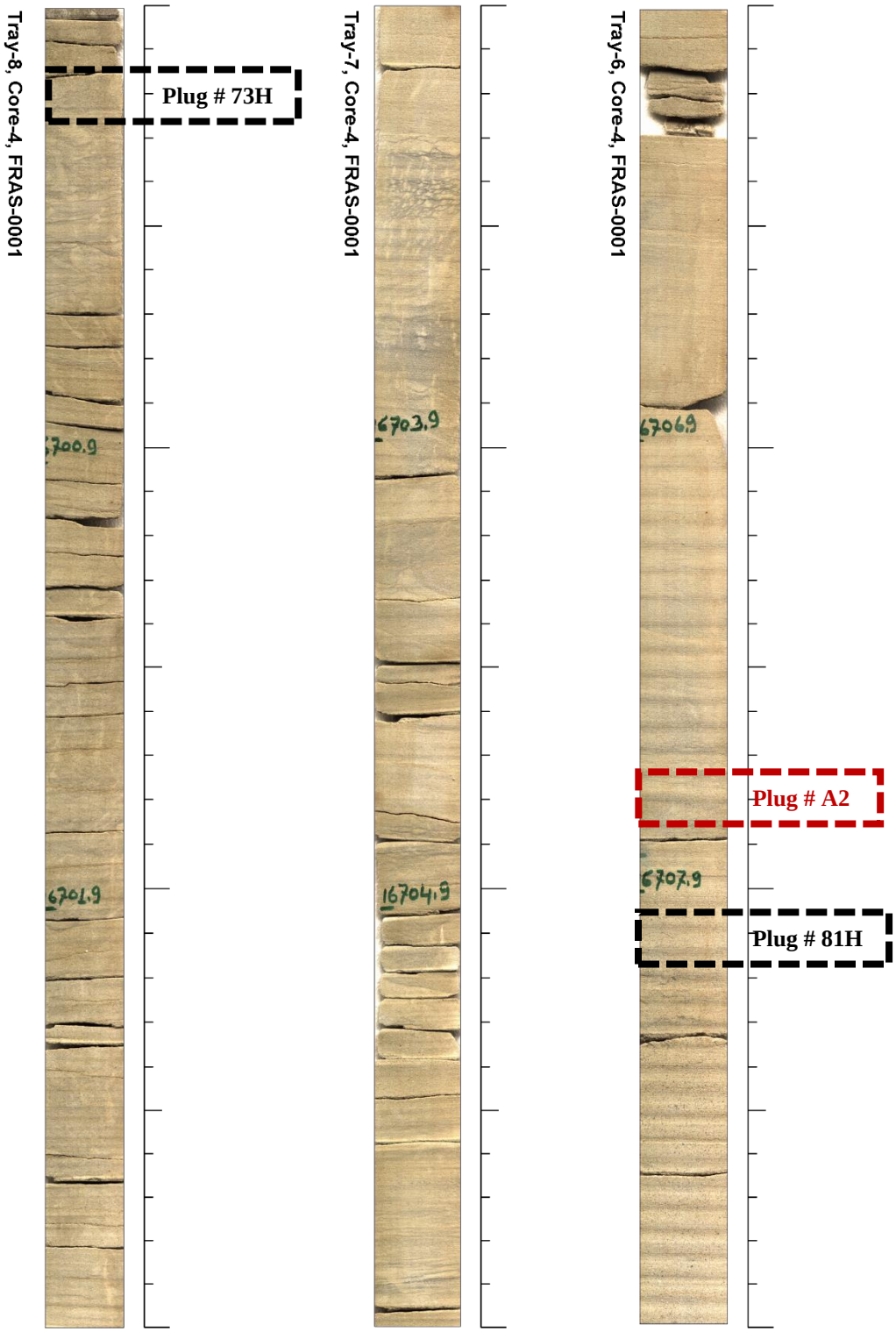

Well-A, Tray 8, 7 and 6

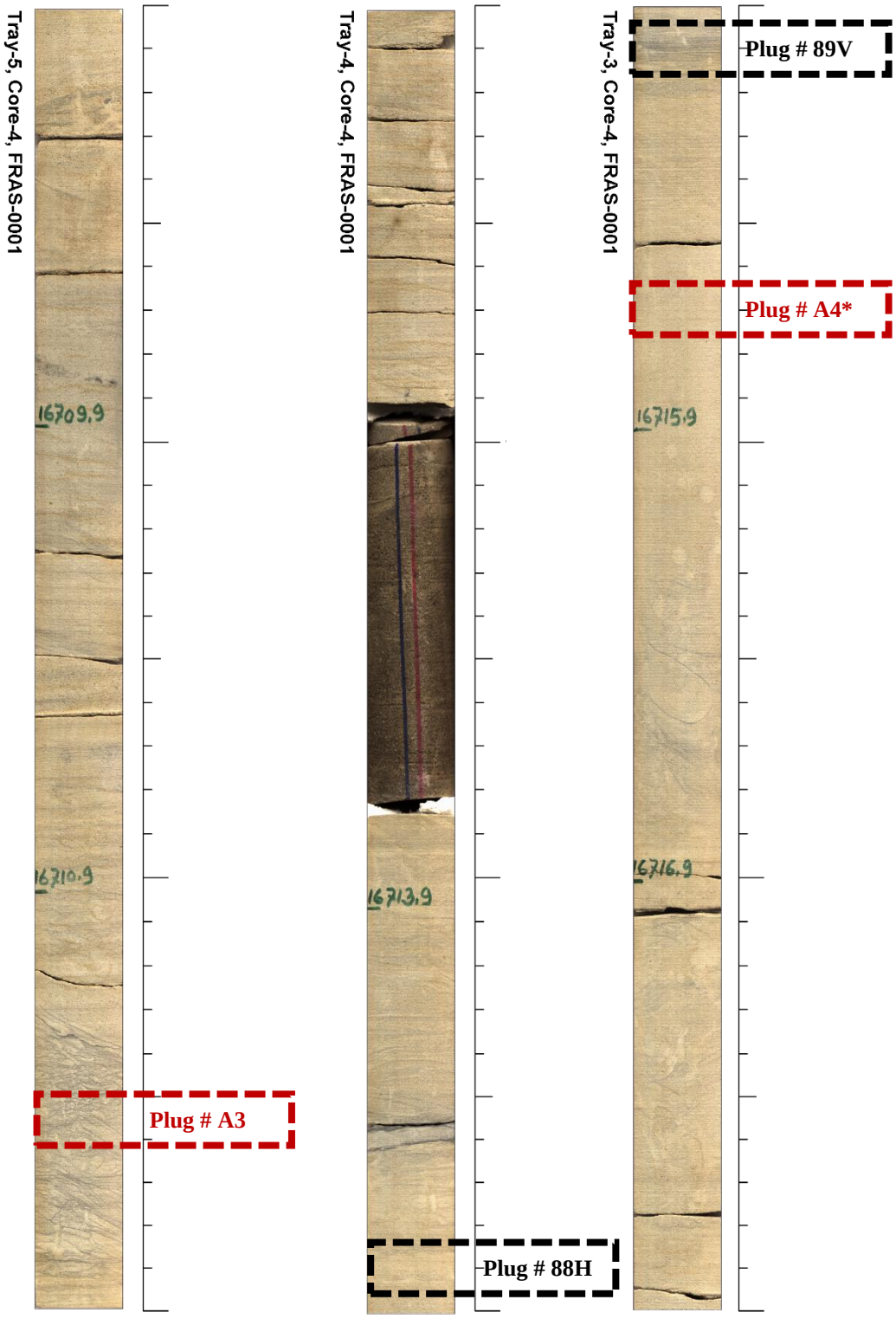

Well-A, Tray 5, 4 and 3

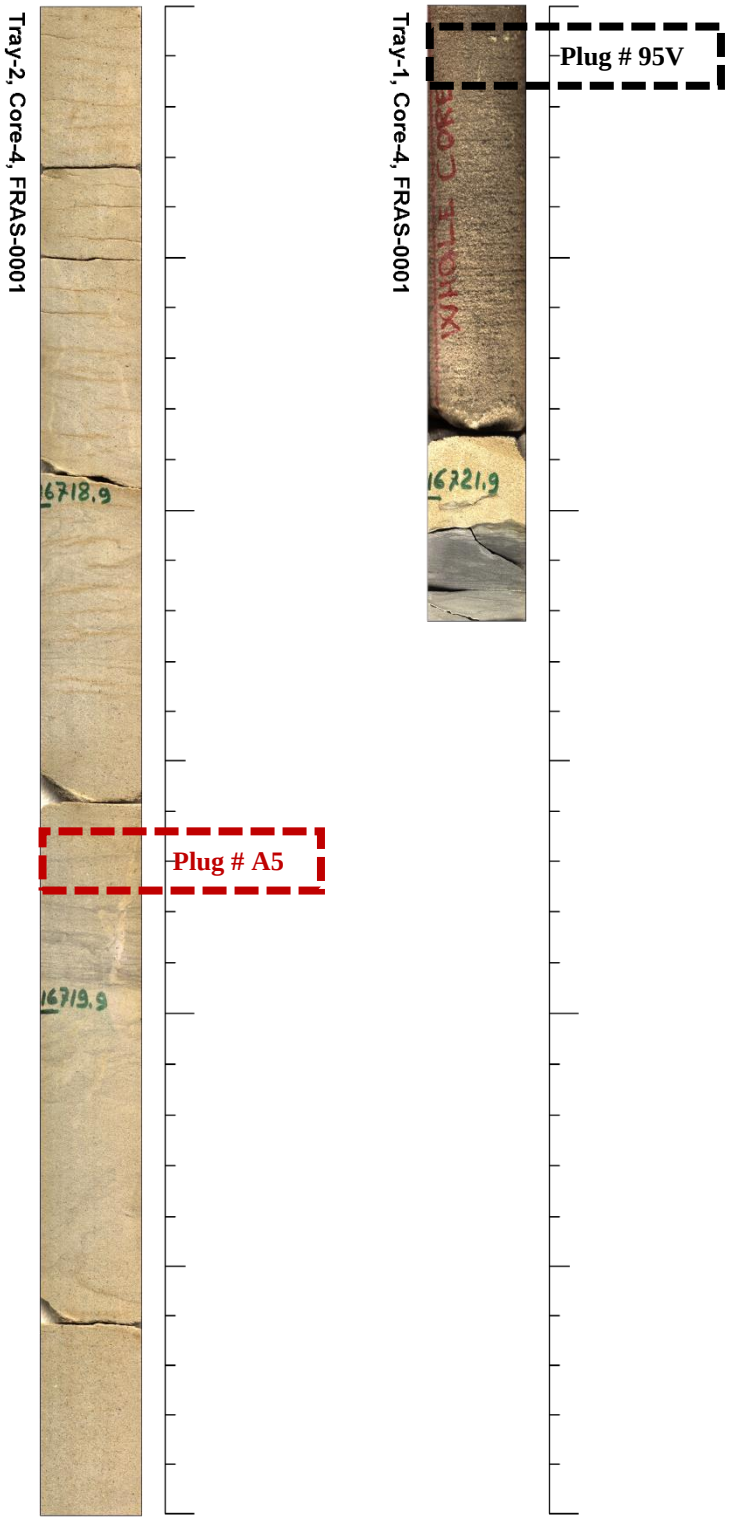

Well-A, Tray 2 and 1

Well-B, Tray 8, 6 and 5

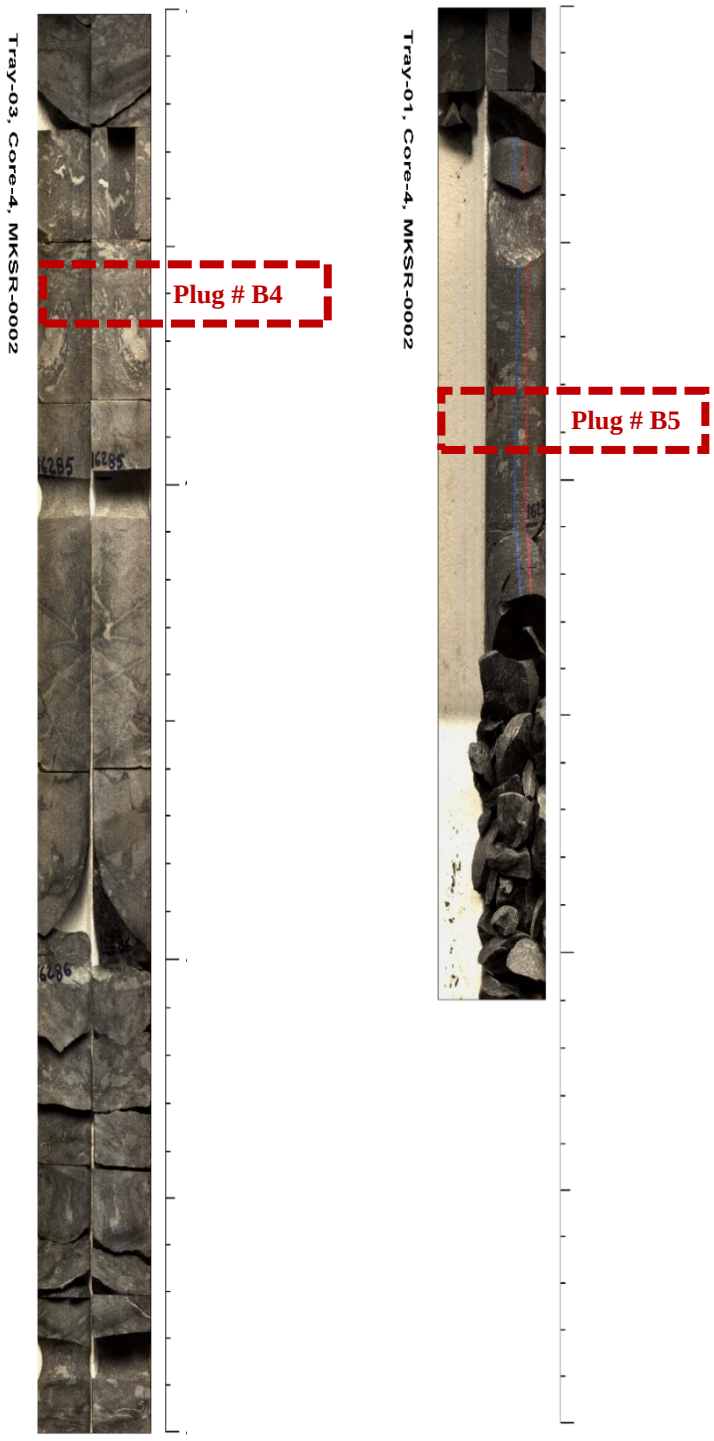

Well-B, Tray 8, 6 and 5

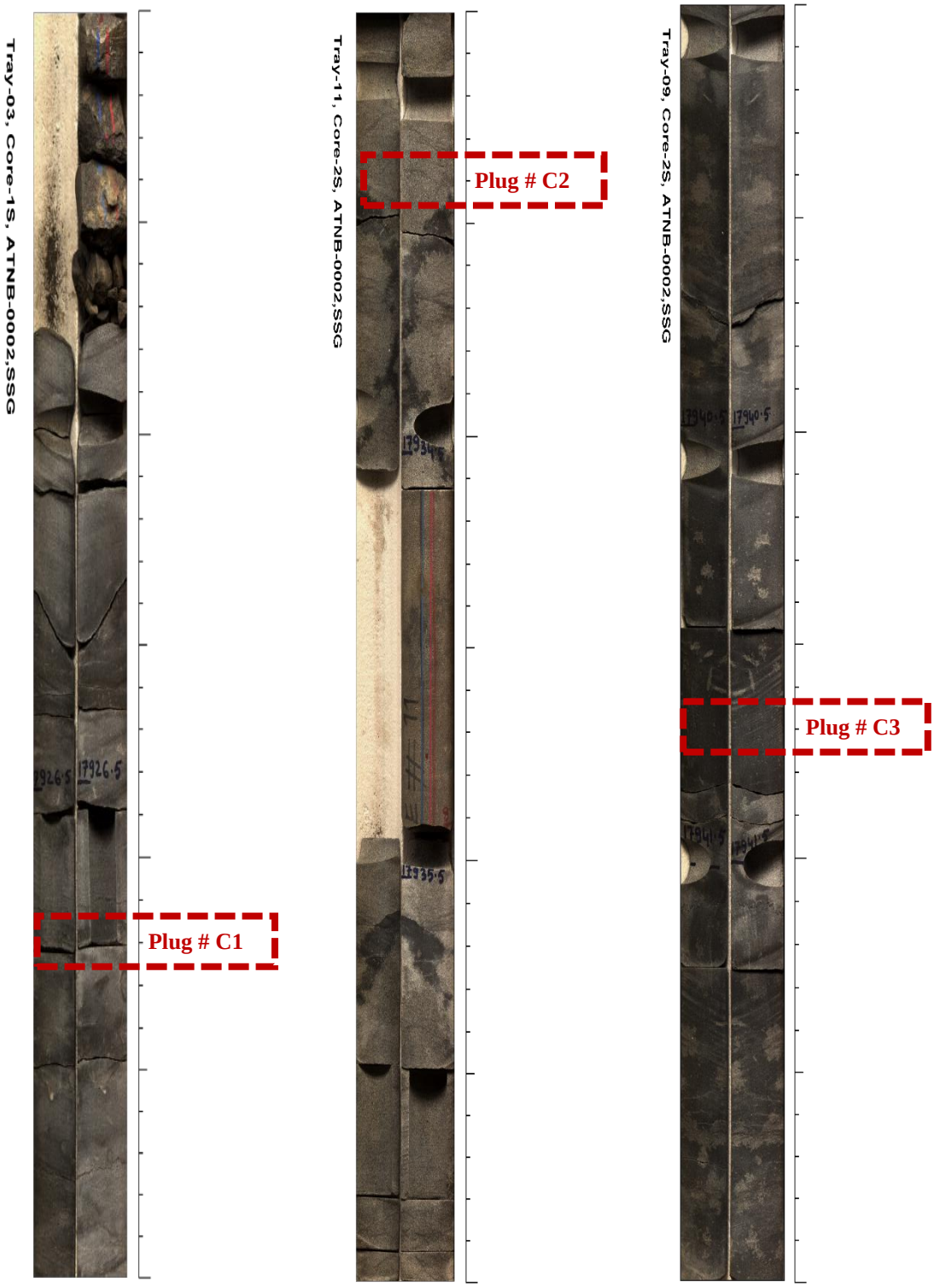

Well-C, Tray 3 (Core 1S), 11 and 9 (Core 2S)

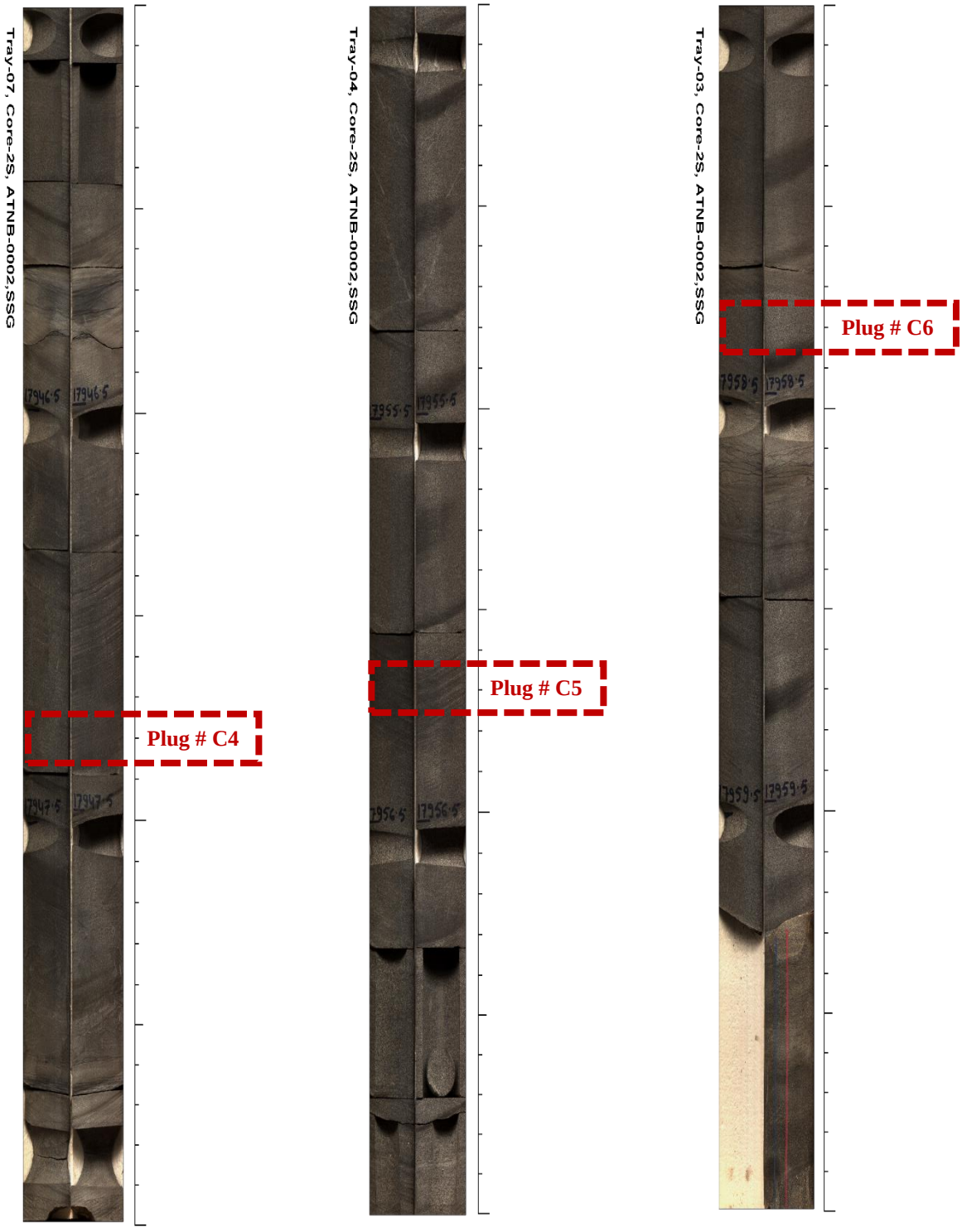

Well-C, Tray 7, 4 and 3 (Core 2S)

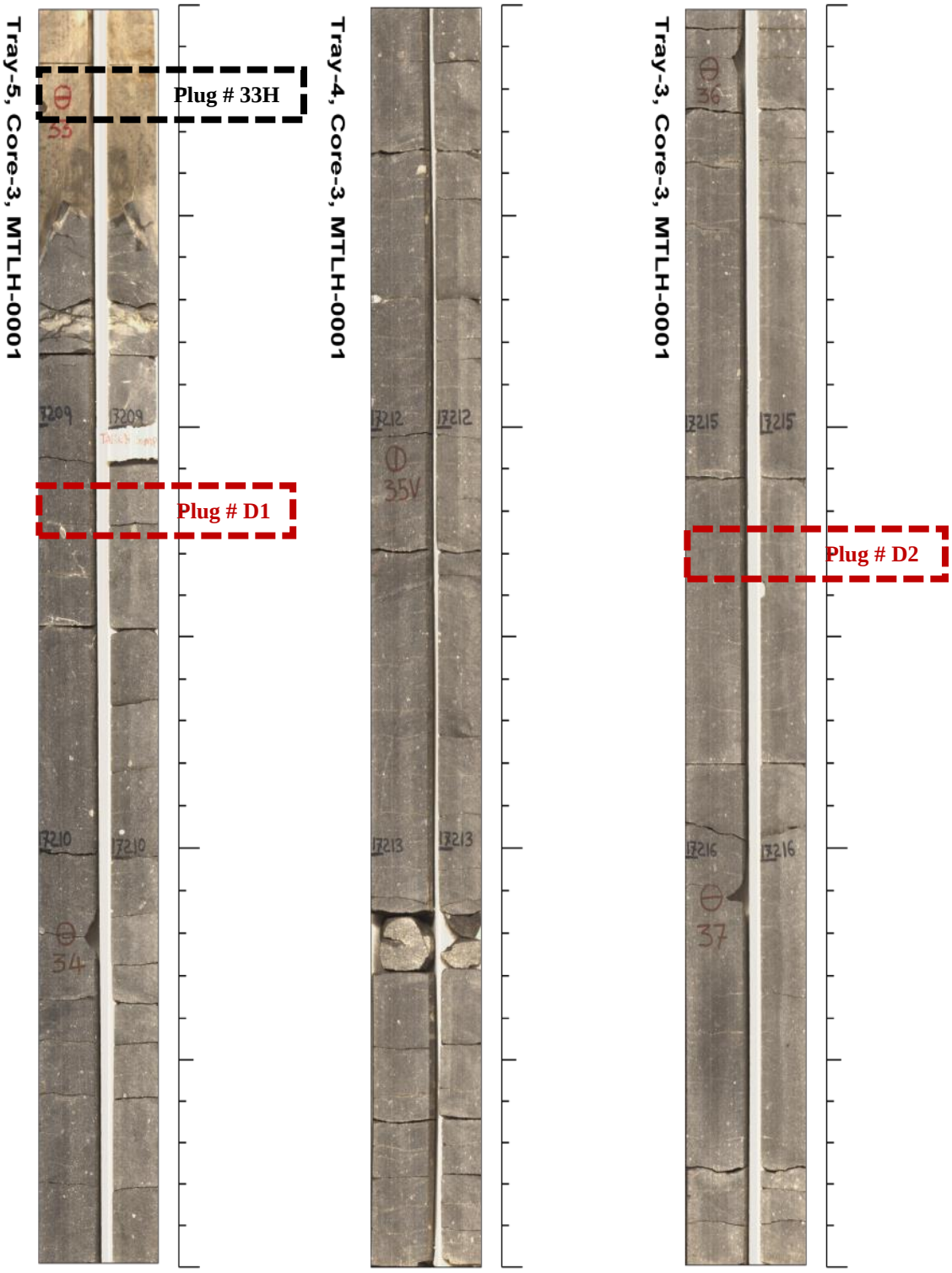

Well-D, Tray 5, 4 and 3

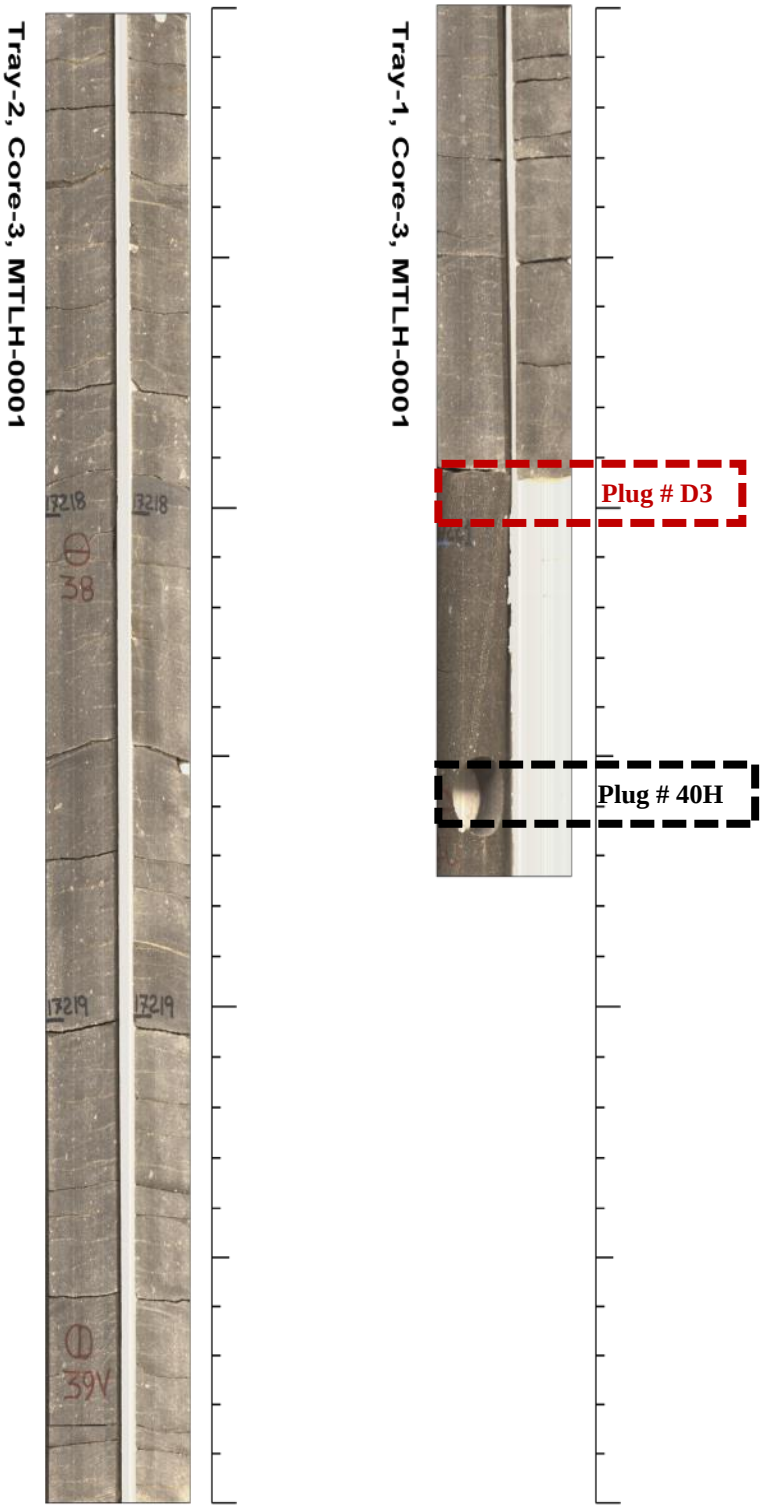

Well-D, Tray 2 and 1

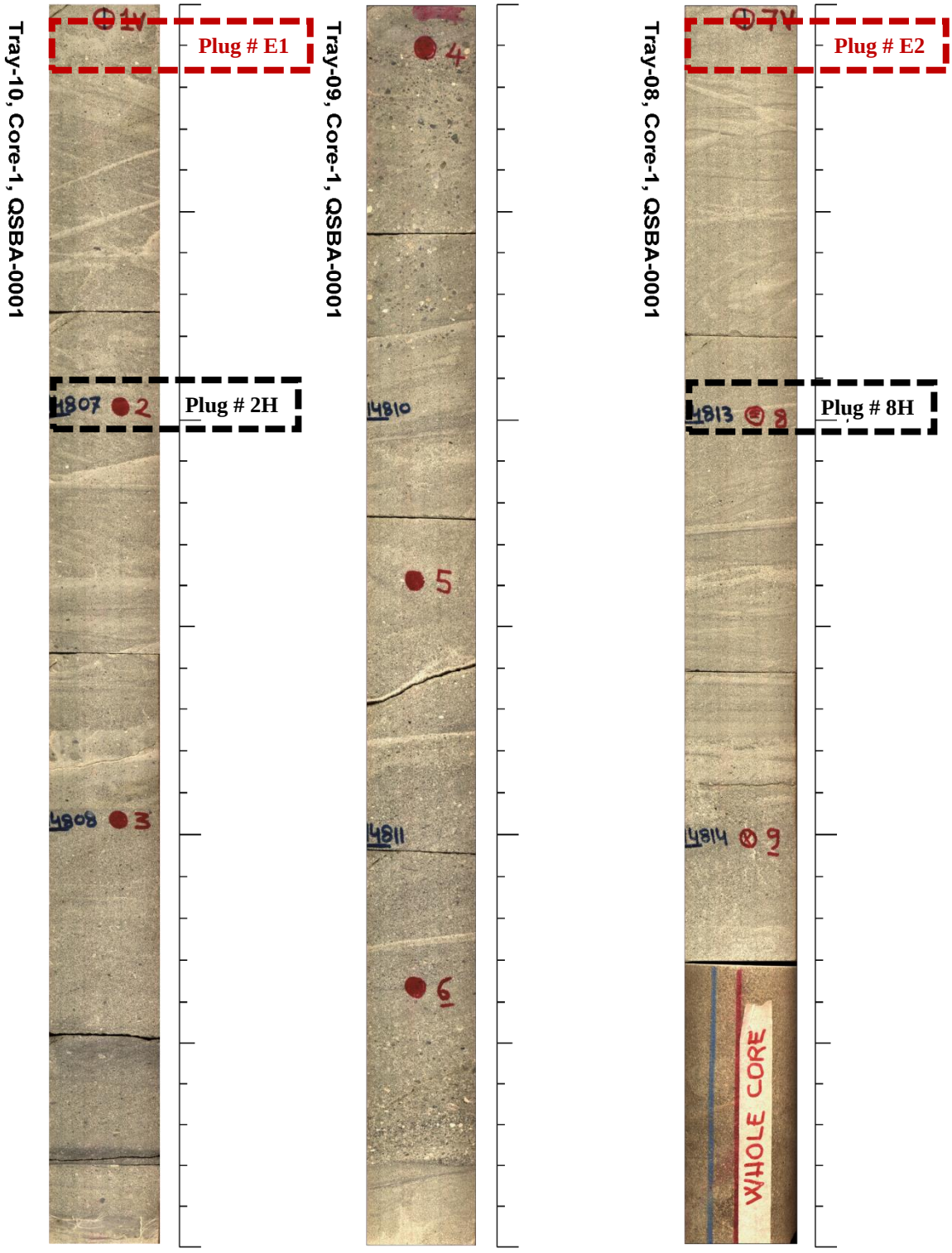

Well-E, Tray 10, 9 and 8

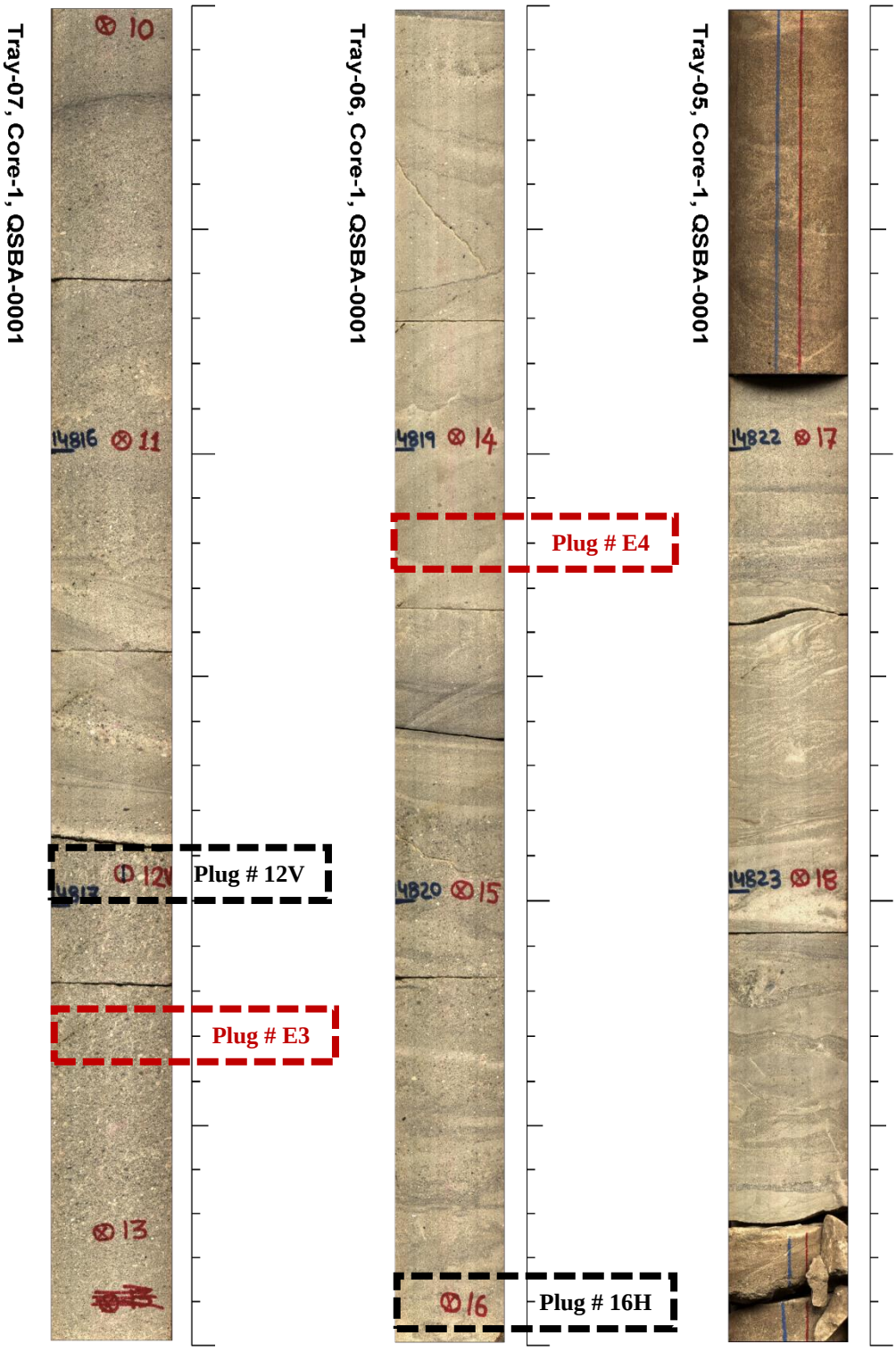

Well-E, Tray 7, 6 and 5

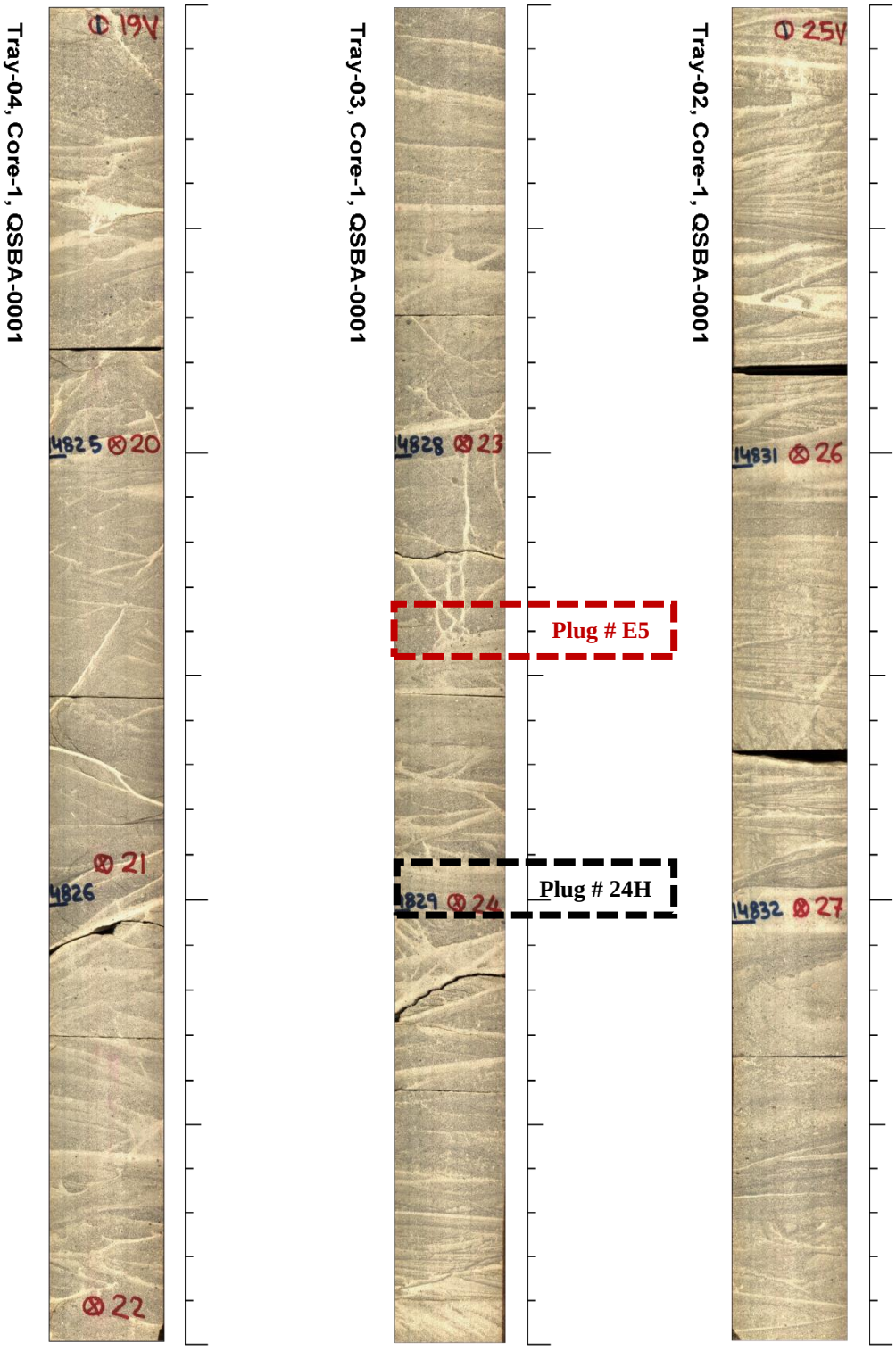

Well-E, Tray 4, 3 and 2

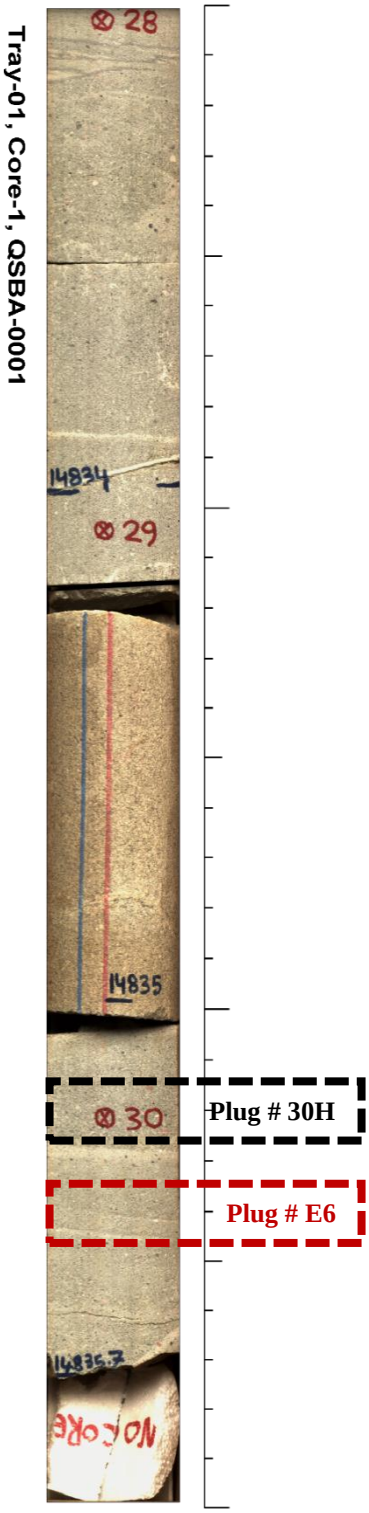

Well-E, Tray 1

Appendix - B

Acoustic Wave Velocity Measurements

-B1-

Observed Velocities and Moduli for File QSBA_SANDSTONE_2H							
Event	Conf	Pore	V_p	$V_s^{(1)}$	$V_s^{(2)}$	Young's Modulus	Poisson's Ratio
	MPa	MPa	m/s	m/s	m/s	GPa	
0	5.1	-0.1	3938	2542	2482	36.80	0.157
1	10.1	-0.1	4132	2673	2610	40.60	0.154
2	15.0	-0.1	4328	2776	2726	44.29	0.161
3	16.0	-0.1	4389	2793	2748	45.22	0.169
4	20.0	-0.1	4550	2858	2820	47.98	0.181
5	16.0	-0.1	4465	2834	2790	46.68	0.171
6	15.0	-0.1	4439	2825	2780	46.26	0.169
7	10.2	-0.1	4298	2750	2700	43.56	0.164
8	5.2	-0.1	4067	2632	2575	39.38	0.153

B 1: P and S waves velocities with Confining Pressure for Sample # 2H, Well E

-B2-

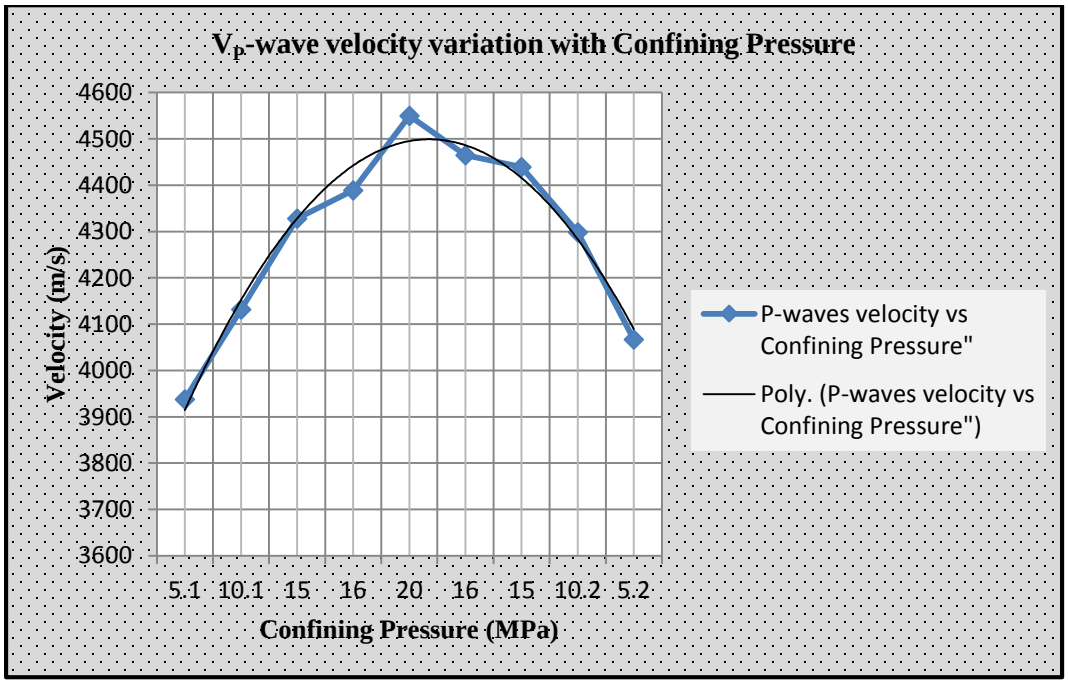

B 2: P-wave velocity variation with confining pressure for Sample # 2H, Well E

-B3-

Observed Velocities and Moduli for File QSBA_SANDSTONE_8H							
Event	Conf	Pore	V_p	$V_s^{(1)}$	$V_s^{(2)}$	Young's Modulus	Poisson's Ratio
	MPa	MPa	m/s	m/s	m/s	GPa	
0	7.0	-0.1	3364	2169	2056	25.68	0.174
1	14.0	-0.1	3731	2428	2276	31.72	0.170
2	21.1	-0.1	4021	2546	2438	36.16	0.188
3	28.0	-0.1	4234	2684	2561	40.06	0.189
4	35.1	-0.1	4395	2758	2659	42.91	0.194
5	28.2	-0.1	4298	2714	2606	41.24	0.190
6	21.4	-0.1	4149	2656	2505	38.65	0.185
7	14.2	-0.1	3924	2505	2377	34.58	0.184
8	7.2	-0.1	3493	2281	2183	28.19	0.155

B 3: P and S waves velocities with Confining Pressure for Sample # 8H, Well E

-B4-

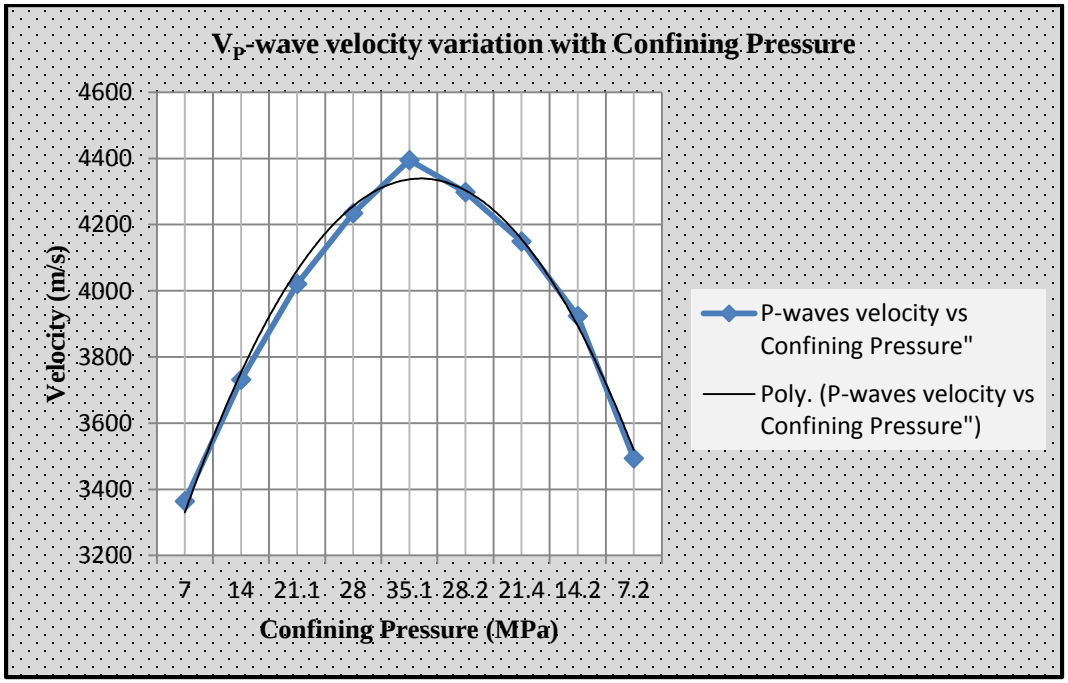

B 4: P-wave velocity variation with confining pressure for Sample # 8H, Well E

-B5-

Observed Velocities and Moduli for File QSBA_SANDSTONE_12V							
Event	Conf	Pore	V_p	$V_s^{(1)}$	$V_s^{(2)}$	Young's Modulus	Poisson's Ratio
	MPa	MPa	m/s	m/s	m/s	GPa	
0	7.0	-0.1	2900	2012	2049	20.93	0.019
1	14.0	-0.1	3337	2257	2283	27.44	0.069
2	21.0	-0.1	3609	2441	2462	32.07	0.072
3	28.1	-0.1	3790	2594	2618	35.57	0.052
4	35.0	-0.1	4016	2721	2747	39.76	0.068
5	28.1	-0.1	3906	2637	2672	37.58	0.071
6	21.2	-0.1	3703	2533	2540	33.90	0.058
7	14.2	-0.1	3445	2347	2364	29.32	0.061
8	7.2	-0.1	2974	2105	2128	22.02	-0.013

B 5: P and S waves velocities with Confining Pressure for Sample # 12V, Well E

-B6-

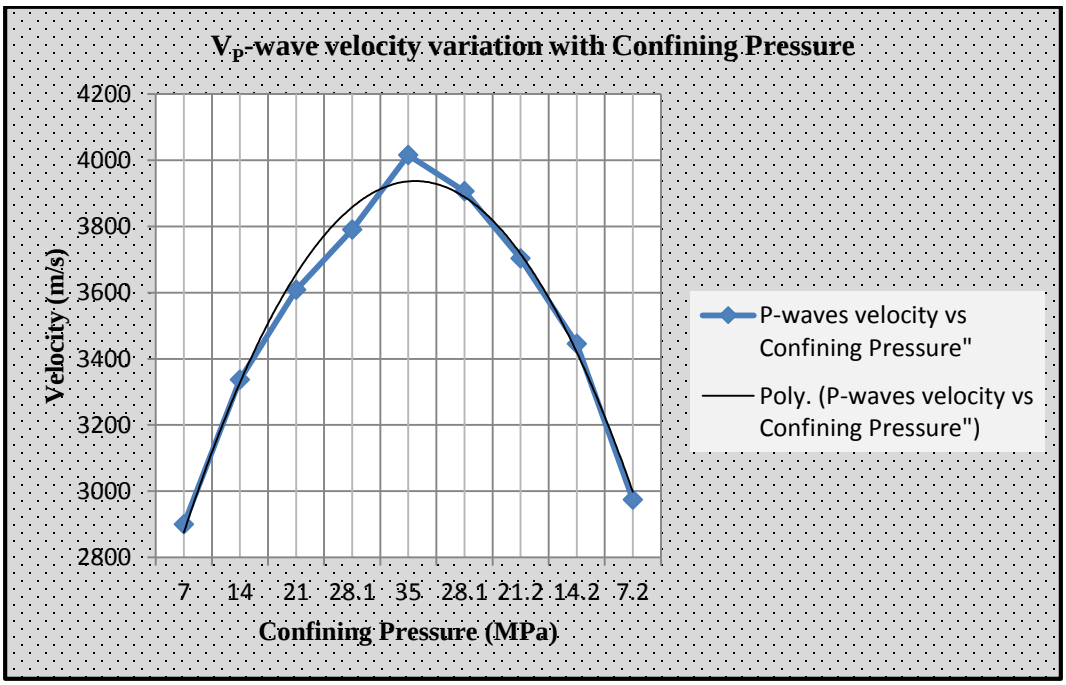

B 3: P-wave velocity variation with confining pressure for Sample # 12V, Well E

Observed Velocities and Moduli for File QSBA_SANDSTONE_16H_WALEED							
Event	Conf	Pore	V_p	$V_s^{(1)}$	$V_s^{(2)}$	Young's Modulus	Poisson's Ratio
	MPa	MPa	m/s	m/s	m/s	GPa	
0	7.0	-0.1	3771	2251	2456	32.05	0.181
1	14.0	-0.1	4090	2429	2664	37.60	0.183
2	21.0	-0.1	4329	2573	2819	42.14	0.183
3	28.0	-0.1	4501	2683	2928	45.60	0.182
4	35.0	-0.1	4651	2763	3008	48.43	0.187
5	28.1	-0.1	4591	2714	2962	46.99	0.191
6	21.1	-0.1	4480	2646	2890	44.72	0.191
7	14.2	-0.1	4295	2528	2777	41.08	0.192
8	7.2	-0.1	3926	2335	2604	35.04	0.173

B 4: P and S waves velocities with Confining Pressure for Sample # 16H, Well E

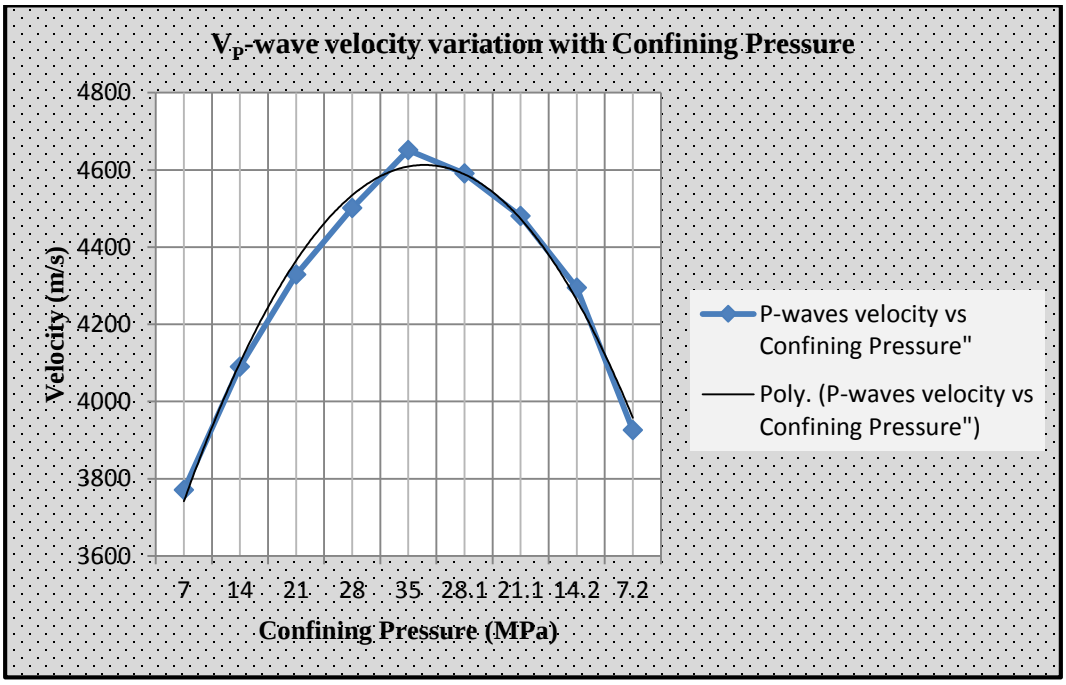

B 5: P-wave velocity variation with confining pressure for Sample # 16H, Well E

Observed Velocities and Moduli for File QSBA_SANDSTONE_24H_WALEED_2							
Event	Conf	Pore	V_p	$V_s^{(1)}$	$V_s^{(2)}$	Young's Modulus	Poisson's Ratio
	MPa	MPa	m/s	m/s	m/s	GPa	
0	7.1	-0.1	4789	2619	2875	46.97	0.255
1	14.0	-0.1	5031	2719	3009	51.27	0.260
2	21.1	-0.1	5165	2972	3121	56.77	0.233
3	28.0	-0.1	5239	3019	3203	58.93	0.228
4	35.1	-0.1	5350	3064	3260	61.08	0.232
5	28.1	-0.1	5316	3036	3222	59.97	0.235
6	21.2	-0.1	5239	2991	3172	58.19	0.236
7	14.1	-0.1	5117	2786	3068	53.41	0.257
8	7.2	-0.1	4874	2626	2890	47.71	0.264

B 6: P and S waves velocities with Confining Pressure for Sample # 24H, Well E

-B10-

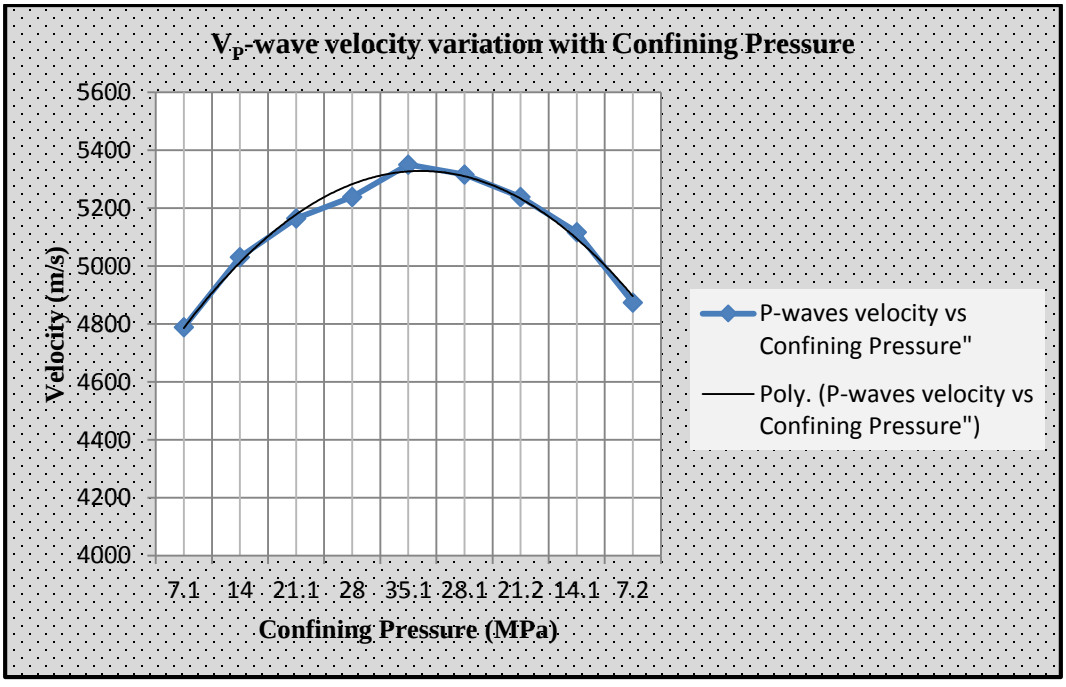

B 10: P-wave velocity variation with confining pressure for Sample # 24H, Well E

Observed Velocities and Moduli for File QSBA_SANDSTONE_30H_WALEED							
Event	Conf	Pore	V_p	$V_s^{(1)}$	$V_s^{(2)}$	Young's Modulus	Poisson's Ratio
	MPa	MPa	m/s	m/s	m/s	GPa	
0	7.0	-0.1	3580	2333	2433	31.42	0.102
1	14.0	-0.1	4034	2572	2683	39.22	0.132
2	21.0	-0.1	4294	2748	2878	44.65	0.124
3	28.0	-0.1	4569	2870	3012	49.77	0.146
4	35.0	-0.1	4747	2954	3109	53.31	0.156
5	28.1	-0.1	4630	2919	3054	51.21	0.144
6	21.1	-0.1	4451	2825	2960	47.65	0.134
7	14.2	-0.1	4189	2673	2794	42.36	0.129
8	7.2	-0.1	3709	2427	2522	33.78	0.099

B 7: P and S waves velocities with Confining Pressure for Sample # 30H, Well E

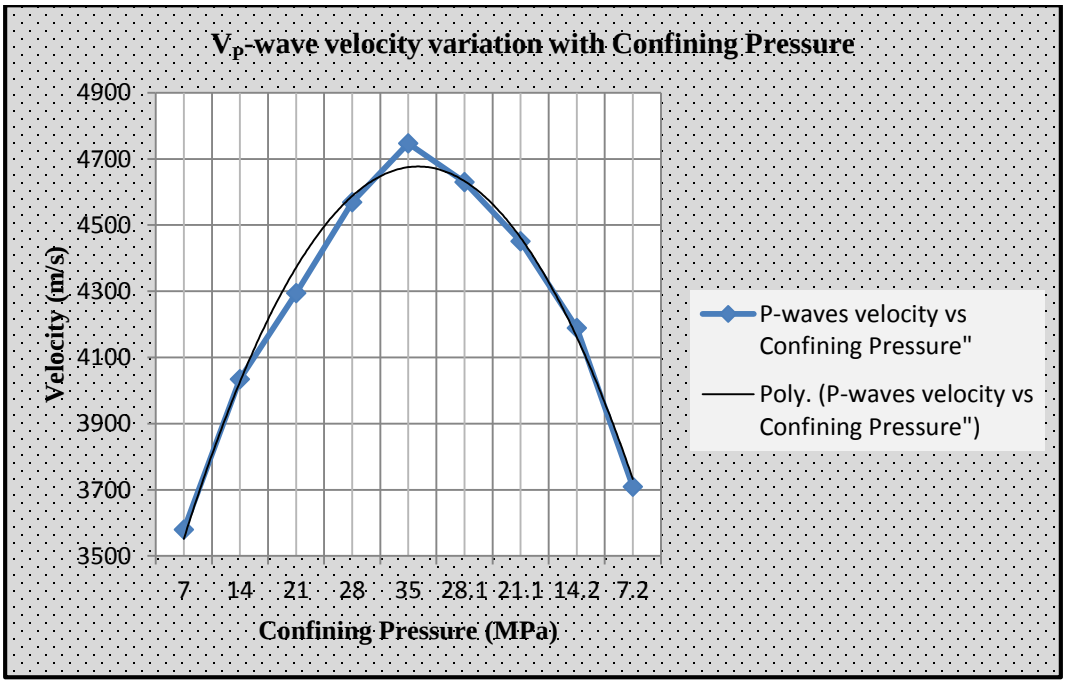

B 8: P-wave velocity variation with confining pressure for Sample # 30H, Well E

-B13-

Observed Velocities and Moduli for File FRAS_SANDSTONE_68H_WALEED							
Event	Conf	Pore	V_p	$V_s^{(1)}$	$V_s^{(2)}$	Young's Modulus	Poisson's Ratio
	MPa	MPa	m/s	m/s	m/s	GPa	
0	7.1	-0.1	3352	2268	2159	26.40	0.113
1	14.0	-0.1	3713	2462	2363	31.96	0.135
2	21.0	-0.1	4031	2590	2529	36.85	0.162
3	27.9	-0.1	4262	2729	2662	41.03	0.167
4	34.8	-0.1	4367	2826	2768	43.63	0.152
5	7.1	-0.1	3531	2360	2272	29.14	0.122
6	14.0	-0.1	3795	2508	2414	33.33	0.137
7	21.0	-0.1	4081	2619	2559	37.74	0.163
8	27.8	-0.1	4272	2745	2681	41.40	0.162
9	35.1	-0.1	4450	2835	2779	44.60	0.170
10	28.0	-0.1	4353	2783	2720	42.77	0.167
11	21.1	-0.1	4182	2692	2624	39.70	0.161
12	14.3	-0.1	3930	2558	2484	35.39	0.150
13	7.2	-0.1	3519	2360	2270	29.01	0.119

B 9: P and S waves velocities with Confining Pressure for Sample # 68H, Well A

-B14-

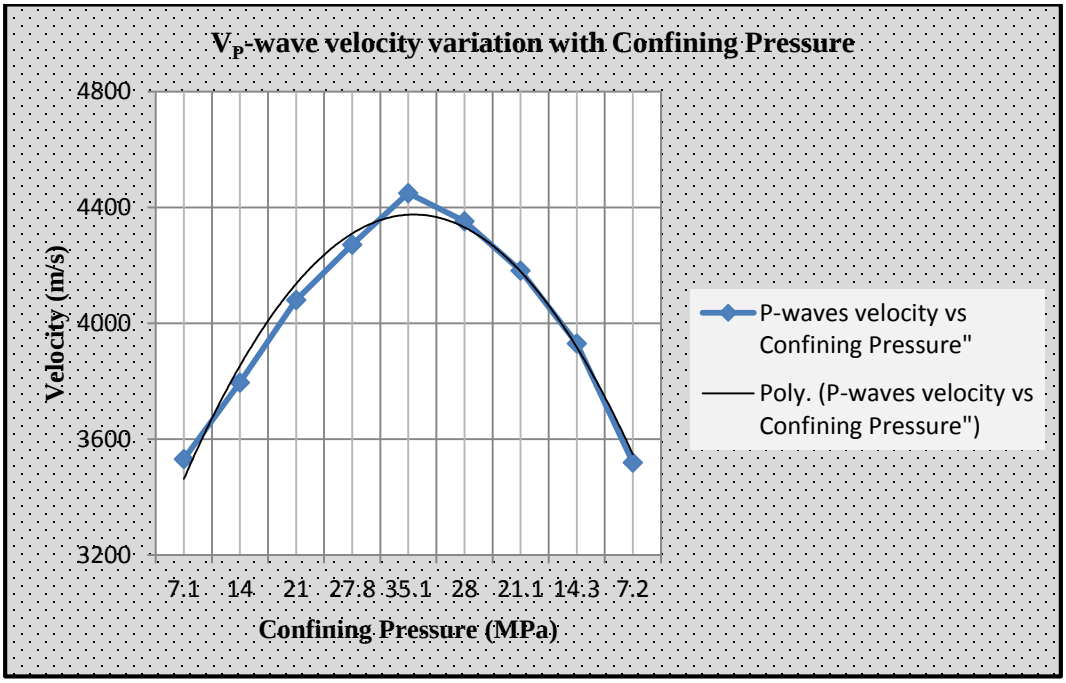

B 14: P-wave velocity variation with confining pressure for Sample # 68H, Well A

-B15-

Observed Velocities and Moduli for File FARS_SANDSTONE_73H_WALEED							
Event	Conf	Pore	V_p	$V_s^{(1)}$	$V_s^{(2)}$	Young's Modulus	Poisson's Ratio
	MPa	MPa	m/s	m/s	m/s	GPa	
0	7.0	-0.1	3386	2121	2212	25.77	0.153
1	14.0	-0.1	3735	2375	2478	31.81	0.135
2	21.1	-0.1	4013	2563	2649	36.70	0.135
3	28.0	-0.1	4214	2689	2781	40.45	0.136
4	35.1	-0.1	4377	2774	2869	43.37	0.145
5	28.1	-0.1	4286	2723	2815	41.67	0.142
6	21.2	-0.1	4150	2635	2729	39.08	0.141
7	14.2	-0.1	3880	2491	2590	34.55	0.125
8	7.1	-0.1	3528	2257	2345	28.48	0.130

B 10: P and S waves velocities with Confining Pressure for Sample # 73H, Well A

-B16-

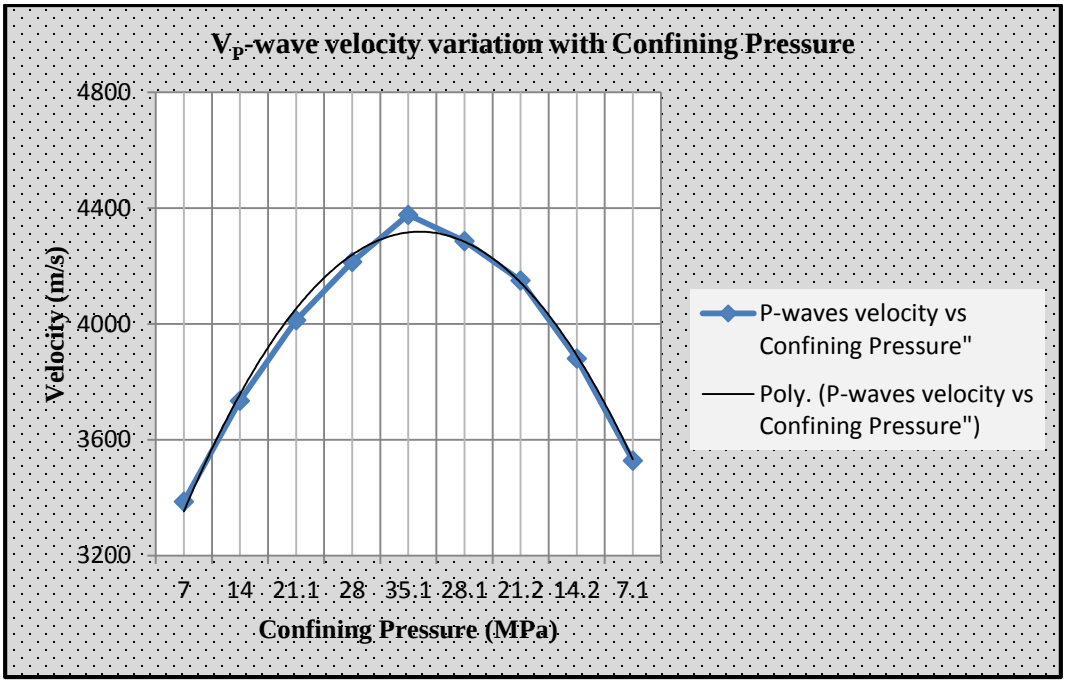

B 11: P-wave velocity variation with confining pressure for Sample # 73H, Well A

-B17-

Observed Velocities and Moduli for File FARS_SANDSTONE_81H_WALEED							
Event	Conf	Pore	V_p	$V_s^{(1)}$	$V_s^{(2)}$	Young's Modulus	Poisson's Ratio
	MPa	MPa	m/s	m/s	m/s	GPa	
0	7.1	-0.1	3318	2191	2078	25.08	0.147
1	14.0	-0.1	3735	2415	2343	31.48	0.159
2	21.0	-0.1	3996	2572	2527	36.09	0.157
3	28.0	-0.1	4227	2691	2666	40.10	0.165
4	35.0	-0.1	4430	2780	2770	43.51	0.177
5	28.1	-0.1	4284	2727	2712	41.27	0.163
6	21.2	-0.1	4135	2639	2610	38.44	0.163
7	14.2	-0.1	3877	2502	2455	34.04	0.154
8	7.1	-0.1	3480	2273	2207	27.61	0.146

B 17: P and S waves velocities with Confining Pressure for Sample # 81H, Well A

-B18-

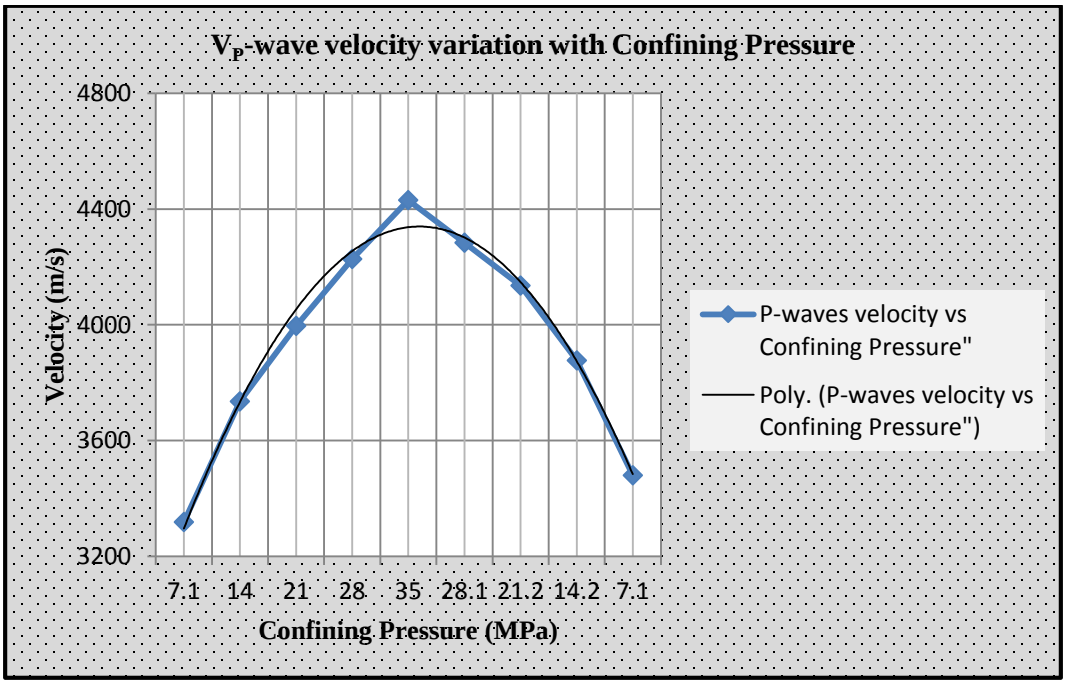

B 18: P-wave velocity variation with confining pressure for Sample # 81H, Well A

Observed Velocities and Moduli for File FARS_SANDSTONE_88H							
Event	Conf	Pore	V_p	$V_s^{(1)}$	$V_s^{(2)}$	Young's Modulus	Poisson's Ratio
	MPa	MPa	m/s	m/s	m/s	GPa	
0	7.0	-0.1	3463	1990	2178	25.04	0.216
1	14.0	-0.1	3799	2200	2373	30.13	0.216
2	21.0	-0.1	3987	2364	2508	33.81	0.202
3	28.1	-0.1	4141	2511	2594	36.86	0.194
4	34.9	-0.1	4246	2602	2664	39.03	0.188
5	28.1	-0.1	4171	2538	2620	37.53	0.191
6	21.3	-0.1	4118	2433	2552	35.66	0.211
7	14.2	-0.1	3894	2324	2446	32.35	0.200
8	7.3	-0.1	3563	2091	2311	27.36	0.191

B 12: P and S waves velocities with Confining Pressure for Sample # 88H, Well A

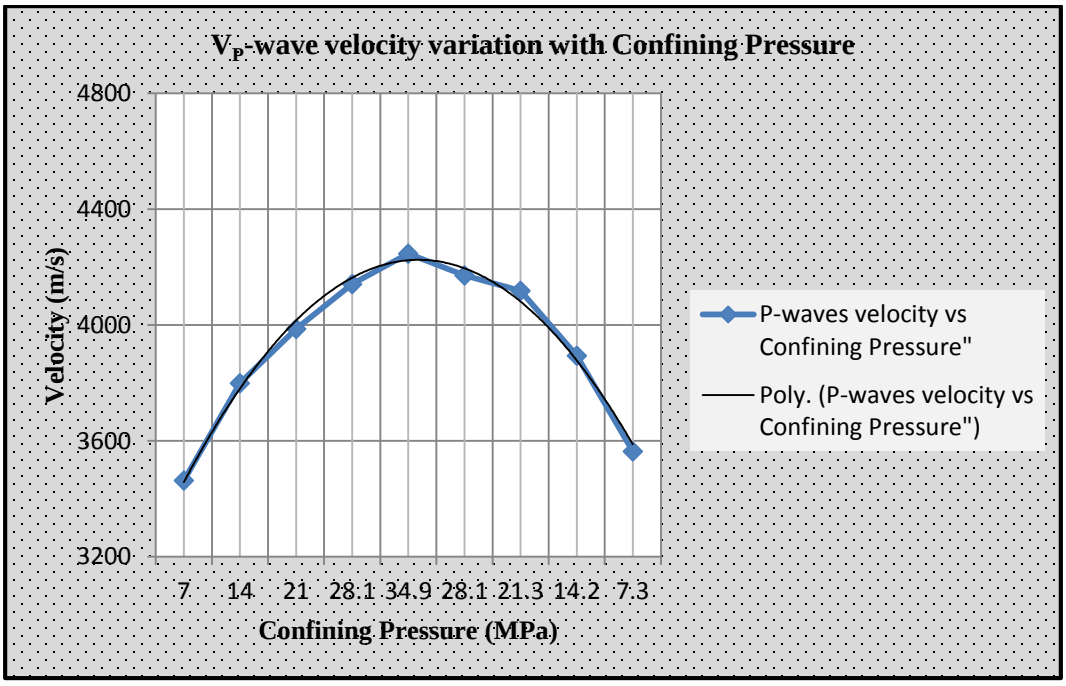

B 13: P-wave velocity variation with confining pressure for Sample # 88H, Well A

Observed Velocities and Moduli for File FARS_SANDSTONE_89V_WALEED_2							
Event	Conf	Pore	V_p	$V_s^{(1)}$	$V_s^{(2)}$	Young's Modulus	Poisson's Ratio
	MPa	MPa	m/s	m/s	m/s	GPa	
0	7.1	-0.1	3115	2244	2227	24.41	-0.031
1	14.0	-0.1	3616	2484	2468	32.71	0.059
2	21.0	-0.1	4013	2671	2660	39.58	0.105
3	28.2	-0.1	4299	2813	2814	44.90	0.125
4	35.0	-0.1	4517	2893	2914	48.77	0.148
5	28.2	-0.1	4401	2857	2863	46.77	0.134
6	21.1	-0.1	4226	2764	2769	43.40	0.125
7	14.2	-0.1	3894	2628	2616	37.60	0.085
8	7.3	-0.1	3390	2391	2379	28.95	0.010

B 14: P and S waves velocities with Confining Pressure for Sample # 89H, Well A

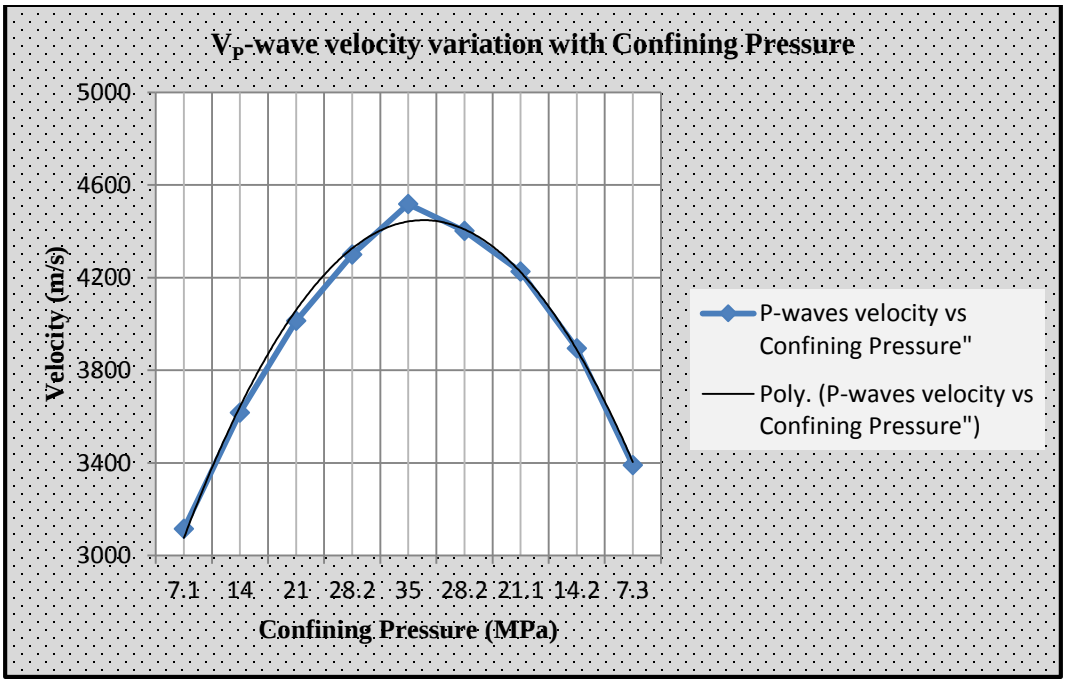

B 15: P-wave velocity variation with confining pressure for Sample # 89V, Well A

Observed Velocities and Moduli for File FARS_SANDSTONE_95V							
Event	Conf	Pore	V_p	$V_s^{(1)}$	$V_s^{(2)}$	Young's Modulus	Poisson's Ratio
	MPa	MPa	m/s	m/s	m/s	GPa	
0	7.0	-0.1	3077	2015	2020	21.48	0.123
1	14.1	-0.1	3475	2278	2289	27.45	0.120
2	21.1	-0.1	3789	2460	2483	32.43	0.130
3	28.0	-0.1	4045	2543	2628	36.28	0.155
4	35.0	-0.1	4285	2669	2734	40.14	0.170
5	28.1	-0.1	4141	2588	2671	37.77	0.162
6	21.1	-0.1	3976	2513	2555	34.95	0.158
7	14.2	-0.1	3657	2356	2391	30.08	0.136
8	7.2	-0.1	3109	2112	2137	22.53	0.062

B 16: P and S waves velocities with Confining Pressure for Sample # 95V, Well A

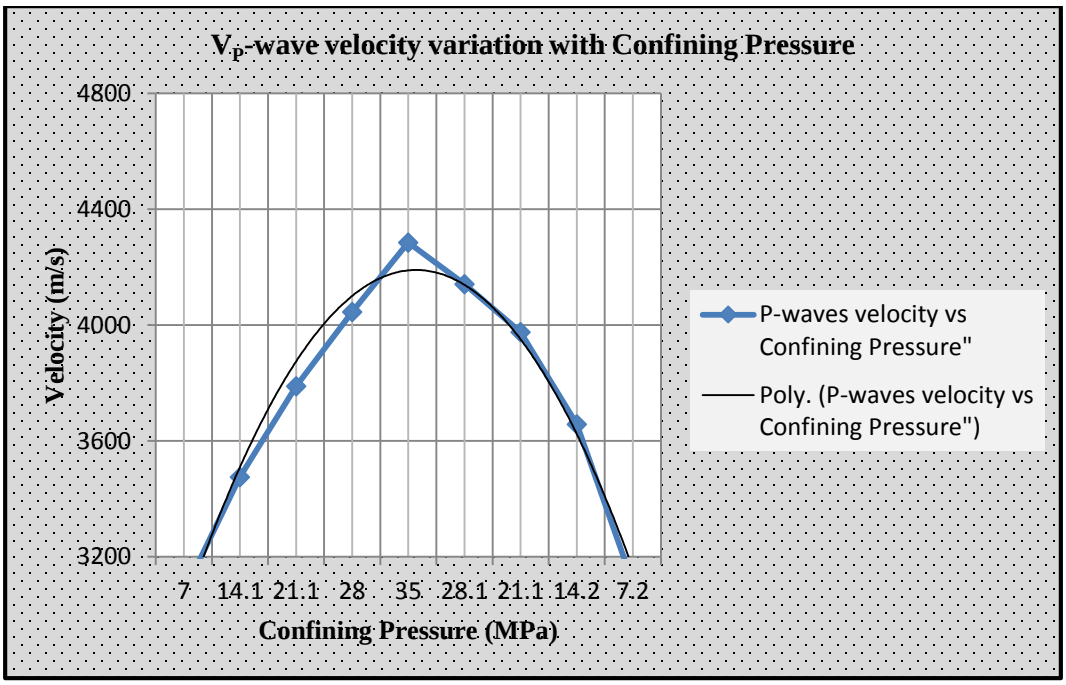

B 17: P-wave velocity variation with confining pressure for Sample # 95V, Well A

Observed Velocities and Moduli for File MTLH_SANDSTONE_33H_WALEED							
Event	Conf	Pore	V_p	$V_s^{(1)}$	$V_s^{(2)}$	Young's Modulus	Poisson's Ratio
	MPa	MPa	m/s	m/s	m/s	GPa	
0	7.1	-0.1	4756	2449	2829	50.18	0.278
1	14.1	-0.1	5042	2583	3000	56.21	0.279
2	21.0	-0.1	5426	2680	3113	61.55	0.301
3	28.1	-0.1	5596	2763	3154	64.47	0.306
4	35.0	-0.1	5596	2840	3196	66.52	0.295
5	28.0	-0.1	5596	2796	3211	66.02	0.298
6	21.1	-0.1	5426	2731	3140	62.85	0.293
7	14.2	-0.1	5152	2640	3046	58.40	0.281
8	7.2	-0.1	4805	2476	2874	51.47	0.275

B 18: P and S waves velocities with Confining Pressure for Sample # 33H, Well D

-B26-

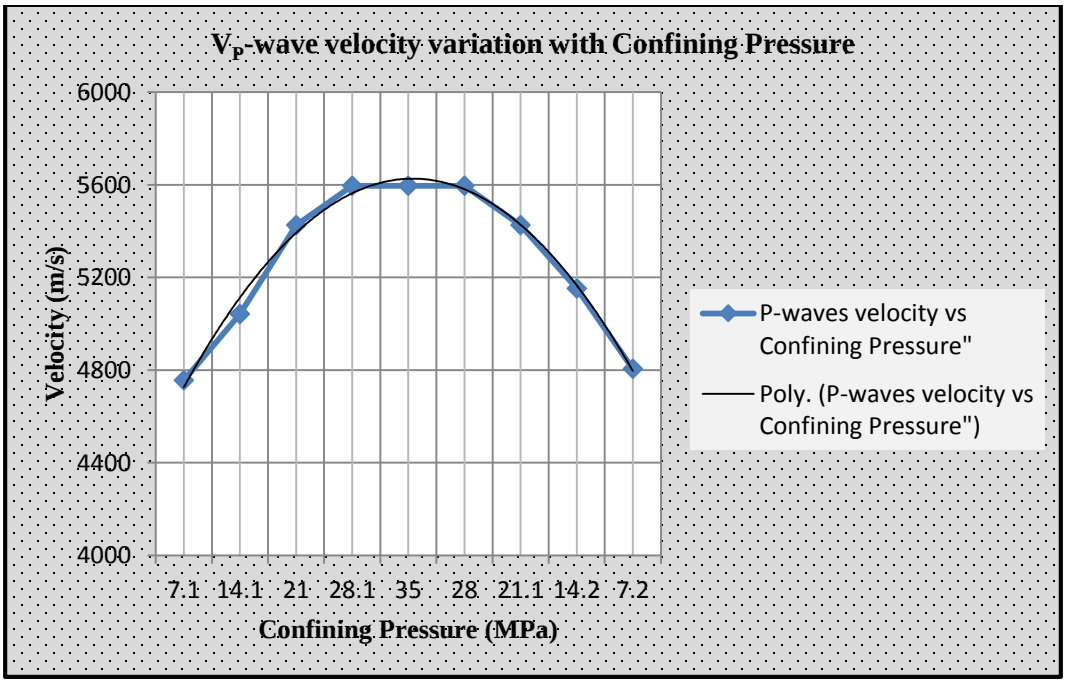

B 26: P-wave velocity variation with confining pressure for Sample # 33H, Well D

Observed Velocities and Moduli for File MTLH_SANDSTONE_40H_WALEED							
Event	Conf	Pore	V_p	$V_s^{(1)}$	$V_s^{(2)}$	Young's Modulus	Poisson's Ratio
	MPa	MPa	m/s	m/s	m/s	GPa	
0	7.1	-0.1	5502	3226	3372	70.60	0.219
1	14.1	-0.1	5550	3246	3394	71.62	0.221
2	21.0	-0.1	5582	3257	3411	72.30	0.223
3	28.0	-0.1	5615	3257	3420	72.73	0.227
4	35.0	-0.1	5632	3268	3422	73.07	0.228
5	28.1	-0.1	5615	3257	3418	72.70	0.227
6	21.1	-0.1	5582	3257	3414	72.35	0.222
7	14.1	-0.1	5550	3246	3394	71.62	0.221
8	7.3	-0.1	5502	3226	3372	70.60	0.219

B 27: P and S waves velocities with Confining Pressure for Sample # 40H, Well D

-B28-

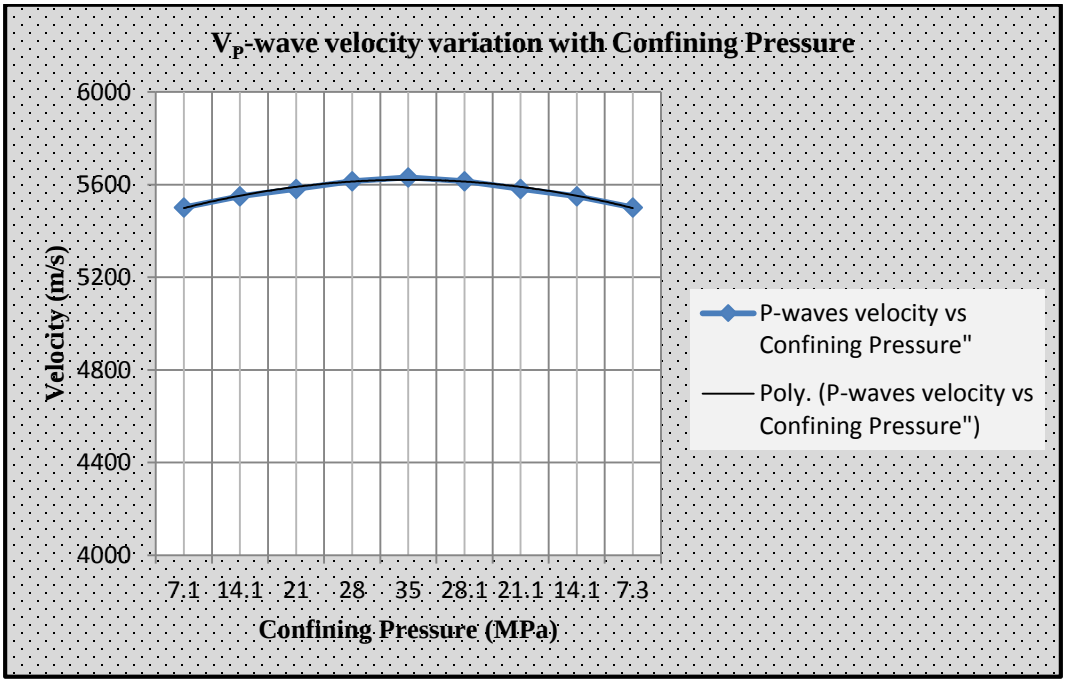

B 28: P-wave velocity variation with confining pressure for Sample # 40H, Well D

Observed Velocities and Moduli for File SHEH_SANDSTONE_116_WALEED							
Event	Conf	Pore	V_p	$V_s^{(1)}$	$V_s^{(2)}$	Young's Modulus	Poisson's Ratio
	MPa	MPa	m/s	m/s	m/s	GPa	
0	7.1	-0.1	4815	2923	3119	54.06	0.175
1	14.1	-0.1	4953	3000	3179	56.84	0.182
2	21.1	-0.1	5058	3069	3235	59.21	0.183
3	28.1	-0.1	5145	3122	3294	61.31	0.182
4	35.0	-0.1	5280	3171	3337	63.71	0.194
5	28.2	-0.1	5235	3156	3321	62.90	0.190
6	21.2	-0.1	5180	3122	3283	61.54	0.191
7	14.1	-0.1	5058	3064	3240	59.21	0.183
8	7.2	-0.1	4910	2982	3169	56.12	0.177

B 29: P and S waves velocities with Confining Pressure for Sample # 116H, Well F

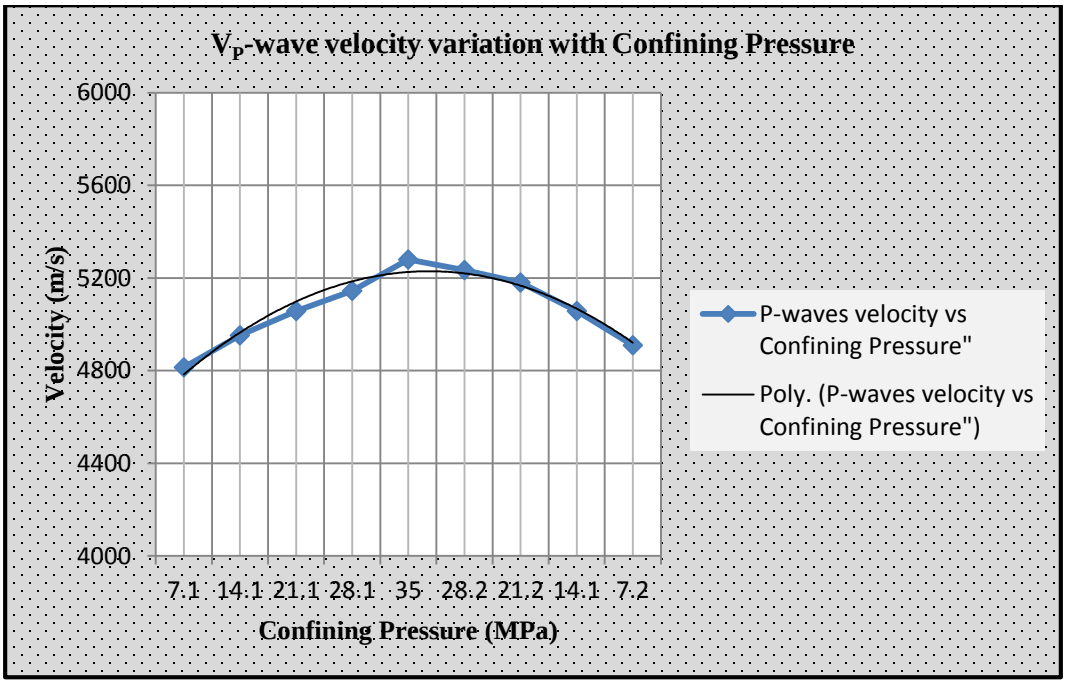

B 30: P-wave velocity variation with confining pressure for Sample # 116H, Well F

Observed Velocities and Moduli for File SHEH_SANDSTONE_118_WALEED							
Event	Conf	Pore	V_p	$V_s^{(1)}$	$V_s^{(2)}$	Young's Modulus	Poisson's Ratio
	MPa	MPa	m/s	m/s	m/s	GPa	
0	7.0	-0.1	5465	3227	3369	69.43	0.214
1	14.1	-0.1	5494	3242	3380	70.05	0.215
2	21.0	-0.1	5524	3253	3397	70.71	0.216
3	28.1	-0.1	5601	3263	3409	71.72	0.225
4	35.1	-0.1	5555	3274	3414	71.51	0.216
5	28.1	-0.1	5585	3265	3414	71.67	0.222
6	21.1	-0.1	5539	3258	3409	71.08	0.216
7	14.2	-0.1	5509	3253	3397	70.57	0.213
8	7.3	-0.1	5479	3237	3380	69.84	0.213

B 19: P and S waves velocities with Confining Pressure for Sample # 118H, Well F

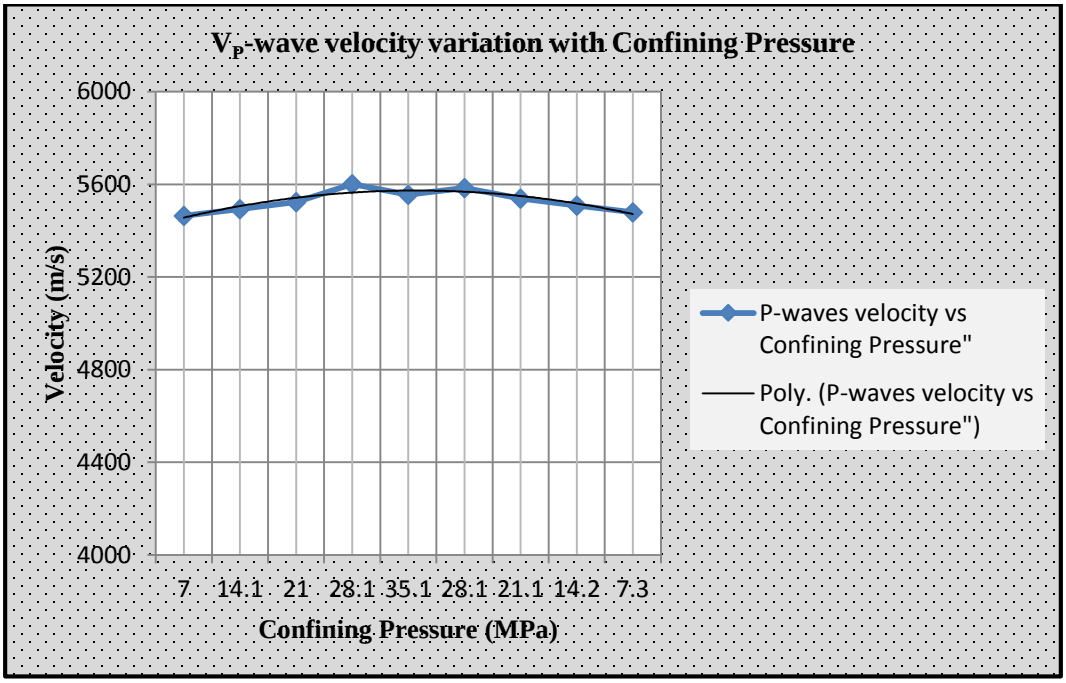

B 20: P-wave velocity variation with confining pressure for Sample # 118H, Well F

Appendix - C

Uniaxial Compressive Strength Results of All Core Plugs

Uniaxial Compressive Strength Results, Well-A

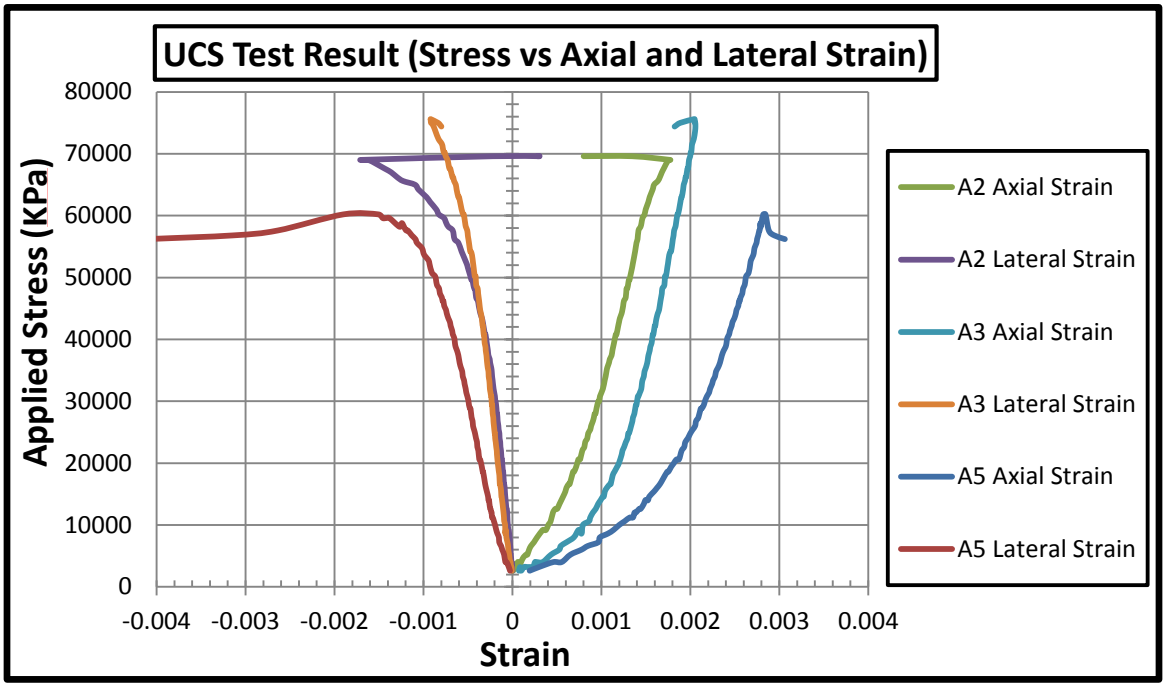

Uniaxial Compressive Strength Results, Well-B

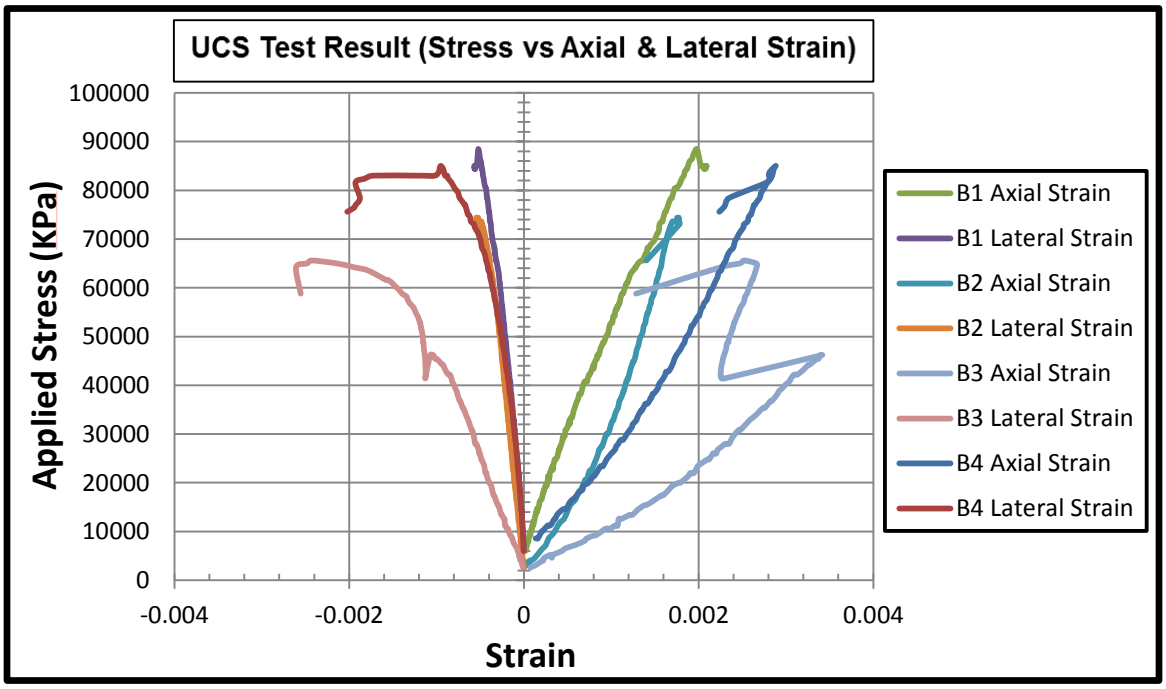

Uniaxial Compressive Strength Results, Well-C

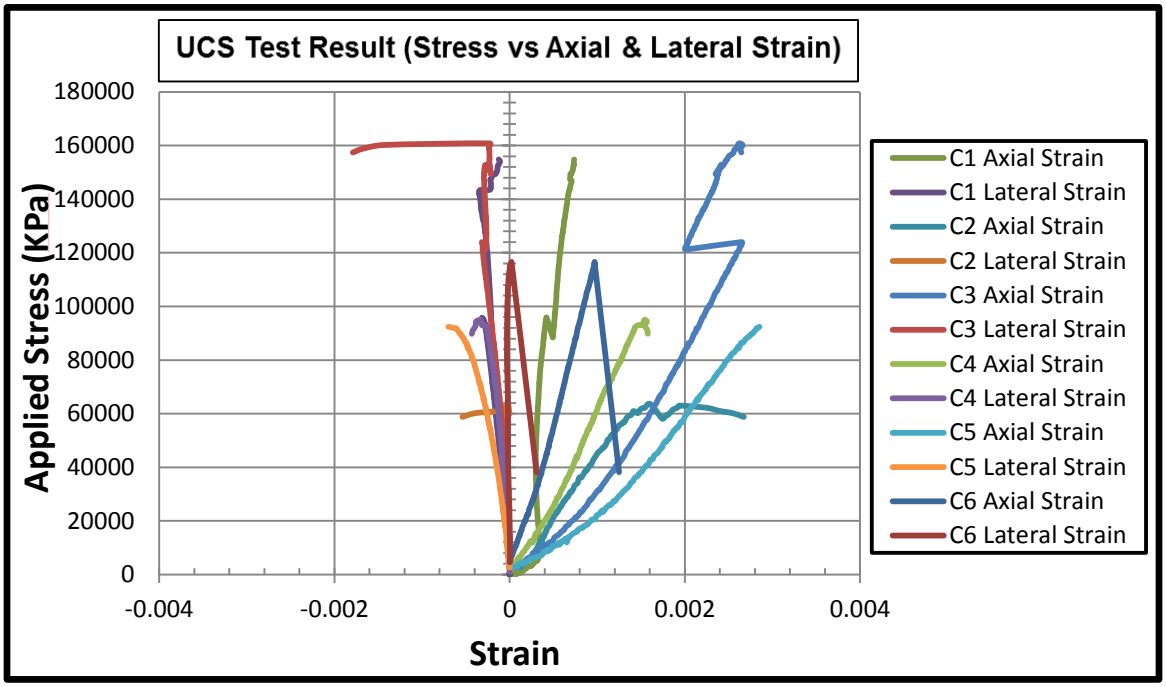

Uniaxial Compressive Strength Results, Well-D

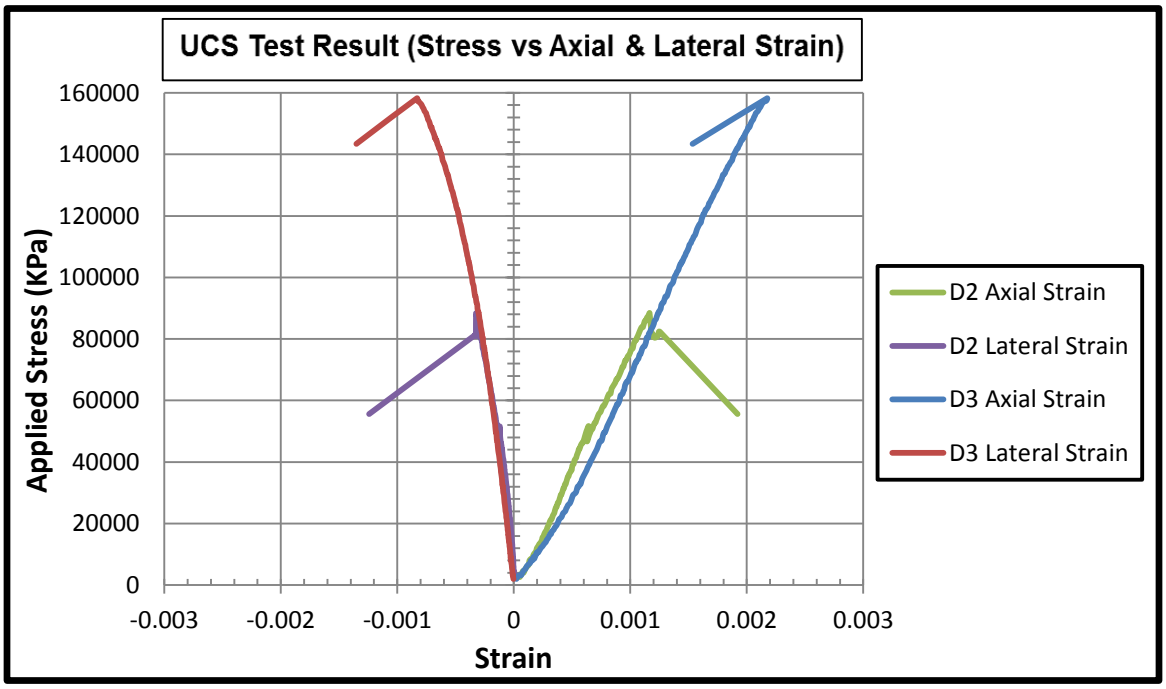

Uniaxial Compressive Strength Results, Well-E

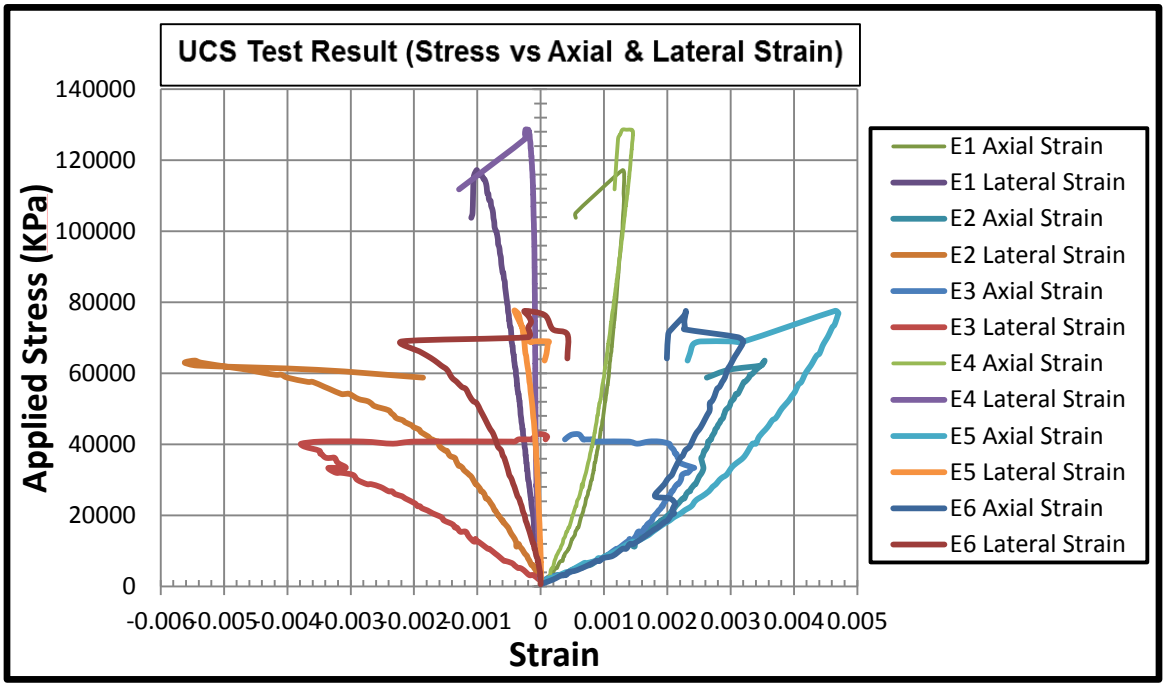

Vitae

Name	:	Waleed Ejaz
Nationality	:	Pakistani
Date of Birth	:	7/18/1989
Email	:	waleed_geoman@yahoo.com
Address	:	House No. 26, Abshar Street, Taj Bagh Scheme Lahore, Pakistan.
Academic Background	:	M.S. in Geophysics, 2016, King Fahd University of Petroleum and Minerals, Dhahran, Saudi Arabia. B.S. in Applied Geology, 2012, University of the Punjab, Lahore, Pakistan.
Publications	:	

1. *Petrophysical trends of the organic-rich Qusaiba Shale, Saudi Arabia. (In Progress)*
   Abouelresh, O.M., Ejaz, W., Alshuhail, A.
   Submitted in Journal of Petroleum Science and Engineering
2. *Electrofacies Characterization in a Tight Siliciclastic Sequence: Sarah Formation, Rub' Al-Khali Basin, Saudi Arabia. (In Progress)*
   Submitted in Unconventional Resources Technology Conference (URTeC) 2016.
3. *Petrophysical and Dynamic Geomechanical Characterization of Lower Silurian Qusaiba Shale, Saudi Arabia.*

Presented in 3rd SEG/DGS Middle East Geoscience Young Professionals and Student Event, 26-28 April 2015 Manama, Bahrain.

4. *Study of Source Rock Maturity and Hydrocarbon Exploration Potential using Petrophysical Analysis, Punjab Platform, Central Indus Basin, Pakistan.*

   Presented in KSEG International Symposium 2012, Jeju Island, Korea.

5. *Study of Source Potential in Pre-Permian Sediments using Well Log Data and Vitrinite Reflectance, Central Indus Basin (Punjab Platform), Pakistan.*

   Presented in Annual Technical Conference (ATC) 2012, Pakistan.